STUDIES OF CARBOHYDRATES AND PEPTIDES BY NMR SPECTROSCOPY AND MOLECULAR MODELLING

PhD dissertation

BY

KRISZTINA FEHÉR

SUPERVISOR: DR LÁSZLÓ SZILÁGYI

UNIVERSITY OF DEBRECEN
DEBRECEN, 2003

Ezen értekezést a Debreceni Egyetem TTK Kémiai Doktori Iskola Heterociklusos vegyületek programjának keretében készítettem a Debreceni Egyetem TTK doktori (Ph.D.) fokozatának elnyerése céljából.
Debrecen, 2002.06.20.

.....

Fehér Krisztina

Tanúsítom, hogy ***Fehér Krisztina*** doktorjelölt 1998 - 2003 között a fent megnevezett Doktori Iskola Heterociklusos vegyületek programjának keretében irányításommal végezte a munkáját. Az értekezésben foglalt eredményekhez a jelölt önálló alkotó tevékenységével meghatározóan hozzájárult. Az értekezés elfogadását javaslom.
Debrecen, 2003.06.20

.....

Dr Szilágyi László
egyetemi tanár
témavezető

ACKNOWLEDGEMENTS

I am grateful to Professor László Szilágyi for his guidance and continuous careful supervision of my work all along the years.

I am greatly indebted to Dr. Katalin E. Kövér and Dr. Gyula Batta for their invaluable help regarding both practical and theoretical aspects of NMR.

I am grateful to Professor Dr. Stefan Berger in University of Leipzig. In his laboratory I had unrestricted access to excellent equipment that has given me a chance to play around any idea I was curious about. I also enjoyed the critical, very thorough discussions with Professor Berger that stimulated me to dig down to the roots of problems.

I would like to thank to Professor Sándor Antus for giving me the opportunity to carry out these investigations in the Organic Chemistry Department of University Debrecen.

Several people were contributing to this work as co-authors of publications and I would like to acknowledge them all, in particular Dr Primož Pristovšek and Dr Anikó Borbás.

I would like to express my thanks to Sára Balla for her practical help in solving our day-by-day problems in the laboratory in Debrecen and for ensuring a warm, friendly atmosphere.

Thanks all the colleagues with whom I was working together in Debrecen and in Leipzig for sharing day-by day problems both in the laboratory and in life.

I gratefully acknowledge the Marie Curie Training Site Fellowship grant HPMT-2000-00183.

Krisztina Fehér

20.06.2003., Leipzig

TABLE OF CONTENTS

SYMBOLS AND ABBREVIATIONS

1D or 2D or 3D	one/two/three dimensional
RDC	residual dipolar coupling
RQC	residual quadrupolar coupling
CSA	chemical shift anisotropy
X	heteronucleus: ^{13}C or ^{15}N
$^{1}J_{X,1H}$	scalar coupling constant of X heteronucleus to directly bonded proton
$^{n}J_{X,1H}$	scalar coupling constant of X heteronucleus to long-range protons
$^{1}D_{X,1H}$	dipolar coupling constant of X heteronucleus to directly bonded proton
$^{n}D_{X,1H}$	dipolar coupling constant of X heteronucleus to long-range protons
LC	liquid crystal
COSY	COrrelated SpectroscopY
TOCSY	TOtal Correlated SpectroscopY
HSQC	Heteronuclear Single Quantum Spectroscopy
HMQC	Heteronuclear Multiple Quantum Correlated Spectroscopy
HMBC	Heteronuclear Multiple Bond Correlated Spectroscopy
NOE	Nuclear Overhauser Effect
NOESY	Nuclear Overhauser Effect Spectroscopy
ROE	Rotating frame nuclear Overhauser Effect
ROESY	Rotating frame nuclear Overhauser Effect Spectroscopy
PES	potential energy surface
E_{pot}	potential energy
GS	grid search
SA	simulated annealing
PGM	peptidoglycan monomer
Ad-PGM	adamant-1-yl-CH_2CO-PGM
BocTyr-PGM	tert-butyloxycarbonyl-L-tyrosyl-PGM
NAG, GlcNAc	N-acetyl-D-glucosamine
NAM, MurNAc	N-acetyl muramic acid
Lac	L-acetyl
Ala	alanine
Dap	diaminopimelic acid

iGln	iso-glutamine
Ad	adamantyl
Tyr	tyrosine
Boc	butyl-oxy-carbonyl
Bu^t	tercier-butyl
MDP	N-acetyl-muramyl-dipeptide
Glc	glucose
Man	mannose
Gal	galactose
NAcGlc	N-acetyl-glucose
GlyVal	glycine-valine
m	meso
CHAPSO	3-[(3-cholamidopropyil) dimethylammonio]-2-hidroxy-1-propanasesulfonate
DMPC	dimyristoyl-DL-α-phosphatidylcholine 1,2-ditetradecanoyl-rac-glycerol-3-phosphocholine
$\mathcal{H}$	Hamiltoinian

Vectors are noted with underlines, tensors are indicated in bold. Other symbols are explained in the text.

1. INTRODUCTION

Matter in the Universe is made up of the same 100 different types of atoms, still a vast variety of different materials are observed. The enormous diversity arises from the various ways the atoms are arranged. Knowing the 3D structure of a molecule is of paramount importance today in chemistry and biology since it determines the large variety of chemical, physical and biological properties of materials.

The concept of structure incorporates the chemical constitution, the stereochemistry and the conformation (3D structure) of molecules. The conformations of molecules are traditionally defined as those arrangements of atoms in space that can be interconverted purely by rotation about single bonds. This definition is usually relaxed in recognition of the fact that small distortions in bond angles and bond lengths often accompany conformational changes, and that rotations can occur about bonds in conjugated systems that have bond orders between one and two.

In crystalline materials positions of the heavy atoms in the molecule can be determined by X-ray crystallography. Problems arise with X-ray crystallography when crystals cannot be grown or a molecule has a dynamic nature. An alternative method for structure determination is nuclear magnetic resonance (NMR) that is steadily gathered importance in the last three decades or so. Applications of high-resolution solution state NMR extend to numerous areas. As an analytical tool the result of chemical synthesis is checked in a fast and efficient way, as far as connectivity, stereochemistry and purity is concerned. In structural studies NMR spectroscopy has made the largest impact on the determination of protein structures in solution, and a pioneer in NMR, Kurt Wüthrich was awarded the Nobel Prize in 2002 for his contributions to this area. The information provided by NMR structures is complementary to X-ray crystallography in many ways. It is performed on molecules in solution or most recently on powder crystals; therefore no single crystal is required. New structures can be obtained which are not available from X-ray studies or a meaningful comparison of the conformations in single crystals and in non-crystalline states can be obtained. It can provide additional information about dynamics on various time scales. The solution conditions for NMR studies (e.g., pH, temperature, ionic strength, buffers) can be varied over a wide range, which opens the possibility for comparative studies, or for investigations of intermolecular interactions with other solute molecules. The NMR studies are often combined or compared with the results of molecular modelling methods,

since NMR parameters provide structural constraints at the atomic level that can be conveniently utilized in computations, while the analysis of calculations give further insight into the characteristics of the chemical system.

This thesis describes conformational studies of two important classes of molecules, glycopeptides and carbohydrates to reveal conformational features of biological relevance. Furthermore, modifications to known NMR methods are proposed to improve measurements of structurally relevant NMR parameters.

2. METHODS

2.1 Structure elucidation by NMR

Any NMR study consists of three stages: experimental data collection, resonance assignment and determination of structurally relevant parameters that are in turn converted to constraints to derive information about the constitution, stereochemistry or 3D arrangement of atoms in the molecule. Further experiments for measuring relaxation and exchange rates give additional information on dynamic aspects.

The NMR parameters are connected to the molecular structure in various ways. When building up the structure of a molecule one typically first searches for evidence of scalar coupling between nuclei as this can be used to indicate the location of chemical bonds. After all bonding relationships within the molecule have been established, the gross structure of the molecule is defined. Spatial proximities between nuclei can be used to define stereochemical relationships within a molecule and to address questions of conformation. Angular relations are provided by scalar coupling constants and residual dipolar couplings. The theory of NMR parameters in terms of spin interactions and their connection to structure is briefly summarized in the followings.

NMR observables in different physical states of matter

Spectral parameters are manifestations of physical interactions of the nuclear spin (1). The various types of spin interactions can be conveniently summarized in terms of the internal nuclear spin Hamiltonian:

$$\mathcal{H}_{\text{int}} = \mathcal{H}_{\text{CS}} + \mathcal{H}_{\text{D}} + \mathcal{H}_{\text{J}} + \mathcal{H}_{\text{Q}}$$

where $\mathcal{H}_{\text{CS}}$ is the Hamiltonian for chemical shielding, $\mathcal{H}_{\text{D}}$ stands for the direct dipole-dipole coupling, $\mathcal{H}_{\text{J}}$ is for the indirect coupling and $\mathcal{H}_{\text{Q}}$ is the quadrupolar coupling Hamiltonian. The shielding is a magnetic interaction of the spin with the magnetic field generated by electrons. The direct or dipolar coupling is a magnetic interaction whereby pairs of nuclei in

close proximity to each other sense one another through space. The J coupling involves an indirect interaction of spins with each other by the mediation of the bonding electrons. The quadrupolar coupling is an interaction of the electric quadrupole moment of the nucleus with electric field gradients.

All these interactions are orientation dependent giving different interaction energies in different directions. The orientation dependence is described by second rank interaction tensors, hence the general form of the interaction Hamiltonian is the following:

$$\mathcal{H} = \text{constant } \underline{I}\ \mathbf{T}\ \underline{J}$$

where $\underline{I}$ is the spin angular momentum vector, **T** is the interaction tensor, $\underline{J}$ is the interacting vector that can be a magnetic or an electric field vector or the spin angular momentum vector of another spin. Table 2.1 summarize the tensors relating the two interacting vectors for all possible interactions.

Table 2.1 Summary of physical interactions of spins. $\underline{I}$ and $\underline{S}$ are theangular spin momentums of spins I and S, respectively, and B_0 stands for the external static magnetic field.

Interaction	**Interacting physical quantities**		**Tensor**
Shielding	$\underline{I}$	$\underline{B_0}$	$\boldsymbol{\sigma}$ shielding tensor
Indirect coupling	$\underline{I}$	$\underline{S}$	**J** indirect coupling tensor
Direct coupling	$\underline{I}$	$\underline{S}$	**D** dipolar coupling tensor
Quadrupolar coupling	$\underline{I}$	$\underline{I}$	**Q** quadrupolar coupling tensor

It is practical to distinguish between intra- and intermolecular relations. Except for J coupling, all interactions have intermolecular contributions for which the interacting vectors are located in different molecules. For liquids, intermolecular interactions can further be subdivided into short-range relations involving molecules within the same diffusion sphere, and long-range relations between molecules at a larger distance. Such classification of interactions is neccessary, because the internal, the short-range and the long-range intermolecular part of interactions are affected by motions in a different way.

Motions present in different physical states have an averaging effect on the interactions due their intrinsic orientation dependence. There are three relevant modes of molecular motion: namely the internal, rotational and translational. Internal motions involve vibrations, rotations of internal groups and chemical isomerizations. Rotations involve a

change in the orientation of molecules in space. Translational motions can be random (diffusion) or biased in a particular direction by an external pressure gradient (convection).

Internal motions and rotations affect primarily the intramolecular spin interactions, while translational motion may influence both intra- and intermolecular motions. The effect of motions on NMR observables in different physical states is summarized in Table 2.2.

Table 2.2 Summary of NMR observables in different physical states of matter

State of matter	**liquid**		**solid**	
Motion	isotropic	anisotropic	single crystal	powder
	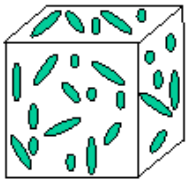	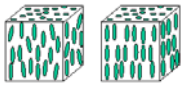	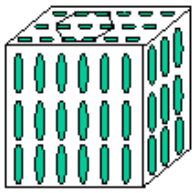	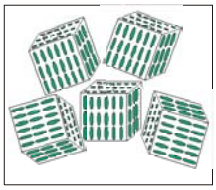
Internal	free	free	restricted	restricted
Rotational	free	restricted	restricted	restricted
Translational	free	free [a]	restricted	restricted
Orientation of molecules	all orietations	statistically oriented	single orientation	all orientations
NMR observables	finit, isotropic value or zero	partially averaged or residual value	values for a single orientation	values for all orientations

[a)] Recently there the translational diffusion were studied by NMR investigating restrictions of translational motion in anisotropic liquid crystals (2)

In liquids, the diffusional motion completely averages the long-range intermolecular interactions, it is, however, not able to average out the short-range intermolecular interactions. This effect, however, hardly can be detected.

In isotropic liquids, all intramolecular interactions are averaged by rotational motions since all orientations are equally likely. This average can be a finite value or zero. A finite residual value is observed for the shielding and the indirect coupling. As a result, resonances of nuclei in an isotropic liquid are shifted by the isotropic chemical shift (simply referred to as chemical shift) and split by the isotropic indirect coupling (the so called scalar coupling). The isotropic averages are, however, zero for both the dipolar and the quadrupolar interactions.

Thus, these terms does not affect directly the isotropic solution state NMR spectra, although they have effects via relaxation as line broadening or through NOE.

There is a considerable rotational motion in anisotropic liquids, but not all orientations are equally probable. The direction dependent rotational motion averages the spin interactions to anisotropic values that are different from their isotropic value. For the shielding it results in a residual chemical shift anisotropy that will add to the isotropic chemical shift. The J anisotropy is usually small and often ignored. The direct and the quadrupolar couplings average to a finite value yielding a residual direct or dipolar coupling (RDC) and a residual quadrupolar coupling (RQC). This latter one appears only in spectra of quadrupolar nuclei as line splitting by the finite value of the RQC.

In the solid state all type of motions are highly restricted, except for certain degrees of internal motions such as group rotations. Due to restricted rotation, intramolecular motions are not averaged. Only one orientation of the molecule is present in single crystals. For each interaction a single value characteristic for the single orientation appear in the spectra. In case of powders all orientations are present and for all interactions values characteristic for all orientation prevail. The most important difference between liquids and solids is, however, that diffusion is completely absent in solids and not able to affect either intra- or intermolecular interactions. This latter is quite significant since molecules are densely packed to each other in the solid phase giving rise to the manifestation of numerous mainly unresolved splittings. This yields very broad, featureless lines in the NMR spectra of solids.

The isotropic NMR parameters, the chemical shift and the scalar coupling constant, are easily measured due to "simplicity" of the spectra, but are difficult to convert to specific structural information as these parameters are sensitive to subtle changes in electron density sometimes in regions of the molecule relatively remote from the nucleus of interest. Instead, empirical rules are deduced for certain classes of compounds and these rules are applied for structural analysis. Measuring NMR spectra in isotropic liquids therefore causes a considerable loss of structural information, but gives the advantage of "easily" interpreted spectra.

In the NMR spectra of solids, broad lines are observed combining high information content with extreme complexity making spectral analysis difficult. This necessitates the use of special manipulations of experimental conditions in order to obtain spectra of comparable resolution as for liquids.

Recently anisotropic sample conditions have been used in order to reintroduce the information content present in orientation dependent spin interactions. A slight degree of

alignment maintained in the solution offers residual values of anisotropic interactions, whereas still retaining simplicity of the spectra. Parameters obtained in this manner are the residual chemical shift anisotropy, the residual dipolar coupling and the residual quadrupolar coupling.

Methods for inducing anisotropy

Alignment of molecules can be achieved by application of electric or magnetic fields, by dissolving the substance in dilute liquid crystals or by other methods.

Application of electric field alignment (3,4) in NMR has not, however, become widespread, due to the need for specially designed probes and the limitation to relatively non-conducting solutions.

Intrinsic partial alignment (5) is observed for molecules possessing sufficiently large magnetic susceptibility anisotropy such as nucleic acids (6), protein-nucleic acid complexes (7), metal binding paramagnetic proteins (8, 9), or proteins with strong diamagnetic susceptibility anisotropy (10, 11) in the presence of strong magnetic field. The degree of orientation depends the inherent anisotropy in magnetic susceptibility of the molecule under study. The magnitude of the resulting RDCs at the available field strengths is, however, small and therefore difficult to measure reliably.

Alignment can be achieved by dissolving the molecule in partially oriented media. Liquid crystalline media have long been used for orienting solutes in order to study their structure (12-14). The degree of solute orientation typically obtained in such a solvent is so large that interpretation of the NMR spectra of molecules with larger size is extremely difficult. Furthermore, the RDCs obtained exceed the chemical shift differences between resonances and as a result the spectra suffer from strong coupling effects.

A tunable degree of alignment was achieved by dissolving molecules in a dilute liquid crystalline phase (15). This reduces the RDCs to an extent that only the largest couplings are observable, thus retaining the resolution, simplicity and sensitivity of the NMR spectra in the isotropic phase. The resulting RDCs are of measurable magnitude (±2-20Hz) compared to values resulting from intrinsic alignment studies. In recent years RDCs have therefore been extensively applied (16-19) for structural studies of proteins, nucleic acids and carbohydrates in the liquid state and proved to improve the precision of structures.

Alignment with bicelles, which usually consist of a long-chain and a short-chain phospholipid, is the most common way to align molecules (20). The mixture in aqueous

solution was shown to form disc-like aggregates which align themselves in the presence of a magnetic field. The short-chain phospholipids are believed to be located primarily at the edges of the disc, whereas the long-chain phospholipids form a stable flat bilayer. These aggregates, commonly referred to as bicelles, adopt a nematic liquid crystalline phase at a given temperature and align themselves in the magnetic field with their director perpendicular to the magnetic field direction. Many different bicelle mixtures for different sample conditions (concentration, molar ration, temperature, ionic strength, pH) are known.

Other liquid crystal based methods use lamellar phases formed by quasi-ternary mixtures of CPCl (cetylpyridinium cloride) or CPBr (cetylpyridinium bromide)/hexanol/bile salt (21-22) or n-alkyl-poly-(ethylene-glycol)/n-alkyl-alcohol based systems (23). Another commonly utilized method to achieve alignment is the use of nematic phases of rod-shaped viruses (24-25), purple membrane fragments (26-27). Furthermore, other approaches have also been introduced such as cellulose crystallites (28-29) and poly-acryl amide gel (30) combined with the application of mechanic pressure.

Relationship between NMR parameters and molecular structure

Parameters conventionally measured in isotropic liquids

The most important NMR parameters in isotropic liquids are the chemical shift and the scalar spin-spin coupling constant. Since these parameters are treated in detail in many text books, here only practical issues relevant for the content of this thesis are discussed.

The chemical shift

The chemical shift is a change of the Larmor frequency of the nuclear spin due to its chemical environment. Phenomenologically the chemical shift arise because the field actually experienced by the nucleus, B_{eff}, slightly differs from the external field, B_0, that would be felt by an isolated, bare nucleus. This effect is characterized by the shielding constant (σ).

$$B_{eff} = B_0 (1 - \sigma)$$

It is useful to divide the nuclear shielding into parts:

$$\sigma^{local} = \sigma^{dia} + \sigma^{para} + \sigma^{IS} + \sigma^{ring} + \sigma^{inter}$$

where σ^{dia} represents the contribution from local diamagnetic electron currents in the vicinity of nucleus I, σ^{para} reflects anisotropic, non-spherical local electron circulations, the σ^{IS} term represents the contribution from the magnetic anisotropy of neighbouring groups (31-32), σ^{ring} represents the effect of aromatic ring currents and σ^{inter} reflects the effect of intermolecular interactions (hydrogen bonding, solvent effects) upon shielding.

For protns, the most important contributions to the chemical shift are the local diamagnetic term dependent on the inductive and mesomeric effects, the shielding term arising from shielding anisotropy of neighbouring bonds and the aromatic ring current effects.

The temperature dependence of the NH/OH proton chemical shifts can be considered as a diagnostic tool for structure determination since it indicates the solvent accessibilty of the proton. A small temperature dependence (< -3 ppb/K) in a non-competitive solvent indicates small accessibility to solvent molecules of the proton in question which can be caused by participation in hydrogen-bonding of the particular proton (33).

The most important shielding contributions in carbon NMR arise from the hybridization state of the observed nucleus effecting local electron distribution, inductive effects of substituents, van der Waals and steric effects between closely spaced nuclei, electric fields originating from molecular dipoles or point charges, hyperconjugation, mesomeric interactions in π-electron systems (delocalization effects), diamagnetic shielding due to heavy substituents (‘heavy-atom’ effect), neighbour anisotropy effects and isotope effects (32).

Scalar spin-spin couplings

Scalar spin-spin coupling constants are widely applied to chemical structure determination due to a large number of groundwork that related these parameters to stereochemical and conformational features. (32, 34-37). The interpretation of the magnitudes of coupling constants in an atomic level is difficult, therefore only selected coupling constants relevant to biomolecular structure will be briefly summarized bellow.

Studies on carbohydrate derivatives have shown that the anomeric one-bond carbon-proton coupling (32, 37) is sensitive to the configuration at C-1 (38). The $^{1}J_{C1/H1}$ values in the

α and β anomers are ca. 170 Hz and ca. 160 Hz respectively. This correlation is fairly general, and can therefore be used in cases, where the determination of $^3J_{HH}$ is difficult.

Probably the most useful spin-spin couplings are those involving nuclei separated by three bonds. Experimentally and theoretically, these coupling constants are found to vary with the torsion angle, ϑ according to the Karplus relation (plotted in Figure 2.1)(32, 39):

$$^3J_{HH} = A + B\cos\vartheta + C\cos^2\vartheta$$

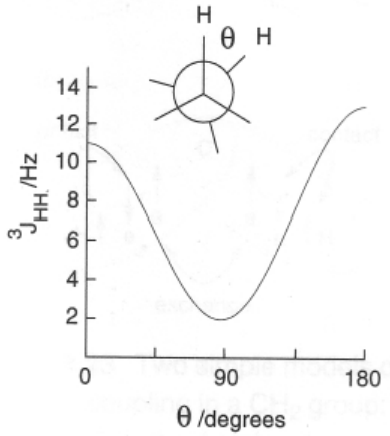

Figure 2.1 Typical dependence of a three-bond coupling constant on the torsional angle ϑ

The utility of three-bond couplings lies principally in conformational analysis. Determination of the interglycosidic bond geometry in oligosaccharides, assignment of the diastereotopic C-6 methylene protons in glycosyl residues are based on vicinal couplings between protons and/or protons and heteronuclei (34-37). The Karplus relation finds valuable applications in studies of protein structures. Couplings between the amide and α protons in a polypeptide chain provide information on the conformation of the protein backbone (35, 36, 40).

The interpretation of three-bond couplings in conformationally mobile molecules is somewhat different. The three staggered conformations, or rotamers, interconvert rapidly so that the observed ^{3}J value is an average, weigthed according to the populations of the three energy minima. Thus:

$$^3J = P_{g-}J_g + P_{g+}J_g + P_t J_t$$

where J_t and J_g are the trans (ϑ = 180°) and gauche (ϑ = ±60°) coupling constants, and P_{g+} + P_{g-} + P_t = 1. The relative populations of the three rotamers can therefore be determined, provided J_t and J_g can be obtained from rigid model compounds.

The Nuclear Overhauser Effect

The NOE is an aspect of nuclear relaxation; it is defined as a change in intensity of a resonance when the transitions belonging to another one are perturbed in some way. The mechanisms, which drive relaxation, are related to molecular motion. (41) The NOE is as follows:

$$\eta_I(s) = (I - I_0) / I_0 \times 100$$

where I_0 is the intensity of a resonance in thermal equilibrium and I the intensity while saturating resonances of S.

According to the Solomon equation the steady-state NOE is proportional to the ratio of the cross-relaxational (σ_{IS}) and the longitudinal relaxational rate (ρ_{IS}), and to the proportion of gyromagnetic ratios (γ) between the pertubed and the observed nucleus:

$$\eta_I(s) = \frac{\gamma_S \, \sigma_{IS}}{\gamma_S \, \rho_{IS}}$$

Since the longitudinal relaxational rate are fairly similar for protons in biomolecules and the cross correlational rate is strongly dependent on the distance between the crossrelaxing protons and on the reorientational time for the interproton vectors, hence the NOE is related to the distance between the two spins. One- and other multidimensional NOE experiments (42, 43) are therefore powerful methods to furnish structural data and to investigate the conformational preferences of larger molecules in solution. The various inter- and intraresidual NOEs are a rich source of information for establishing sequence specific assignments and solution structures for peptides and proteins. (44)

Parameters measured in anisotropic liquids

Structural information present in orientation dependent spin interactions may be obtained in anisotropic liquids. NMR parameters obtained in this manner are the residual chemical shift anisotropy, the residual dipolar coupling and the residual quadrupolar coupling.

The partially averaged values of NMR parameters (N stands for a general NMR parameter) are composed of an isotropic part and an anisotropic part:

$$N = N^{iso} + N^{aniso}$$

The isotropic value is a constant as it equals the trace of the interaction tensor.

$$N^{iso} = 1/3\ (N_{xx} + N_{yy} + N_{zz})$$

For the shielding and the indirect coupling this is a finite value. The isotropic averages of both the dipolar and the quadrupolar interactions are zero. In the followings only the residual dipolar coupling will be discussed.

The residual dipolar coupling

The RDC (45-47) between two nuclei depends on the intermolecular distance, r_{ij}, and on Θ, the angle between the internuclear vector and the static field:

$$D_{i,j} = (\mu_0 \hbar \gamma_i \gamma_j / 4\pi \langle r^3_{ij} \rangle) \langle 3\cos^2\Theta_{ij} - 1 \rangle /2$$

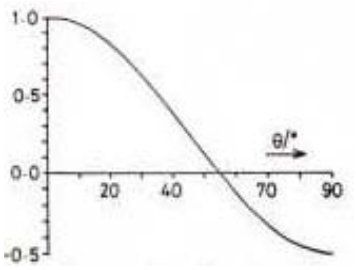

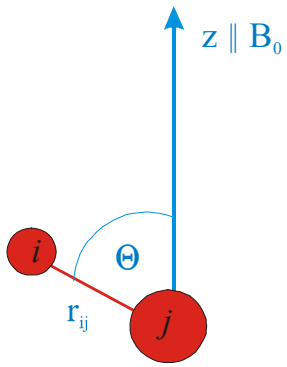

Figure 2.2 Dependence of dipolar interaction on molecular parameters and plot of the $3\cos^2\Theta_{ij}-1$ function

where γ is the gyromagnetic ratio of the spins. The angle brackets indicate time averaging over instantaneous values of angles and distances on time scales short compared to the reciprocal of the splitting. The sign of the RDC for internuclear vector aligned along the field ($\theta_{ij} = 0^o$) is opposite compared to vectors with perpendicular orientation to the field ($\theta_{ij} = 90^o$). the RDC values go through zero periodically at multiples of the magic angle (54.74^o, 125.26^o, etc).

Interpretation of tensorial interactions is a complicated issue, because the experimentally obtained information is a convolution of structural and dynamic contributions. In solution state, the time dependence arises from several sources. These include fluctuations in the internuclear distance, changes in the orientation of the internuclear vector with respect to the magnetic field due to overall molecular reorientation as well as internal motions. Deconvolution of the various contributions is required

It can assumed that the distance vibrations occur on very different time scales and thus their averages can be computed independently (48). Therefore $< r^3_{ij} >$ can be approximated as simply $r^{3\,eff}_{ij}$ and omitting time averages. To separate effects of the overall molecular reorientation and the internal motions, an intermediate coordinate system is introduced fixed onto a rigid fragment of the molecule. Tumbling and alignment of this molecule fixed coordinate frame (with axes denoted as Z, X, Y) with respect to the external magnetic field (laboratory frame x,y,z, with z axis aligned along B_0) reflects only the global reorientation, but is independent of the internal motions.

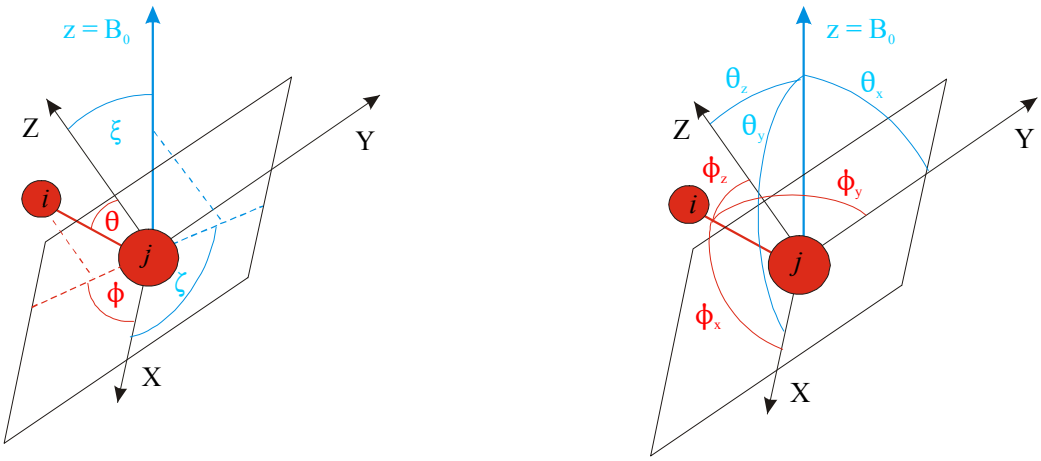

Figure 2.3 Introduction of laboratory frame as a polar coordinate system (left side) and as a Cartesian coordinate system (right side). Angles characterizing structural information for a rigid subunit are in red, whereas the global reorientation manifest in the time dependence of angles are in blue. (Notations of the angles follow the literature (45, 10))

Thus, by the introduction of the molecular frame the internal motions are separated from the global reorientation. The former is characterized by the angles between the internuclear vector and the molecule fixed coordinates system. In polar coordinates, these are the θ and ϕ, in Cartesian coordinates the ϕ_z, ϕ_x and ϕ_y. In a general case these are time dependent, whereas for a rigid subunit assuming no internal motions, they may be considered being independent of time. Likewise, the overall reorientation is characterized by the time

dependent polar (ξ and ζ) or Cartesian angles (θ_z, θ_x, θ_y) between the molecular frame and the laboratory frame.

The Saupe orientation tensor (49) or alignment tensor describes how the molecule coordinate frame (Z, X, Y) is oriented in the laboratory frame (z, x, y). It was originally formulated using Cartesian coordinates as follows:

$$\mathbf{S} = \begin{matrix} S_{Xx} & S_{Xy} & S_{Xz} \\ S_{Yx} & S_{Yy} & S_{Yz} \\ S_{Zx} & S_{Zy} & S_{Zz} \end{matrix}$$

$$S_{Pq} = \langle\, 3 \cos\theta_p \cos\theta_q - \delta_{pq} \,\rangle / 2$$

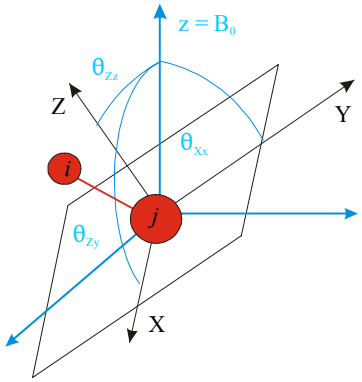

where P, q are Cartesian coordinate axes of the molecular and the laboratory frame, respectively, θ_P, θ_q are angles between the molecular frame axis and the laboratory axis, δ_{pq} is the Krönecker delta, $p = q \Rightarrow \delta_{pq} = 1$, $p \neq q \Rightarrow \delta_{pq} = 0$ and angular brackets denote time average. By using the order tensor the RDC is now:

$$D_{i,j} = (\mu_0 \hbar \gamma_i \gamma_j \ / 4\pi \ r^{3\,eff}_{ij}) \ \Sigma \ S_{Pq} \cos(\phi_P) \cos(\phi_Q)$$

The internal geometry is represented by the direction cosines describing the orientation of the internuclear vector within the molecular frame, whereas the global reorientation is characterized bythe Saupe order tensor. The tensor is symmetric and traceless; therefore 5 independent elements have to be determined.

$$S_{xy} = S_{yx} \qquad S_{xz} = S_{zx} \qquad S_{yz} = S_{zy} \qquad\qquad S_{xx} + S_{yy} + S_{zz} = 0$$

Measurements of five RDC 's corresponding to five independent dipolar interactions combined with the knowledge of the structure of a rigid subunit assuming no internal dynamics, allow the determination of the Saupe's order tensor.

Diagonalization of the order tensor that transforms the order tensor into a coordinate frame where it is diagonal. This coordinate system is referred to as the principal axis frame

where the tensor is expressed only in terms of its principle values S'_{xx}, S'_{yy}, S'_{zz} where $|S'_{zz}| > |S'_{yy}| > |S'_{xx}|$. The transformation relates the orientation of the principal alignment axes to the initial molecular frame and is represented in terms of three Euler angles. The principle values can be recast into a principal order parameter, S_{zz}, and an asymmetry parameter, η which describes the deviation from axially symmetric ordering:

$$\eta = \frac{S_{xx} - S_{yy}}{S_{zz}}$$

μ runs from 0 for an axially symmetric tensor to 1 for the tensor with the highest possible asymmetry. The RDC can be expressed in a polar coordinate frame using principal components of the order matrix as follows:

$$RDC = -D^{stat} \; S'_{zz} \left(\left(3/2 \cos^2\theta - 1/2 \right) + \left(\mu/2 \sin^2\theta \cos 2\phi \right) \right)$$

$$D^{stat} = \mu_0 \hbar \gamma_i \gamma_j \; / \; 4\pi \; r^{3\,eff}_{ij}$$

where θ and ϕ are polar angles (depicted in Figure 2.3, left side) defining the orientation of the internuclear vector with respect to the principle axis system of the alignment tensor, S_{zz} is the principal order parameter, μ is the asymmetry parameter, D^{stat} is the static dipolar coupling subsuming various physical constants.

NMR experimental techniques

The unique feature of NMR spectroscopy is its ability to define relationships between specific nuclei within a molecule or even between molecules. This is generally obtained by correlating one nucleus with another by exploiting the following phenomena (50):

- through-bond interactions: J couplings, via bonding electrons.
- through-space interactions: the nuclear Overhauser effect mediated through manifestation of dipole-dipole coupling in spin relaxation
- chemical exchange: the physical exchange of spins with two different locations.

The homonuclear correlation experiment, COSY, (51, 52) identifies those nuclei that share a J-coupling, which, for protons, operate over two, three and, less frequently, four bonds. This information can therefore be used to indicate the presence of a bonding pathway. The correlation of nuclei within the same coupled network or chain of spins established with

the aid of the TOCSY experiment (53-56). Crosspeak overlap in homonuclear correlation spectra may be resolved by exploiting the higher chemical shift distribution of the heteronuclei in experiments such as HMQC/HSQC-COSY/TOCSY (57-59). One-bond heteronuclear correlation methods (HMQC or HSQC) (60-63) identify the heteroatoms to which the protons are directly attached and can, for example, provide carbon assignments from previously established proton assignments. Long-range heteronuclear correlations over two- or three-bonds (HMBC) (64-66) provide a wealth of information on the skeleton of the molecule and can be used to infer the location of carbon-carbon or carbon-heteroatom bonds. These correlations can be particularly valuable when proton-proton correlations are absent. As an alternative to the collection of a full 2D dataset, the 1D analogue (67-71) can prove advantageous in some circumstances. The 1D equivalents of 2D sequences are in general faster and can be recorded with higher digital resolution. Measurements based on the NOE (41, 72-75) are used to define the 3D structure and stereochemistry of a molecule since this effect maps through-space proximity between nuclei. In the case of medium sized molecules the NOE become negligible. In such cases one can take advantage of the Rotating-frame Overhauser Enhancement (ROE). (76-79, 41)

Measurement of coupling constants

There is a wide array of experimental methods (81) for the accurate determination of coupling constants. Methods can be classified into two general categories on the basis of the measured NMR parameter: frequency resolved methods and intensity-based methods. In frequency resolved methods (82) the splitting of the signal caused the coupling between nuclei is detected and the resulting characteristic lineshape is analysed to determine the coupling constant. In the simplest case (weak coupling) the coupling can be extracted as a frequency difference between peak maxima. Intensity-based approaches (83-86) utilize the fact that the efficiency of magnetization transfer is dependent on the magnitude of the coupling, therefore its value is encoded in, and can therefore be determined, from signal intensity.

The frequency-resolved versus intensity-based methods are somewhat complementary as they are often subject to different sources of systematic error. They also differ in applicability to different ranges of molecular size as the frequency resolved methods suffer from a degradation of precision as the linewidths increase. This fact makes them useful to

small to medium sized molecules while for macromolecules the attainable precision is limited by the linewidths.

The issue of how much precision can be obtained from frequency domain spectra and how the data can be most efficiently acquired is actually a complex problem (87). Possible sources of multiplet splitting distorsions are the followings: the effects of transverse relaxation (88) when linewidths are comparable to the magnitude of splittings, the effects of cross-correlated relaxation manifested as differential line-broadening and the second order dynamic frequency shift. (89)

The BIRD sequence

The BIRD sequences (90, 91) (BIlinear Rotational Decoupling) act as group selective pulses being able to distinguish between directly and remotely bonded protons on the basis of the magnitude of their heteronuclear coupling constant. There are four basic BIRD sequences differing only in the relative phases of individual pulses (Figure 2.4).

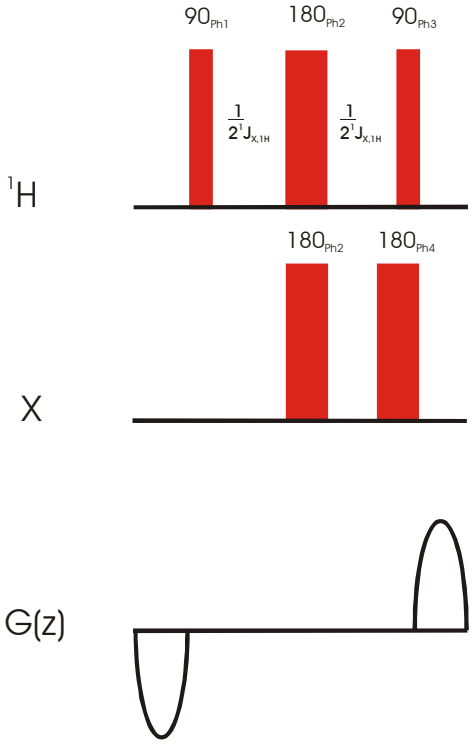

	ph1	ph2	ph3	ph4
G-BIRD(d)	x	x	x	x
	x	x	x	y
	x	y	-x	x
	x	y	-x	y
G-BIRD(r)	x	x	-x	x
	x	x	-x	y
	x	y	x	x
	x	y	x	y

Figure 2.4 The BIRD sequence

Two of them with relative phases of the ^{1}H pulses (x, x, x) and (x, y, -x) invert spins coupled via direct, large one-bond couplings and have no effect on multiple bonded spins coupled via long-range couplings. These sequences are denoted as BIRD$^{(d)}$. The BIRD$^{(r)}$ pulses with

relative phases on ^{1}H pulses of (x, x, -x) and (x, y, x) have the opposite effect. The original BIRD sequences also invert the magnetization of the heteronucleus thus preventing the heteronuclear chemical shift evolution. This effect can be removed by the addition of a 180^o pulse on the heteronucleus simultaneously with the first or the last 90^o ^{1}H pulse. The BIRD$^{(r)}$ sequence is surrounded by two gradients of opposite signs in order to purge out the fraction of magnetization that does not experience perfect rotation by the sequence.

The DANTE sequence

Selective and bandselective pulses affect only a selected region of the spectral window. There is two approach to produce such a selective pulse: soft pulses, which are of longer duration on reduced radiofrequency power and preferably have a characteristic shape, and the DANTE sequence (Delays Alternating with Nutation for Tailored Excitation) (92).

The DANTE sequence employs a series (N) of short hard pulses of tip angle α, where $\alpha << 90^o$, interspersed with fixed delays (τ) for free precession:

$$[\tau/2 - \alpha - \tau/2]_N$$

The total length of the selective pulse is the product of N, τ, and t_p, where t_p is the duration of each hard pulse and the net on-resonance tip angle is the sum of the individual pulses.

Limitations of the DANTE approach arise when very small τ durations are required which pulse transmitters are unable to deliver. Another complication is the presence of strong sidebands at multiples of the hard pulse frequency, 1/ τ. If only a single spectral window is required to be affected by the pulse, then the hard pulse repetition frequency must be adjusted by varying τ to ensure that the sidebands do not coincide with other resonances.

The DANTE sequence is still a method of choice on older instruments or on newer ones without waveform generations, but its simplicity in terms of calibration (only one parameter, τ to be adjusted) is still a major advantage.

Excitation sculpting

Recent methods have combined selective pulses with pulse field gradients to produce experimentally robust sequences with a number of desirable properties. They are based on pulse field gradient spin-echo sequences (PFGSE):

G - S - G

where G is the gradient and S represents any selective 180^{o} pulse scheme. The bracketing gradients are identical and act in opposition for those spins, which experience the selective inversion pulse and thus, the second gradient refocus the dephasing effect of the first one. Spins outside the selectively affected bandwidth do not experience the pulse and are influenced by the cumulative effects of the gradients and become fully dephased in the transverse plane and thus become unobservable. The gradient echo therefore achieves clean resonance selection according to the profile of pulse S. The phase profile of the selected resonances is also dictated by the phase properties of the selective pulse S, which may not be ideal. Repeating the gradient echo (with a different gradient strength to avoid refocusing of the previously dephased unwanted magnetisation) cancels any remaining phase errors and the resulting pure-phase excitation profile depends on the inversion properties of the selective pulse. The double pulse field gradient spin-echo sequence (DPFGSE) (93-94) is therefore the following:

$(G_1 - S - G_1)\ (G_2 - S - G_2)$

Experimentally it is an enormous benefit since it makes implementation of the selective sequence straightforward and gradients ensure excellent suppression of unwanted resonances.

2. 2 Methods for structure calculation

Computational chemistry or molecular modelling is an increasingly useful tool in modern chemistry. Many chemical and physical properties can be calculated with theoretical methods, most of them, however, require knowledge about the 3D structure of the molecular system to be studied.

Molecular modelling studies involve three stages. First, the level of theory is selected by which the internal potential energy (E_{pot}) is calculated. The alternatives are the followings: the quantum theory at different level of simplification or the molecular mechanics. These models enable the energy of any arrangement of atoms and molecules in a system to be calculated, and to determine how the energy of the system varies as the positions of the atoms and molecules change. After the selection of the appropriate model and the desired property, the calculation is carried out, such as energy minimization, a molecular dynamics, a Monte Carlo simulation, a conformational search, etc. Finally, the calculation must be analysed to compute molecular properties.

Potential energy of the molecular system

The concept of potential energy surfaces (PES) is central to computational chemistry (95). The internal energy consists of the kinetic energy (E_{pot}) resulting from motion and the potential energy (E_{pot}) resulting from position of the atoms or configuration of molecules within a force field. In an isolated system the total internal energy of the system is constant as stated by the principle of conservation of energy. The PES describes the energy of a molecule in terms of its structure, as a function of the nuclear coordinates. The structure, energetics, properties, reactivity, spectra and dynamics of molecules can in principle be understood in terms of the PES. For all except the simplest system, the E_{pot} is a complicated, multidimensional function of the coordinates. Therefore a wide array of methods has been developed for exploring the PESs. Calculations examine thePES using single point calculations, optimisations, and molecular dynamic simulations and other simulation procedures.

Particularly interesting points are the stationary points on the PES (Figure 2.5), where the first derivative of the E_{pot} is zero with respect to the internal or Cartesian coordinates. At a

stationary point the forces on all the atoms are zero. Minimum points are correspond to stable, equilibrium geometries. There may be a very large number of minima on the PES. The minimum with the very lowest energy is known as the global energy minimum. Thermodynamics and kinetics of reactions can be calculated from the energy of the minima for reactants, products and transition states. The shape of the valley around a minimum as given by the second derivative or Hessian, determines the vibrational spectrum. Each electronic state of a molecule has a separate potential energy surface, and the separation between these surfaces yields the electronic spectrum. Properties of molecules such as dipole moment, polarizability, NMR shielding, etc. depend on the response of the energy to the applied electric and magnetic fields.

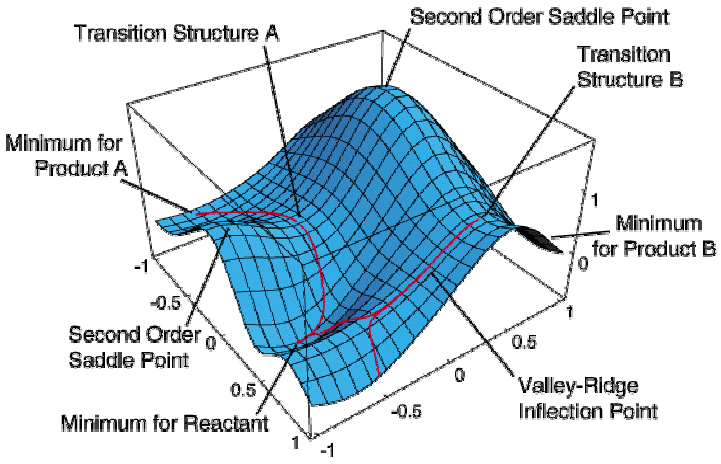

Figure 2.5 The potential energy surface with important points indicated

Mathematical models for the calculation of the E_{pot} involve quantum theories including quantum mechanics (ab-initio, semiempirical models) and density functional theory and classical approaches such as molecular mechanics (force-field based) methods.

Quantum theories versus molecular mechanics

There are a number of quantum theories at different level of simplification for treating molecular systems such as the molecular orbital theory (ab-initio), the semi-empirical methods, the Hückel theory and the valence bond theory. An other alternative is the density functional theory.

Quantum mechanics deals with the electrons in a system, so a large number of particles must be considered and calculations are time-consuming. Force field methods ignore

the electronic motions and calculate the energy of a system as a function of the nuclear positions only.

Molecular mechanics (96) assumes that the energy of a molecular system comprises additive and non-interacting terms. These are the sum of all diatomic bond stretches, the sum of all tri-atomic bond angle deformations, the sum of all tetra-atomic bond torsions, the sum of all non-bonded van der Waals repulsions and the sum of all electrostatic attractions of individual bond dipoles. Each of these functions are mathematically extremely simple and computationally fast to evaluate, provided that simple parameters such as stretching force constants, bond dipole moments, etc. are known. The total potential energy is the sum over all these terms.

$$E_{pot} = E_{bond} + E_{valence\ angle} + E_{torsion\ angle} + E_{electrostatic} + E_{van\ der\ Waals}$$

The goal of a forcefield is to describe entire classes of molecules with reasonable accuracy. In a sense, the forcefield extrapolates from the empirical data of a small set of models, used to parametrize the forcefield, to a larger set of related models.

Molecular mechanics of course cannot provide properties that depend upon the electronic distribution in a molecule. Applications beyond the capability of most forcefield methods include for instance: electronic transitions (photon absorption), electron transport phenomena, proton transfer (acid/base reactions), and stereoelectronic effects.

Molecular mechanics for carbohydrates

The force-field specifically developed for carbohydrates is the HSEA (Hard Sphere Exo-Anomeric) force field (97-98). The approximation of the HSEA methods is to treat each monosaccharides building up an oligosaccharide as rigid geometry units and considering only variations in the interglycosidic torsion angles. The glycosidic linkage is influenced by electronic and steric factors: stereoelectronic effects such as the exo-anomeric effect, non-bonding attractions-repulsions between atoms and interresidual H bonds.

The exo-anomeric effect

The exo-anomeric effect (99, 100) relates to the preference of the aglycone atom for the synclinal position around the glycosidic C-O bond. The exo-anomeric effect causes the aglyconic atom to assume an orientation in which Φ is $\sim+60^{o}$ in β-glycosides and $\sim-60^{o}$ (or

300°) in α-glycosides. Shortening of the C1-O1 bond is also the geometrical consequence of the exo-anomeric effect.

In terms of molecular orbital theory the exo-anomeric effect can be interpreted as a preference for conformations that allow an overlap between a lone pair on the glycosidic oxygen and the antibonding orbital of the C1 – O(ring) as depicted in Figure 2.6. This is permitted by the synclinal arrangements.

Figure 2.6 Interpretation of exo-anomeric effect: favoured conformations allow an overlap between a lone pair on the glycosidic oxygen and the antibonding orbital of the C-1 – O(ring).

The conformation is, however, influenced not only by electronic, but also steric effects. In β-glycosides with equatorial aglycone the -synclinal (300° or -60°) arrangement suffers from repulsion between the aglycone and the axial hydrogen atom on C2. The antiperiplanar arrangement, which is not favoured by the exo-anomeric effect, is also disfavoured by a steric repulsion between the aglycone and equatorial hydroxyl group at position 2. The exo-anomeric effect is usually included into the force-field in the form of a torsional potential.

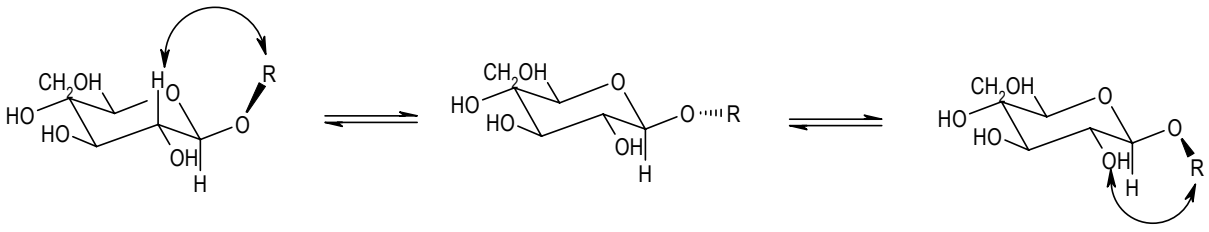

+synclinal (+60°) **-synclinal (300° or -60°)** **antiperiplanar (180°)**

Figure 2.7 Three possible staggered arrangement of the aglycone for β-glycosides with indication of steric repulsions

Non-bonding interactions

Non-bonding attractions and repulsions arising between dipoles are accounted for by the van der Waals term, whereas interactions between partial charges are taken into consideration by the electrostatic or Coulombic term of the energy expression.

H bonds

H bonds are accounted for either by explicitly including a separate H bonding term into the energy expression of the force field or arise from the van der Waals interaction between the donor and acceptor groups.

Hydrogen bonds (101) are generally identified by geometric and energetic criteria. Energetically, hydrogen bonds are favoured, if in the equilibrium between bonded and non-bonded systems, the hydrogen bonded system is lower in energy. The geometric criteria involve a characteristic distance and an angle. If the distance between the hydrogen and the acceptor is significantly smaller than the sum of the van der Waals radii for the two atoms, then a hydrogen bond is present. For the hydrogen - oxygen pair, the van der Waals radius of O is ca. 1.4Å and that of H is about 1.2Å yielding a sum of 2.6Å. As for the angle criterion it must be considered that the hydrogen share a nonbonding orbital with the acceptor in addition to its bonding orbital. So the angle formed by the three atoms must make either a tetrahedral or trigonal planar angle. But in reality this ideal geometry cannot be expected in every case.

Solvent effects

Carbohydrates in polar solvents usually form H bonds only to neighbouring molecules, mainly solvent molecules, while simulation in vacuum is dominated by conformations stabilized by intramolecular H bonds (102) where the coulombic and H bonding terms are overestimated. Stable conformers will be predicted arising from H bond stabilization where none exists because of competition of solvent molecules for H bonding partners.

Several different approaches have been proposed to treat solvation effects (103). In the simplest approach the dielectric constant is set distance dependent which will simulate the damping effect of the solvent. An alternative strategy is to set the dielectric constant to a high value, which will achieve a similar effect except that electrostatic interactions are not scaled in favour of small internuclear distances. An alternative approach is to treat the solvent as a dielectric continuum by adding a solvent specific energy term to the energy expression of the force field (102). The best approach is the inclusion of explicit solvent molecules into the calculation, this, however,considerably increases the computation time.

Conformational analysis

The conformational analysis locates conformations that are at minimum points on the energy surface, that is, those corresponding to the equilibrium geometries. The relative

populations of a molecule's conformations can be calculated using statistical mechanics via the Boltzmann distribution, though it is important to remember that the statistical weights involve contributions from all the degrees of freedom, including the vibrations. Nevertheless one has to keep in mind that even though the global minimum energy conformation has the lowest energy, it may not be the most highly populated because of the contribution of the vibrational energy levels to the statistical weight of each structure. Moreover, the global minimum energy conformation may not be the active (i.e. functional) structure.

Conformational search methods can be conveniently divided into the following categories: systematic - deterministic search algorithms, model building methods, random - stochastic - probabilistic approaches. Here only the systematic search and a random method, the simulated annealing will be briefly summarized.

Systematic methods for exploring conformational space (deterministic search)

A systematic search explores the conformational space by making regular and predictable changes to the conformation as illustrated in Figure 2.8. The simplest type of systematic search (often called grid search*)* is as follows. First, all rotatable bonds in the molecule are identified. The bond lengths and angles remain fixed throughout the calculation. Each of these bonds is then systematically rotated through 360° using a fixed increment. Every conformation so generated is subjected to energy minimization to derive the associated minimum energy conformation. The search stops when all possible combinations of torsion angles have been generated and minimized.

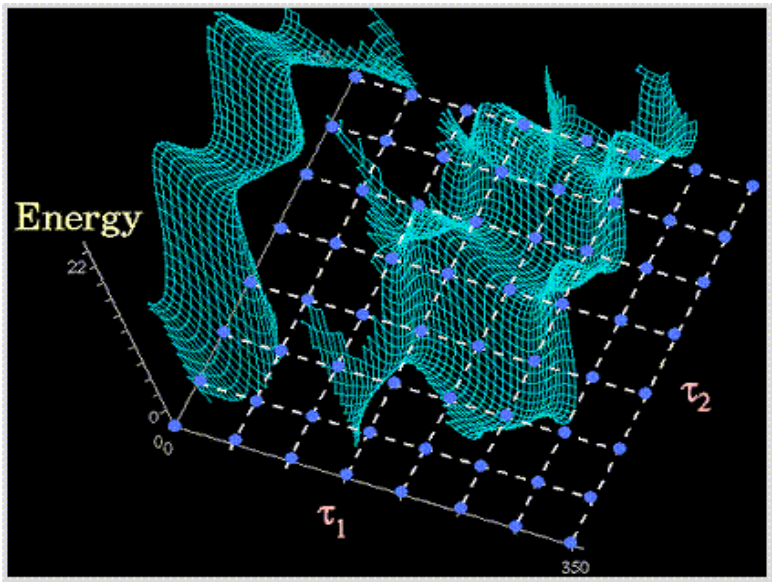

Figure 2.8 Grid points sampling the PES

A major drawback of the grid search is that the number of structures to be generated and minimized increases steeply with the number of rotatable bonds, a phenomenon known as a combinatorial explosion. Any systematic search ultimately requires a balance to be made between the resolution of the grid and the available computer resources.

Stochastic or random search

The random search explores the energy surface of the molecule in a way that it is not possible to predict the order in which conformations will be generated. A random search can move from one region of the energy surface to a completely unconnected region in a single step. The advantage of this approach is that one can obtain an approximate solution efficiently, because only a small portion of the conformational space is explored. The disadvantage is that there is no guarantee that the result is the global minimum. In a systematic search there is a defined endpoint to the procedure, which is reached when all possible combinations of bond rotations have been considered. In a random search, there is no natural endpoint; one can never be absolutely sure that all of the minimum energy conformations have been found. The usual strategy is to generate conformations until no new structures can be obtained. This usually requires each structure to be generated many times and so the random methods inevitably explore each region of the conformational space a large number of times.

Simulated annealing

Simulated annealing is an application of molecular dynamics designed for conformational searching. In this process, structures are heated to temperatures at which increased atomic motion will occur in an attempt to drive molecules out of their local energy wells. At high temperatures, the system is able to occupy high-energy regions of conformational space and thus to pass over high-energy barriers. Structures are then cooled slowly to trap them in the new local energy minimum. As the temperature falls, the lower energy states become more probable in accordance with the Boltzmann distribution. At absolute zero the system should occupy the lowest energy state (i.e. the global minimum energy conformation). Although simulated annealing cannot guarantee to find the global minimum, but if the same answer is obtained from several different runs then there is a high probability that it

corresponds to the true global minimum. Several simulated annealing runs may enable a series of low energy conformations of a molecule to be obtained.

The simulated annealing has the property that it allows uphill directions. This property allows the search to escape from local wells by moving uphill, therefore it has the ability to avoid being trapped at a local minima.

Analysis of simulations

Calculations will generate a large amount of conformers which must be analysed. Clustering of conformations will select conformational families, the members of which are similar to each other regarding selected molecular parameters. Conformational energy differences are typically very small (in the order of 1-5 kcal/mol) and even small errors might lead to incorrect assignment of global minimum conformer.

CONFORMATIONAL STUDIES

3. CONFORMATIONAL INVESTIGATIONS OF MODIFIED CELL WALL PEPTIDES

NMR and molecular modelling investigations were carried out on novel lipophilic derivatives of the monomeric peptidoglycan of the bacterial cell wall. In order to understand the importance of such studies the role of the bacterial cell wall and its biological significance is briefly described. Then follows a survey of literature on conformational investigations of natural or synthetic peptidoglycan fragments or derivatives. Finally conclusions of the conformational investigations on the new synthetic derivatives are discussed.

3.1 The unique cellular structure in bacteria: the cell wall

Bacteria are single-cell, microscopic organisms that lack a nuclear membrane around their genetic material, therefore are called prokaryotic. A general scheme of the most common cellular organelles in bacteria is depicted in Figure 3.1. The most important internal structures are the cytoplasm, the nucleotide region containing the genetic material and the ribosomes which are the protein synthesizing factories of the cell. The inner material is separated from the rest of the world by the cellular membrane and the cell wall

.

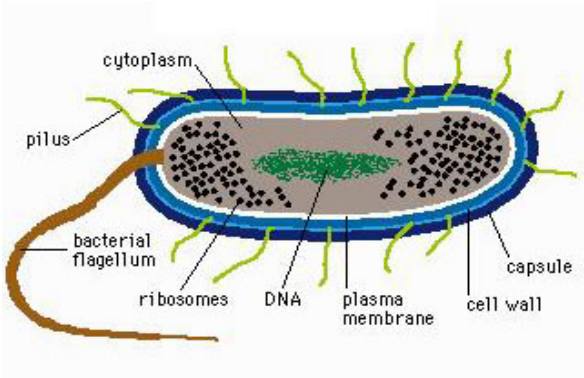

Figure 3.1 Universal structures in bacteria

Eukaryotic and prokaryotic cells by definition are distinguished on the basis of the presence or absence of the nuclear membrane around their genetic material. Another important difference between them is the presence or composition of the cell wall. Eubacteria and Archaebacteria are two major classes of bacteria, both are prokaryotic, but peptidoglycan

containing cell wall can only be found in the cells of Eubacteria. The Archaebacteria also have a cell wall, but it is composed of proteins, a complex carbohydrate, or other unique molecules but not peptidoglycan. Eukaryotic cells of plant cells, algae, and fungi also have cell walls which are usually composed of cellulose or chitin but never contain peptidoglycan. Animal cells and protozoans, which are also eukaryotic, lack cell walls. The fact that the cell wall of Eubacteria is composed of peptidoglycans not found in other species, can be exploited in fighting against bacterial infections.

The membrane and the cell wall carry out different functions. The membrane is composed of a bilayer of phospholipids embedded with proteins. It serves as an osmotic barrier preventing the flow of material into the cell, where the solute concentration is much higher than in the surroundings of the cell. The membrane must also act as a selective barrier since the cell needs to get nutrients in and waste out. The cell membrane is able to prevent most molecules getting inside the cell, but not for water. There is also a great pressure on the membrane from the interior. Without something supporting the membrane the cell would swell and burst. It is the cell wall that protects bacteria from osmotic lysis and also determines the shape of the cell. The cell wall is therefore a critical structure in Eubacterial cells.

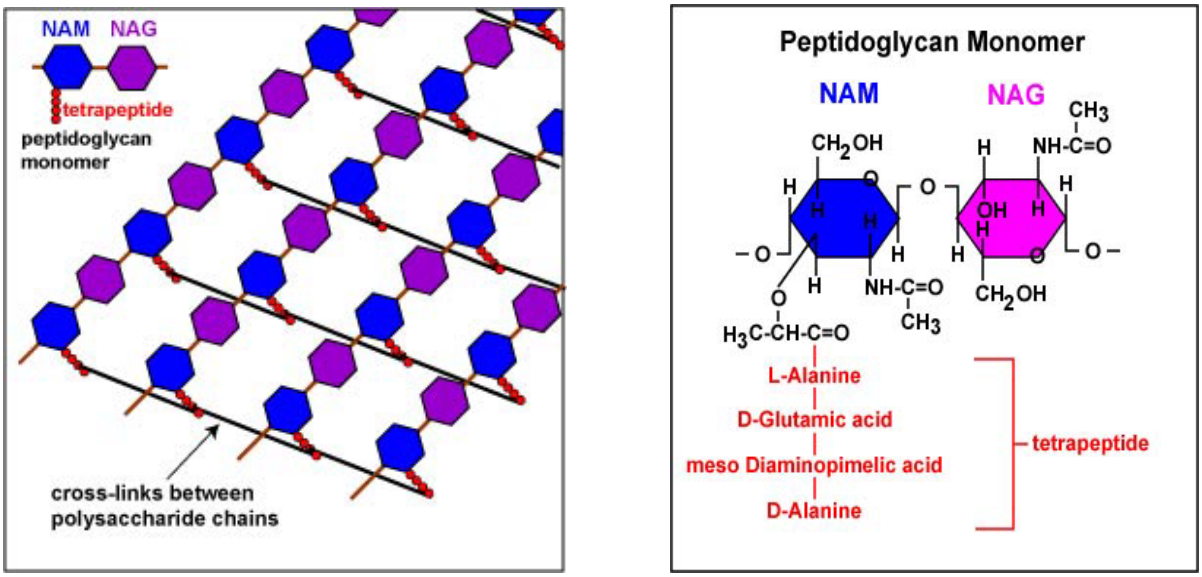

Figure 3.2 The structure of the peptidoglycan polymer and the composition of the peptidoglycan monomer

The cell wall is composed of peptidoglycan. The peptidoglycan, also called murein, is a semirigid polymer consisting of interlocking chains of identical glycopeptide subunits as can be seen in Figure 3.2, left side. A peptidoglycan monomer (Figure 3.2, right side) consists of two joined amino sugars, β-1,4-linked N-acetyl-D-glucosamine (NAG, GlcNAc) and N-

acetylmuramic acid (NAM, MurNAc), with a tetrapeptide consisting of alternating L- and D-amino acids connected to the NAM. These monomers are then bonded together to form glycan chains. The individual glycan chains are then linked to one another by means of pentaglycine cross links between the tetrapeptides coming off of the NAMs. These cross bridges linking the rows of sugars together provide tremendous strength to the cell wall, functioning much like a molecular chain fence around the bacterium.

3.2 Biological activity and conformation of peptidoglycans

Peptidoglycan fragments and substances derived from them exhibit versatile biological activities that depend upon size and composition (104).

One of the most prominent and also well-documented activities of peptidoglycans is the effect on the mammalian immune system. The immune system recognizes the material of the bacterial cell wall as antigens and consequently induces immune defences in the host to defend the body against bacterial infection. The immune response is stimulated even without the presence of the actual infection and creates the basis for active immunization against bacterial disease. Low molecular weight peptidoglycan fragments, either obtained from natural sources or prepared synthetically, are mostly devoid of the toxic properties characteristic for large peptidoglycans, but still retain marked immunomodulating activity (105-108).

Immunomodulators are also used in cancer immunotherapy that aims to find immunological manoeuvres that can raise host anticancer reflections (109-112). The two branches of the immune response – humoral and cell-mediated – act both independently and in concert to combat tumour progression, the success of which depends on the immunogenicity of the tumour cells. Despite the immune system is able to discriminate between transformed cells and normal cells by virtue of the presence of unique antigens on tumour cells, it is, however, not always able to detect and kill cancerous cells because various strategies have also evolved to escape immune surveillance. Attempts are being made to trigger the immune system into an early and efficient response against malignant cells, and various therapeutic methods are being developed to enhance the strength of the immune response against tumours. Many substances endowed with immunomodulating properties have therefore been developed and studied for antitumor activity.

If the structural basis of the biological functions could be inferred from spectroscopic studies, it would be of value in design of analogues. Therefore the next section summarizes conformational investigations on low molecular weight peptidoglycans.

The peptidoglycan monomer

The peptidoglycan monomer (PGM) that is used in this study is obtained from *Brevibacterium divaricatum.* PGM is obtained after lysozyme hydrolysis of uncross-linked peptidoglycan polymer isolated from the culture fluid of penicillin treated bacteria. (113) This disaccharide pentapeptide is water soluble, non-toxic and non-pyrogenic and has the chemically well-defined structure as depicted in Figure 3.3 (113, 114).

It has been shown that PGM possesses marked immunostimulating activity and could therefore be used as an adjuvant with various antigens (115-121).

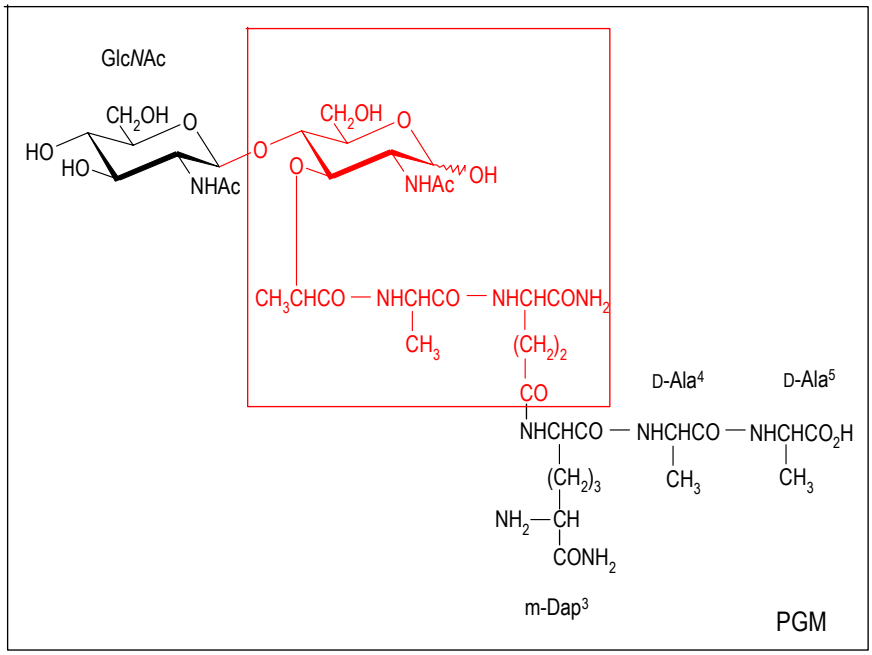

Figure 3.3 Structure of PGM and MDP as enligthed in red

Conformational studies of the peptidoglycan monomer (PGM)

The first NMR study of the PGM molecule has appeared as early as 1982 by Klaic (122) reporting ^{13}C assignment of PGM in D_2O based on experimental comparisons with ^{13}C shifts of the monomeric amino acid units.

^{1}H and ^{13}C NMR pH titrations have been carried out (123) in order to determine the number and the positions of free amino and carboxyl groups. PGM was shown to consume equal amounts of acid and base, hence it was concluded that it contains equal numbers of charged groups. The pH dependence of signals showed that PGM contains two dissociable groups, namely the carboxyl group of the C terminal alanine and the amino group of the $mDap^{3}$ at the D chiral center.

Later a preliminary investigation in DMSO solution by ^{1}H NMR spectroscopy has been reported (124). It has been suggested that the $DAla^{5}$-NH group is involved in H bonding as indicated by the amide proton chemical shift temperature dependencies. As a H bond donor the $DiGln^{2}$-δCO was proposed on the basis of the assumption that the $DiGln^{2}$ residue in question is rotationally restricted, although this latter argument is based on the large chemical shift non-equivalence for the $DiGln^{2}$-βCH_2 protons. A cyclic structure was proposed for the C-terminal pentapeptide of PGM that was supported by NOE interactions involving the $DiGln^{2}$ and the MurNAc residues.

A detailed conformational study of PGM in aqueous solution was carried out by Matter et. al. in 1997 using a combined approach of 2D NMR spectroscopy, restrained simulated annealing (SA) and molecular dynamics (MD) calculations (125). From simulated annealing, a set of conformers was obtained, all characterized by a well-defined extended N-terminal peptide part additionally stabilized by the bound disaccharide. The C-terminal part, on the other hand, exhibited more conformational flexibility in agreement with experimental data and MD simulations. Not only the interglycosidic bond but also the glycopeptide linkage was proven to exist in a single, well-defined conformation, for which no conformational changes were detected during the MD simulations. In contrast, conflicting experimental data for the *N*-acetyl group of GlcNAc was found and explained using a conformer population analysis based on ROE intensities and coupling constants accounting for a conformational equilibrium with one dominantly populated rotamer. It was demonstrated that in the preferential conformation in aqueous solution, the ε-amino group of mDap is exposed and, therefore, readily available for possible chemical reactions.

Fragments: the muramyl-dipeptide (MDP)

Many fragments can be obtained from the bacterial cell wall depending on the micro-organism, direction of the fermentation process and on the use of different enzymes or chemical treatment for the hydrolysis of the peptidoglycanic polymers. The smallest known biologically active unit with the peptidoglycanic structure is the N-acetyl-muramyl-dipeptide

(MDP) (structure can be seen in Figure 3.3 inside), which is a monosaccharide-dipeptide. This simple glycopeptide elicit immunomodulatory and other biological effects. Several studies appeared to reveal conformational characteristics by NMR and molecular modelling methods (126-133).

Complexes

It was proposed, that partial hydrophilic character of the PGM molecule could be modified by complexation of PGM with bivalent metals (134-135), since the coordination of the metal with active hydrophilic groups as possible coordination sites may enforce rearrangement of the lipophilic parts of the molecule. Another reason for the preparation of bivalent metal complexes is based on the fact that metals could play an important role in the stability, distribution, biotransformation and elimination of biologically active substances.

Dervatives

A large number of novel compounds representing smaller parts of the original PGM molecule have been synthesized and found to possess immunomodulating properties (136-137). Structurally related compounds that have been derived from MDP can roughly be divided into three groups:

1. compounds that have a modified peptide moiety
2. compounds that have a modified N-acetylmuramyl structure
3. des-muramyl peptides

3.3 Novel derivatives with increased lipophilicity

Outstanding hydrophilicity and the weak lipophilic character of PGM may be modified by preparation of derivatives bearing apolar groups. In this manner a new equilibrium between the hydrophilic and the lipophilic nature of the molecule is established which may have an influence on the immunomodulating effect by inducing a prolonged activity *in vivo* and increase the affinity against target cells.

Two novel derivatives of PGM, namely, (adamant-1-yl)-CH_2CO-PGM (Ad-PGM) (138) and tert-butyloxycarbonyl-L-tyrosyl peptidoglycan monomer (BocTyr-PGM) (139) starting from the unprotected PGM molecule have been synthesized. The structures are

depicted in Figure 3.4. Both derivatives exhibited immunostimulating activity comparable to the activity of the parent PGM. (138-140)

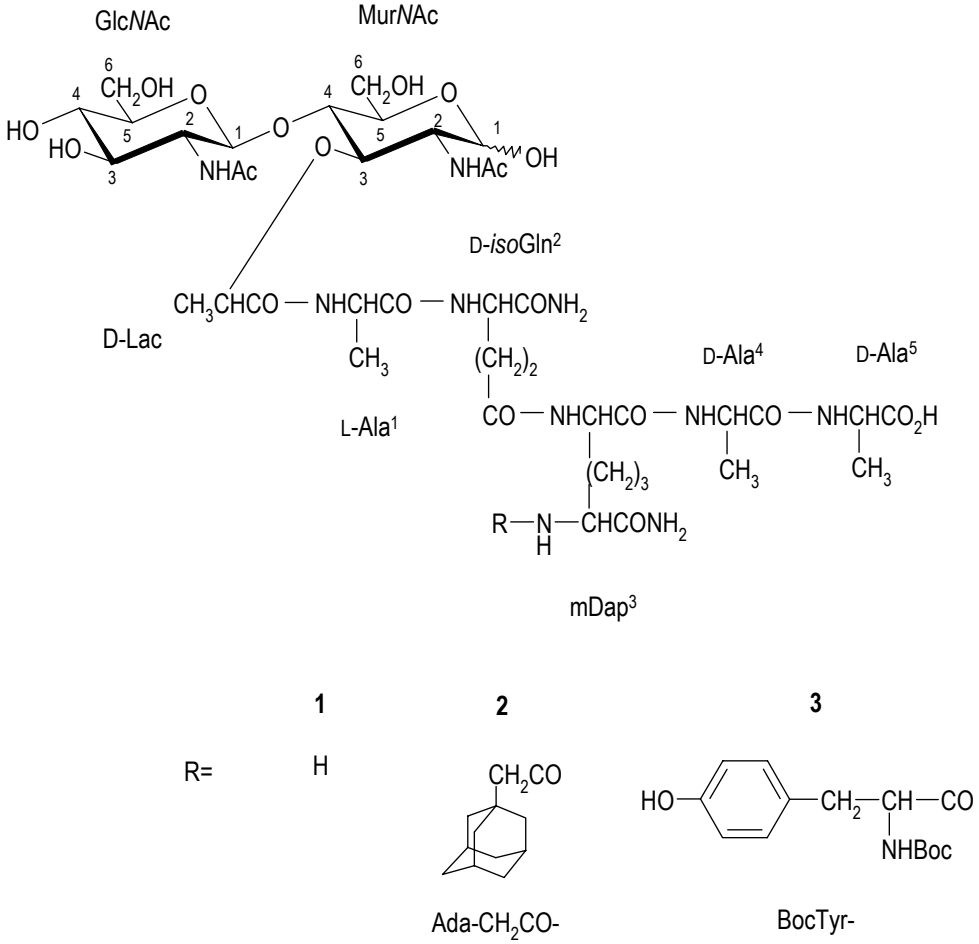

Figure 3.4 Structures of PGM, Ad-PGM and BocTyrPGM

All three compounds are substrates for N-acetylmuramyl-L-alanine amidase, as well. The results indicated that the substitution of the free amino group in the PGM molecule with bulky lipophilic substituents did not markedly affect either the immunostimulating activity or the susceptibility towards hydrolysis by N-acetylmuramyl-L-alanine amidase.

In view of the similar in vivo behaviour of these three compounds, it was of interest to determine whether these activities are related to similarities in the molecular conformations or, on the opposite, eventual conformational differences may not exert sizeable influence on the biological activity. We have therefore conducted a comparative study of the conformations of the synthetically modified derivatives Ad-PGM and BocTyr-PGM with respect to the unsubstituted PGM using NMR spectroscopy and molecular modelling. In particular full assignments of the ^{1}H and ^{13}C spectra, using 2D NMR techniques, for all three compounds in DMSO solutions were obtained. NOESY/ROESY experiments have provided

interproton distance restraints that were used in distance geometry modelling calculations to derive conformational preferences for each of these molecules. These data were supplemented with information available from chemical shifts, temperature dependence of amide proton shifts and proton-proton scalar couplings.

3.4 Results and discussions

The relevant NMR spectral data are summarized in Table 3.1 (chemical shifts), 3.4 (proton-proton couplings and amide proton temperature coefficients) and 3.2 (selected NOEs). The entire list of data for Tables 3.1 and 3.2 can be found in Appendix A and B, respectively. In the course of the discussion only smaller parts of the Tables 3.1 and 3.2 containing relevant data are inserted. NOEs only for the dominant isomer with the reducing MurNAc moiety in α-anomeric form are listed.

Comparison of the data obtained for the parent molecule PGM and the derivatives Ad-PGM and BocTyr-PGM revealed differences in various conformation-related NMR parameters, such as amide ^{1}H chemical shifts (Table 3.1) and their temperature dependence (Table 3.4) as well as ^{1}H/^{1}H NOEs (Figure 3.5, Table 3.2). On the other hand, no significant differences were observed in the ^{3}J(NH,Hα) values (Table 3.4).

The geminal protons of the Dap-$CONH_2$ group display conspicuously large chemical shift non-equivalence (ca. 0.8 ppm) in the unsubstituted parent molecule PGM mainly as a result of a sizeable downfield shift of the resonance for NH_2^E (see in Table 3.3). $CONH_2^Z$ and $CONH_2^E$ refer to one of the amide protons in Z or E position with respect to the C=O oxygen, respectively. The downfield shift of the NH_2^Z resonance is much less pronounced with respect to those in the substituted derivatives Ad-PGM and BocTyr-PGM, whereas shifts of $CONH_2$ proton resonances of the *i*Gln-residue are very similar in all three compounds and also show reduced shift non-equivalences (see Table 3.1).

Table 3.3 Part of Table 3.1**:** ^{1}H and ^{13}C chemical shift data for PGM, Ad-PGM and BocTyr-PGM

	PGM		Ad-PGM		BocTyr-PGM	
	^{1}H	**^{13}C**	**^{1}H**	**^{13}C**	**^{1}H**	**^{13}C**
m-Dap^3-ε$CONH_2^E$	8.107	-	7.248	-	7.355	-
m-Dap^3-ε$CONH_2^Z$	7.287	-	6.912	-	6.938	-

The temperature coefficients for all $CONH_2$ protons are in the range of -5 to -7 ppb/K except that for Dap-$CONH_2^E$ in PGM which is ca. twice as large (Table 3.4). The resonance

shift and non-equivalence effects observed for Dap-$CONH_2$ protons in PGM are therefore unlikely to be caused by protection from the solvent through H-bonding; rather, they may be related to steric/conformational differences with respect to Ad-PGM and BocTyr-PGM that both bear bulky substituents attached to the end of the Dap side chain.

Table 3.4 ^{1}H NMR coupling constants and amide temperature coefficients for PGM, Ad-PGM and BocTyr-PGM

Residue	**^{3}J(NH,Hα) [Hz]**			**Δδ/ΔT [-ppb/K]**		
	PGM	Ad-PGM	BocTyr-PGM	PGM	Ad-PGM	BocTyr-PGM
β-GlcNAc	8.4 (8.4[a]; 9.6[b])	7.6	8.4	5.4 (11.8[b])	4.5	4.4
α-MurNAc	5.7 (7.9[a]; 7.5[b])	5.7	6.1	11.7 (4.3[b])	11.4	10.0
L-Ala[1]	~7 (8.0[a]; 5.4[b])	7.0	n.a.	~10 (13.8[b])	7.0	~6
D-iGln[2]	8.1 (8.0[a]; 7.8[b])	8.1	7.0	7.8 (13.7[b])	6.7	4.8
m-Dap[3] (α)	7.5 (7.6[a]; 6.8[b])	7.6	7.8	0.4 (10.5[b])	5.9	5.2
D-Ala[4]	~7 (7.2[a]; 6.8[b])	8.1	n.a.	~10 (10.4[b])	7.5	~6
D-Ala[5]	6.4 (6.4[a]; 6.9[b])	7.2	~5	-8.1 (12.5[b])	5.5	2.2
m-Dap[3] (ε)	----	8.1	n.a.	----	6.1	~6
D-iGln-$CONH_2^E$	n.a.	n.a.	n.a.	6.4	5.3	~5
D-iGln-$CONH_2^Z$	n.a.	n.a.	n.a.	5.4	4.9	~7
m-Dap-$CONH_2^E$	n.a.	n.a.	n.a.	~14	5.9	~5
m-Dap-$CONH_2^Z$	n.a.	n.a.	n.a.	4.6	5.3	5.4

[a] In DMSO from ref. (124)

[b] In H_2O from ref. (125)

A similar phenomenon is observed for Ala[5]-NH in Ad-PGM: a relatively large downfield shift, with respect to PGM and BocTyr-PGM (Table 3.5), associated with a temperature coefficient of -5.5 ppb/K; the latter indicating appreciable solvent exposure. The same amide proton appears, however, largely protected from solvent in both PGM and BocTyr-PGM, as indicated by the somewhat exceptional, large positive, and low negative, respectively, temperature coefficients, see Table 3.4. The exceptional temperature coefficient for Ala[5]-NH

in PGM was also noticed earlier. (124) The conformational preferences at the N-terminus of Ad-PGM may therefore be different from those in PGM and BocTyr-PGM.

Table 3.5 Part of Table 3.1**:** ^{1}H and ^{13}C chemical shift data for PGM, Ad-PGM and BocTyr-PGM

	PGM ^{1}**H**	**Ad-PGM** ^{1}**H**	**BocTyr-PGM** ^{1}**H**
D-Ala^{5}-NH	7.547	8.072	7.513

Conformational differences are reflected in the NOESY cross peak patterns as well. Part of the observed NOEs arises from intraresidue dipolar contacts (*not* listed in Table 3.2 in Appendix D). The majority of the *inter*residue NOE contacts occur between neighbouring residues as evidenced by αN(*i,i+1*) and βN(*i,i+1*) sequential (44) cross peaks (Table 3.2). In fact, all possible sequential contacts, either of αN or βN-type,(44) could be observed along the hexapeptide backbone starting with D-Lac except for the DiGln^{2}-δ/mDap^{3}-αNH and the DAla^{4}-β/DAla^{5}-NH. Sequential cross peaks like those mentioned are usually observed for small, unstructured peptides in aqueous solution.(141)

On the other hand, NOEs between the carbohydrate and peptide moieties (NOEs #2-20, Table 3.6) are indicative of less conformational freedom at the N-terminal part of the peptide chain. Strong interglycosidic NOEs (#1) were detected between GlcNAc-H1 and MurNAc-H4 in all three molecules investigated (Table 3.6).

Inspection of the amide regions in the NOESY maps for PGM, Ad-PGM and BocTyr-PGM (Figure 3.5) reveals characteristic differences especially with regard to the long-range NOEs (Table 3.2). Of the three compounds PGM clearly features the largest number of long-range NOEs. There are 13:7:10 long-range NOEs in derivatives PGM, Ad-PGM and BocTyr-PGM, several indicating contacts between the MurNAc (especially the N-acetyl methyl and MurNAc-2,3 protons) and the N-terminal peptide residues. The number of such contacts is reduced in Ad-PGM, whereas practically none is observed in BocTyr-PGM (discussed NOEs #6, 11, 17, 18, are indicated in Figure 3.6 are listed in Table 3.6,).

Table 3.6 Part of Table 3**:** NOESY/ROESY cross peak intensities for PGM, Ad-PGM and BocTyr-PGM

	Proton1	Proton2	PGM	Ad-PGM	BocTyr-PGM
1	GlcNAc-1	MurNAc-4	s	s	s
2	GlcNAc-3	D-Lac-β	-	-	w [i)]
3	MurNAc-2	D-Lac-α	-	m	-
4	MurNAc-2	D-Lac-β	m	s	m
5	MurNAc-2	L-Ala^1-NH	m	m	w
6	MurNAc-2	D-iGln^2-NH	w	-	-
7	MurNAc-NH	D-Lac-α	s	s	m
8	MurNAc-NH	D-Lac-β	s	m	w
9	MurNAc(CH_3)	L-Ala^1-NH	w	w	-
10	MurNAc(CH_3)	L-Ala^1-β	-	-	w
11	MurNAc(CH_3)	D-iGln^2-NH	w	-	-
12	MurNAc(CH_3)	D-iGln^2-$CONH_2^E$	w	w	w [g)]
13	MurNAc(CH_3)	D-iGln^2-$CONH_2^Z$	w	w	-
14	MurNAc(CH_3)	D-Ala^4-β	-	-	w
15	MurNAc-3	D-Lac-β	m	m	w
16	MurNAc-3	L-Ala^1-NH	m	w	-
17	MurNAc-3	D-iGln^2-NH	w	-	-
18	MurNAc-3	D-iGln^2-$CONH_2^E$	w	-	-
19	MurNAc-4	D-Lac-β	-	-	w
20	MurNAc-4	L-Ala^1-NH	w	w	-

g) Ambiguous: MurNAc(CH_3) and GlcNAc(CH_3) overlap

i) Ambiguous: GlcNAc-3 and GlcNAc-5 overlap

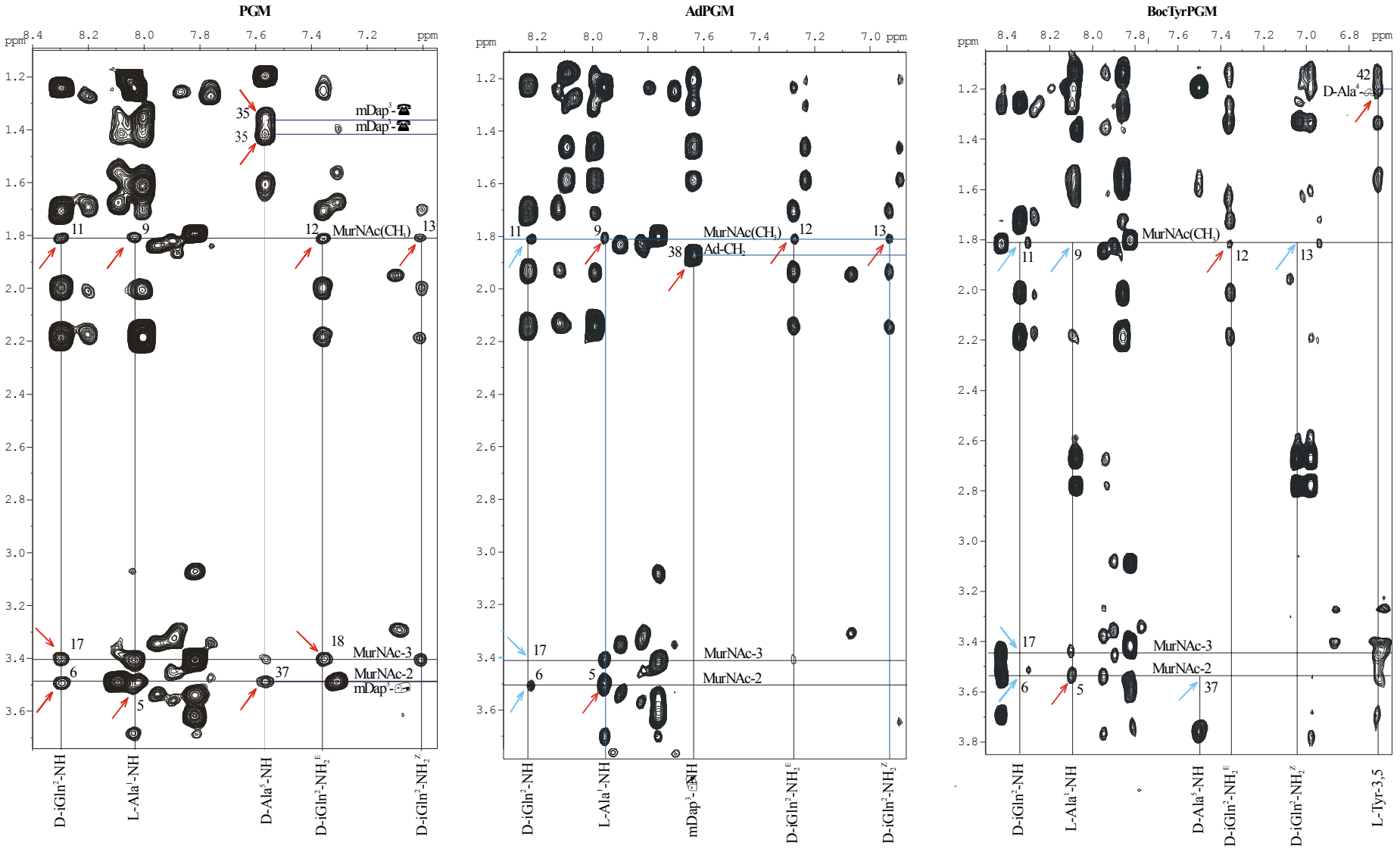

Figure 3.5 Partial NOE maps of PGM (left), Ad-PGM (middle) and BocTyr-PGM (right) emphasizing the presence (arrows in red) or absence (arrows in blue) of characteristic long-range cross peaks. Cross peaks are labelled using peak numbers in Table 3.2.

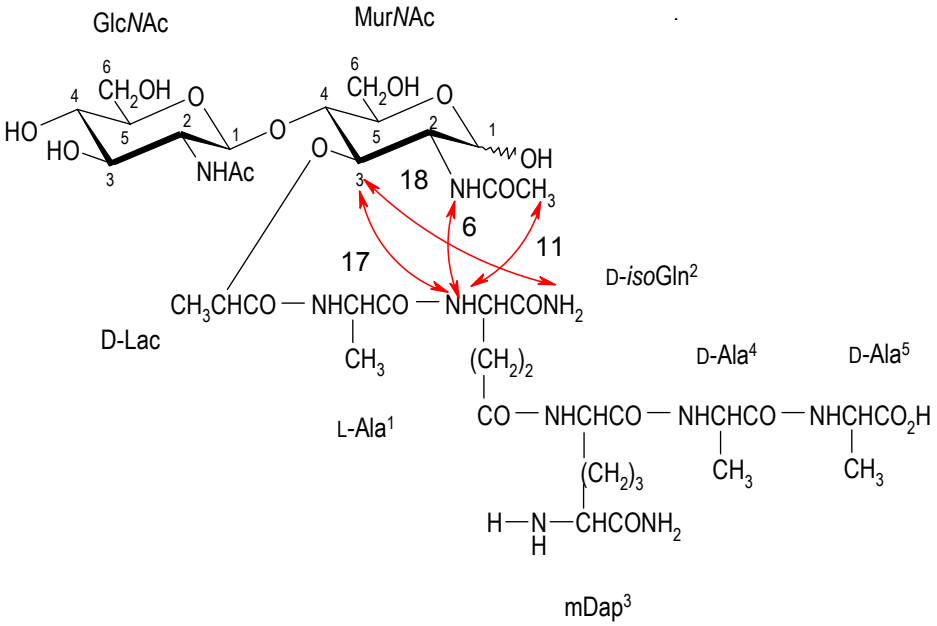

Figure 3.6 Contacts between the MurNAc (especially the N-acetyl methyl and MurNAc-2,3 protons) and the N-terminal peptide residues in PGM

Long-range NOEs involving any of the adamantyl ring protons are conspicuously missing in Ad-PGM. On the other hand, Tyr aromatic protons display some contacts with the C-terminal residues of the peptide moiety (such as #33, 36 and 42, see, Table 3.7).

Table 3.7 Part of Table 3.2: NOESY/ROESY cross peak intensities for BocTyr-PGM

	Proton1	**Proton2**	**BocTyr-PGM**
33	m-Dap^3-β,β’	L-Tyr-3,5	w
36	m-Dap^3-γγ’	L-Tyr-3,5	w
39	m-Dap^3-εNH	L-Tyr-α	s
40	m-Dap^3-εNH	L-Tyr-β,β’	m
42	D-Ala^4-β	L-Tyr-3,5	w

The structures resulting from distance geometry calculations were divided in clusters of conformations according to selected main chain dihedral angle values (see Experimental), and the most populated cluster with low energy was chosen to represent the preferred conformations. Selected structures from the representative clusters are shown with an identical orientation of the two sugar units for each of the molecules in Figure 3.7.

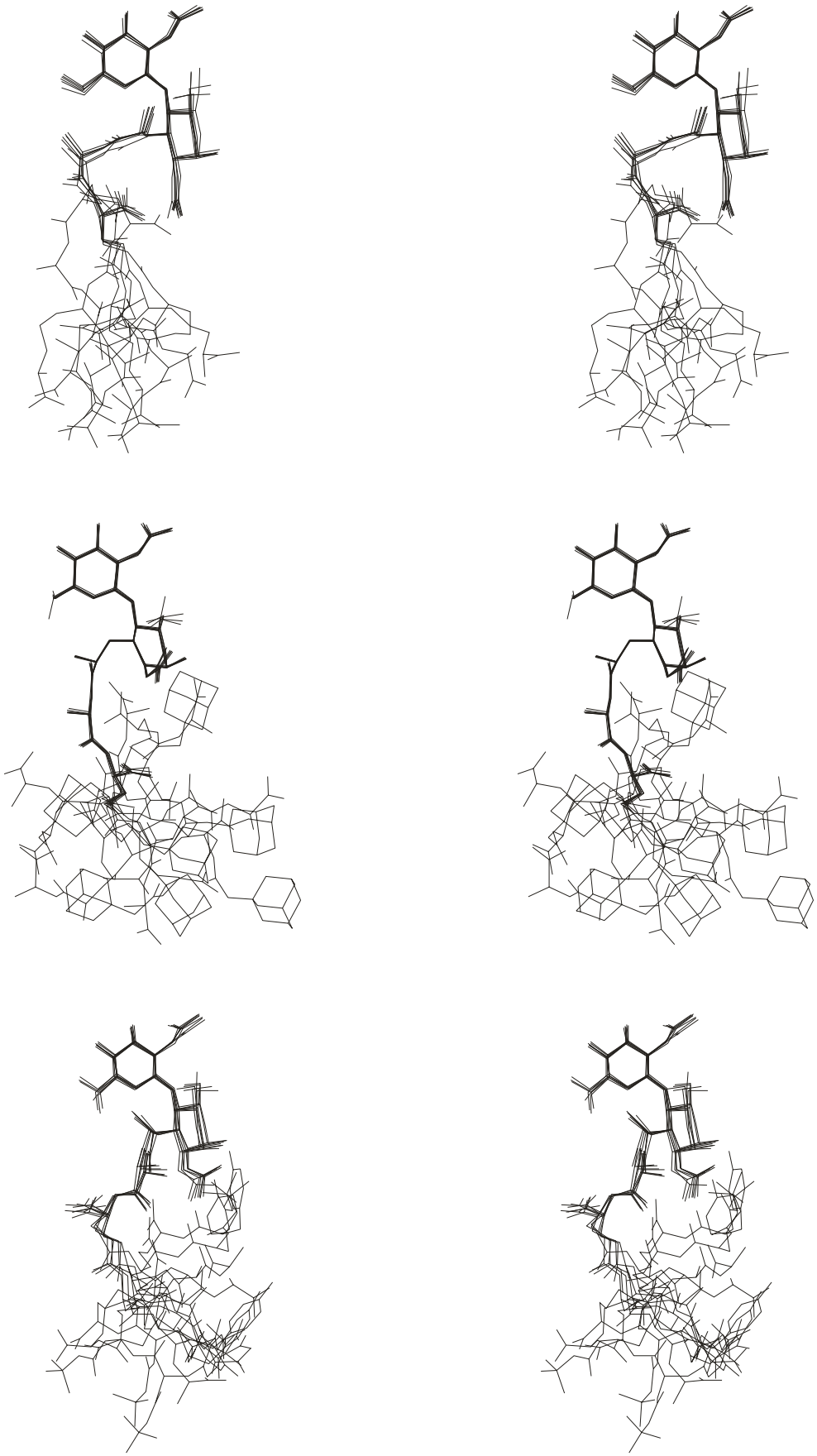

Figure 3.7 Stereoview of nine structures from the most populated clusters with low energy for PGM, Ad-PGM and BocTyr-PGM superposed at the heavy atoms of the NAG, Mur, Lac, Ala and iGln moieties

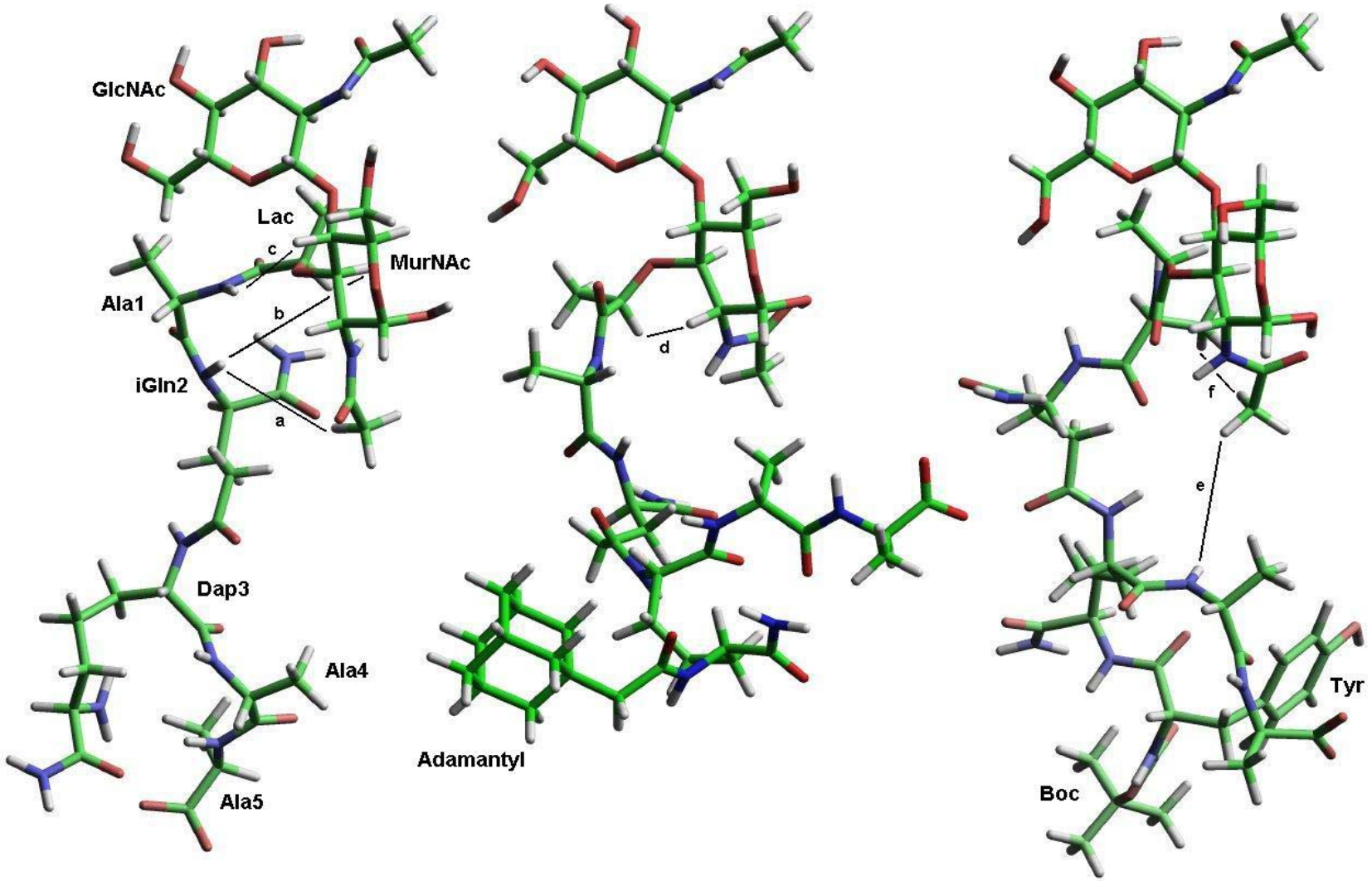

Figure 3.8 Representative structures for the preferred conformation of PGM (left) and derivatives Ad-PGM (middle) and BocTyr-PGM (right). Selected long-range NOEs are displayed as lines and labelled according to Table 3.2. An identical orientation of the two sugar moieties was chosen for all three molecule.

In Table 3.8 some statistical data is shown regarding the main chain dihedral angle values used for clustering of conformations, and a comparison with the values for PGM from an explicit water simulation (125) is given. Additionally, the calculated values for selected $^3J_{HN,\alpha}$ coupling constants (44, 142) are shown for the representative clusters. The latter are reasonably similar to the experimental values (Table 3.4).

Table 3.8 Average values of selected dihedral angles (in degrees)[a] and ^{3}J(HN,Hα) coupling constants (in Hz) calculated[b] for the representative clusters of PGM, Ad-PGM and BocTyr-PGM

Residue	PGM [c]	Ad-PGM	BocTyr-PGM
iGln^2-χ_2	-67 (81)	-64	56
iGln^2-χ_1	-161 (177)	164	131
iGln^2-ψ	-74 (77)	-77	-72
iGln^2-ϕ	80 (123)	76	130
Ala^1-ψ	58 (130)	126	100
Ala^1-ϕ	55 (-160)	175	0
Lac-ψ'	-7 (-166)	-136	-172
Lac-ϕ'	165 (84)	62.8	112
α-MurNAc-ϕ'	121 (-161)	-106	115
β-GlcNAc-ψ	120 (118)	123	121
β-GlcNAc-ϕ'	165 (164)	162	165
^{3}J(iGln^2-α)	8.5 (n.a.)	7.3	7.7
^{3}J(Ala^1-α)	6.8 (n.a.)	6.5	6.6
^{3}J(MurNAc)	5.4 (n.a.)	8.5	8.7
^{3}J(GlcNAc)	8.7 (n.a.)	8.2	8.6

a) For the definition of the dihedral angles, see text

b) Using Karplus parameters from ref. (44)

c) Values in parentheses are those for PGM calculated for solution in water; from ref. (125)

The orientation of the Lac-Ala^1-*i*Gln^2 moiety is similar, though not identical, for PGM and Ad-PGM, but differs more strongly with BocTyr-PGM. With PGM the orientation of the N-terminal peptide domain relative to the disaccharide moiety is characterized by NOEs from the *i*Gln^2 to MurNAc (#6, 11, 17 and 18 in Table 3.6, Figure 3.6) while with Ad-PGM the Lac

moiety displays a different orientation that leads to an interesting NOE contact with MurNAc-H2 (#3 in Table 3.6; Figure 3.9).

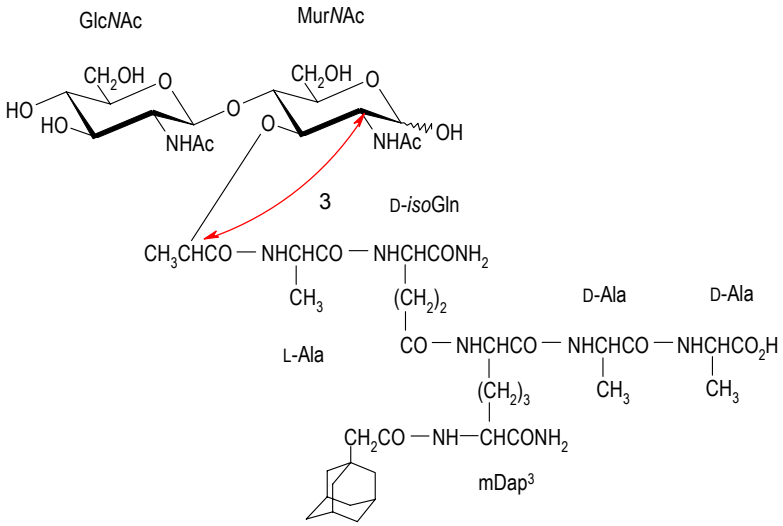

Figure 3.9 NOE contact from Lac to MurNAc-H2 in Ad-PGM

On the other hand, BocTyr-PGM displays unique contacts of the MurNAc to Lac as well as to Ala[4] (#19 and 15 in Table 3.6; and Figure 3.10).

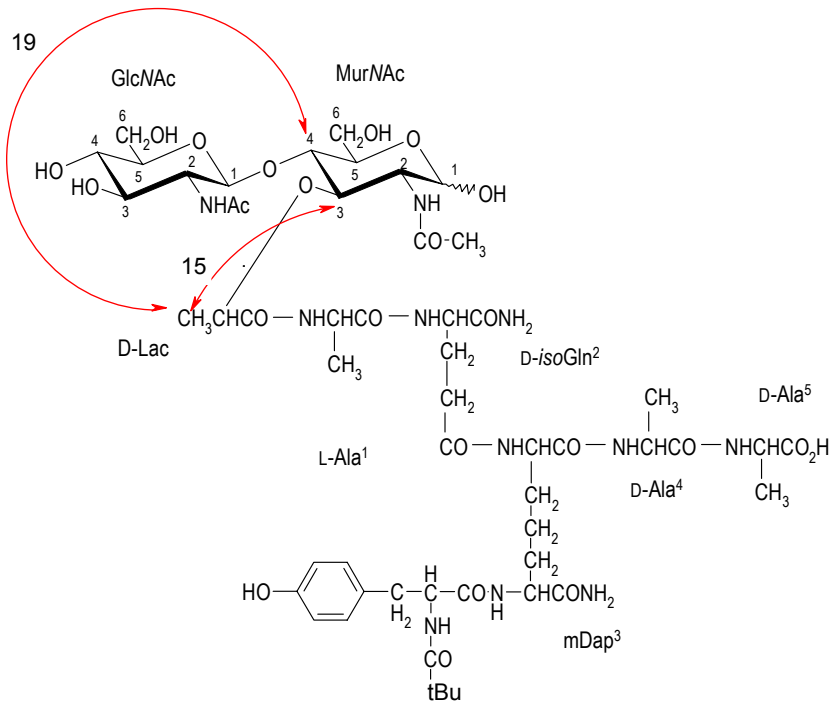

Figure 3.10 NOE contacts from Lac to MurNAc-H2 in BocTyr-PGM

The structure of PGM can be used for an explanation of the unusual *positive* temperature coefficient of the Ala^5-NH chemical shift (Table 3.5). The latter could be caused by the protection of Ala^5-NH from solvent by the side chain of Dap^3 that is attracted towards the negatively charged Ala^5-C-terminus by the positively charged Dap^3-εNH_3^+ group. Such a charged group is absent in Ad-PGM and BocTyr-PGM, where the respective temperature coefficients are in the negative range. Additionally, PGM shows long-range NOEs from the *i*Gln^2 to the sugar moiety (see above); the resulting conformations partially protect Dap^3-NH from solvent and may lower its temperature dependence (Table 3.4) although the exact mechanism is not evident from the NOE pattern. The preferred conformation of PGM in DMSO as determined in the present study is rather different from the average structure of PGM that has been calculated in water, (125) except for the disaccharide conformation as can be seen by comparing the torsion angle values in Table 3.8. Ad-PGM**,** on the other hand, is devoid of any remarkable NOEs, including those involving the adamantyl moiety, or anomalous amide chemical shift temperature dependences. Correspondingly, the calculated structures are also the least constrained by distance restraints of the three molecules.

BocTyr-PGM, however, displays a network of hydrophobic interactions also involving the Bu^t of Boc and aromatic protons, exemplified by the NOEs Mur-NAc(CH_3) to Ala^4-β (#14), Tyr-3,5 to Ala^4-β (#42), and Tyr-3,5 to Bu^t(Boc) (#43) in Figure 3.11.

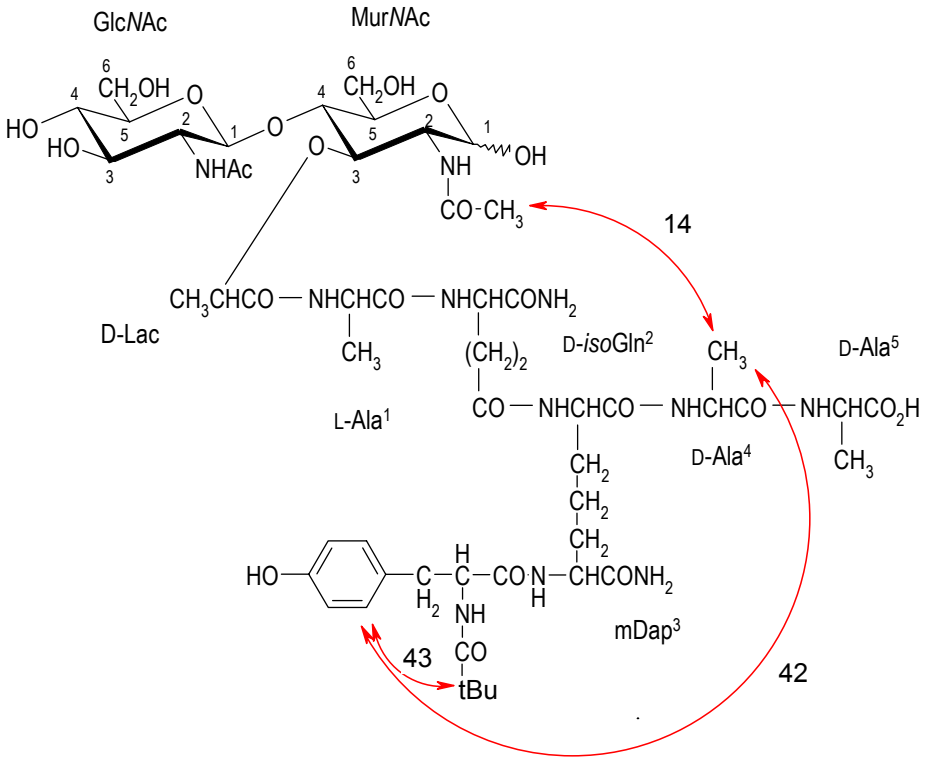

Figure 3.11 Hydrophobic contacts in BocTyrPGM

The resulting structures fully expose Dap-NH but somewhat hide the Ala^5-NH from solvent in partial agreement with the temperature coefficients (Table 3.4). The high-field shift of Ala^5-NH in PGM and BocTyrPGM relative to Ad-PGM seems to be connected with its protection from solvent. The low-field shift of the Dap^3-NH_2^E and -NH_2^Z protons in PGM relative to Ad-PGM and BocTyrPGM (cf. Table 3.3) is most probably caused by the proximity of the Dap^3-εNH_3^+ amino group.

The results shown above suggest that the lipophilic substituents attached to the Dap^3-εNH_2 amino group of the parent PGM molecule introduce changes in the conformational preferences of the peptide moiety. In PGM electrostatic interactions between charged end groups (Ala^5-COO^- and Dap^3-εNH_3^+) apparently promote folded conformations with participation of the long Dap side chain as indicated by the unique, long range NOE contacts between Ala^5-NH and Dap^3 side-chain protons (#34, 35 and 37 in Table 3.9, Figure 3.12).

Table 3.9 Part of Table 3 NOESY/ROESY cross peak intensities for PGM, Ad-PGM and BocTyr-PGM

	Proton1	Proton2	PGM	Ad-PGM	BocTyrPGM
34	m-Dap^3-β,β'	D-Ala^5-NH	w	-	w
35	m-Dap^3-γ,γ'	D-Ala^5-NH	m	-	-
37	m-Dap^3-ε	D-Ala^5-NH	w	-	-

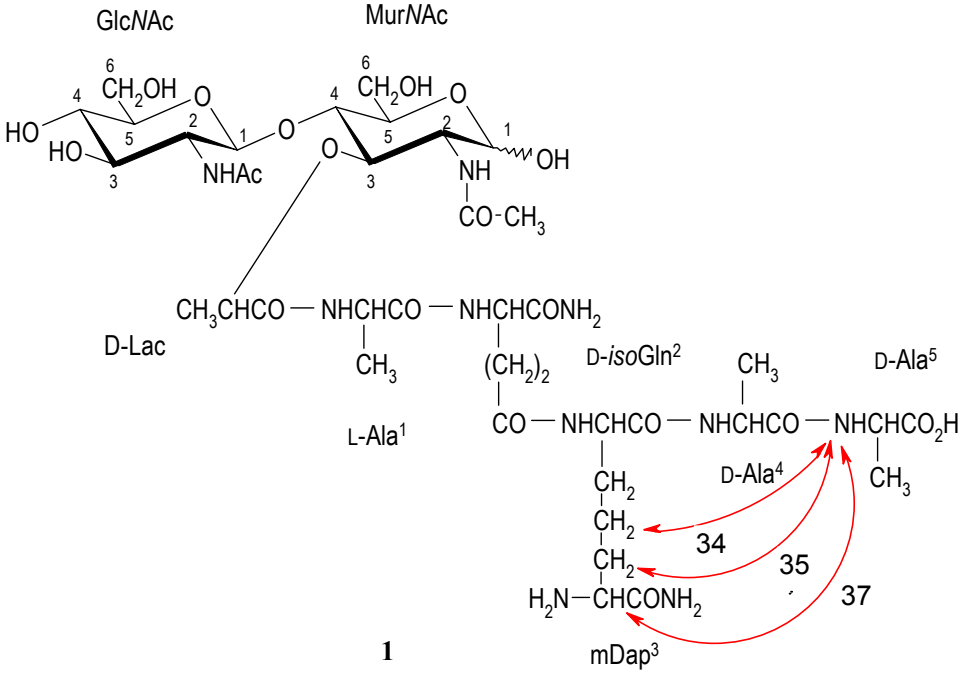

Figure 3.12 Unique, long range NOE contacts between Ala^5-NH and Dap^3 side-chain protons indicating folded conformations with participation of the long Dap side chain as indicated by the induced by electrostatic interactions between charged end groups in 1 PGM

3.5 Conclusion

Derivatives wherein such interactions are suppressed by acylation of the Dap^3-εNH_2 are characterized by more extended conformations of the peptide chain. The above long range interactions are missing in Ad-PGM and, conspicuously, no NOEs can be observed involving any of the adamantly ring protons. Of the two acylated derivatives studied Ad-PGM appears to be less constrained than BocTyr-PGM, the latter being characterized by hydrophobic contacts of methyl, the aromatic and the Bu^t groups.

The differences in conformational preferences revealed in solutions for DMSO do not, however, seem to influence the biological activities such as immunostimulation and binding to N-acetylmuramyl-L-alanine amidase. (139-140) This may indicate that peripheral parts of the peptide chain such as the C-terminus and end groups of the long Dap side chain do not significantly contribute to the binding to receptors or enzymes, participating in these biochemical interactions, under physiological conditions.

4. CONFORMATIONAL PREFERENCES OF DIGLYCOSYL DISULFIDES

4.1 Carbohydrates with unusual interglycosidic linkages

Oligosaccharides containing unusual two-bond interglycosidic linkages

Analogues of oligosaccharides in which an N, S, Se or C-atom replaces the glycosidic O-atom are well known and have been investigated in detail (143-158). Such carbohydrate heteroanalogues are potential inhibitors of glycoside hydrolyse enzymes because the non-O-glycosidic bond is usually resistant to hydrolysis.

Oligosaccharides with 1-6 and other three-bond linkages

On the other hand, few structures featuring a three-bond interglycosidic connection (-X-Y-, with X, Y = O, N, C, S), in place of the natural two-bond coupling between monosaccharide units, are known (159-161). Some representatives of the latter also occur in Nature as components of important antitumor antibiotics (162-163). Three-bond interglycosidic linkages (3BIGL, -X-Y-, with X,Y = O, N, C, S) in place of the natural two-bond connection (2BIGL), between monosaccharide units in di- or oligosaccharides are relatively rare. Some important natural oligosaccharides such as tunicamycin, moenomycin-A or sialyl T_N feature, significantly, 3BIGLs. An interesting subgroup, incorporating two heteroatoms in the interglycosidic chain, also occurs in Nature as part of important antitumor antibiotics. 3BIGLs with X=O and Y=C, such as the 1-6 bonds in polysaccharides are, on the other hand, more frequent, e.g., in dextran, amylopectin or inulin.

The disulfide linkage

Disulfide linkages play an essential role in establishing tertiary structures of proteins, in the formation of cyclopeptides and in many biologically relevant systems. This structural motif is, however, virtually nonexistent within carbohydrates of either synthetic or natural origin. Obvious exceptions are symmetric disulfides formed through oxidation of 1-thioaldoses and some glycosyl-aryl/alkyl disulfides that have been known for a long time (164-165). A few cyclic disulfide derivatives of mono- and disaccharides (166-167) have also

been described. Some neoglycoproteins represent recent examples of interesting hybrid structures in which glycosyl units are attached to proteins through S-S linkages. (168-169)

4.2 Structures investigated: disulfide disaccharides

A novel class of glycomimetics, non-symmetric oligosaccharides containing a three-bond disulfide (X,Y = S) linkage in place of the interglycosidic oxygen, has recently been reported (170). Structures of the derivatives are depicted in Figure 4.1.

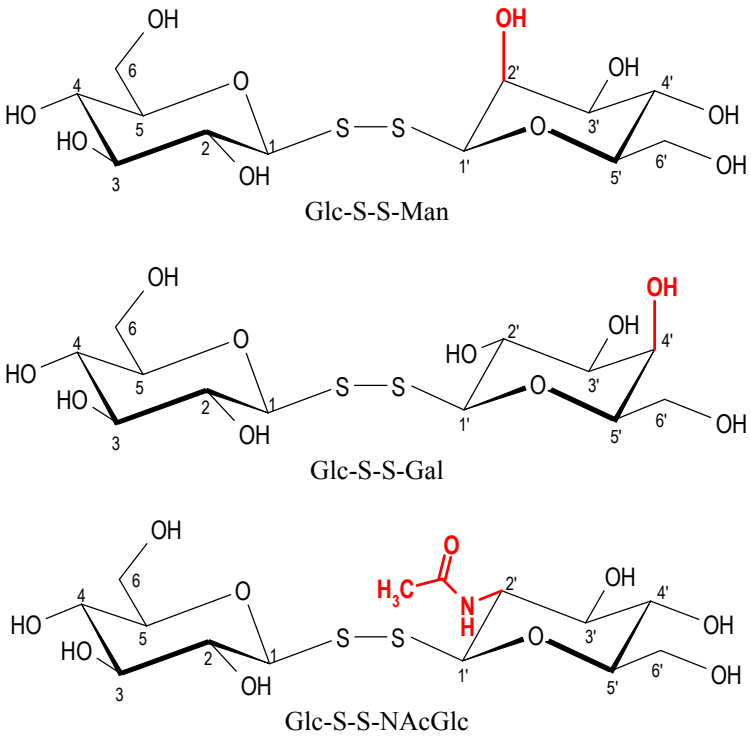

Figure 4.1 Structure of non-symmetric disulfide disaccharides

Such structures are of interest for several reasons: i) added flexibility within the resulting compounds with respect to the reference natural glycosides, ii) increased distance between components in terms of the number of connecting bonds (3 vs. 2), iii) extension of the available conformational space as a result of i) and ii), iv) altered electronic and steric properties of the linker atoms and v) inherent axial chirality of the disulfide bond. All these characteristics play a significant role in biological interactions involving carbohydrates such as in cell recognition or proliferation or in carbohydrate metabolism. (171)

The conformation around the glycosidic linkage has been shown to be the single most important factor in determining the molecular shape of oligosaccharides (172). This property

is fundamental in influencing biological activity such as binding to enzymes or receptors. It is of note in this respect that a peculiar conformation around the unusual three-bond (CNOC) interglycosidic linkage in calicheamicin was shown to be the key structural element that enables this molecule to bind in the minor groove of DNA and hence to exert its biological action (173). It is also known that the chemical reactivity of the SS-bond depends strongly on the CSSC dihedral angle (174). The value of this parameter was observed to be close to 90° in unconstrained disulfides.

Therefore the objective of the present study was to gather information on the relevant interglycosidic torsion angles in these compounds by conformational analysis based on the comparison of NMR data and modelling calculations.

The interglycosidic linkage in the derivatives under study is characterized by three torsional angles as depicted on Figure 4.2 : $\Phi_A = O^{ring}{}_A - C1_A - S - S$; $\omega = C1_A - S - S - C1_B$; $\Phi_B = S - S - C1_B - O^{ring}{}_B$.

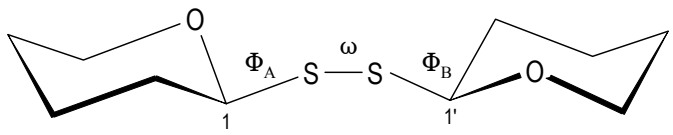

Figure 4.2 Definition of torsion angles characterizing the interglycosidic linkage

4.3 NMR methods for investigating the conformation about the interglycosidic linkage

The most frequently used NMR methods (175, 176) for investigating the solution conformation of carbohydrates are the interglycosidic NOEs, methods for identifying H bonds (temperature dependent hydroxide chemical shifts, ^{2}D isotope shifts) (177-179) and the measurement of homo- and heteronuclear vicinal coupling constants. A major difficulty in determining 3D structure of carbohydrates from NMR data is the flexibility of the conformation around the glycosidic link. When multiple conformations are present in solution, NMR data reflect time-averaged conformational ensembles and constituent conformations can rarely be determined directly. To further complicate matters, the average is not a linear one, because the geometric parameters are usually related to the experimental data in a non-linear way. As internal flexibility becomes significant and NMR parameters are used

as empirical constraint in modelling calculations, this may lead to the generation of virtual conformers, which represents structures that are not physically present. (180-181) Experimental NMR data are, therefore, usually compared to ensemble averaged theoretical parameters derived from model calculations (175, 181, 172) rather than used as constraints. These studies result in the location of the preferred regions in the conformational space rather than in the location of some well-defined points.

Conformational studies of three-bond interglycosidic linkages are difficult because the monosaccharide units are in longer distance from one another. The usual approach based on 3-bond proton-carbon couplings cannot be applied. The vicinal ^{13}C-^{13}C scalar coupling constant between the anomeric carbons contains information on the torsion angle around the disulfide bond. This may be small because torsion angles close to 90^{o} are anticipated (174), and difficult to measure because of low sensitivity of the corresponding measurement techniques. An additional difficulty is that the number of interresidue NOEs is expected to be small due to the larger distance between monosaccharide units.

As a further approach to explore conformational features RDCs may be measured. The RDC has an inverse cubic dependence on the separation between the nuclei and a squared cosine dependence on the angle between the internuclear vector and the static field. For directly bonded pairs of atoms such as a ^{1}H-^{13}C in direct connection, the internuclear distance is accurately known, and the measured RDC provides information on the orientation of the internuclear bond vector. Straightforward interpretation of RDC data is possible only for carbohydrates which can be represented by a single conformer (182). For these cases the orientation tensor defining the alignment of the whole molecule is obtained by fitting $^{1}D_{C,H}$ data to model structure. This method is effective for models which have restricted and symmetric internal motions around the glycosyl linkages.

Interpretation of RDCs in highly flexible oligosaccharides with several conformational minima requires a different approach. In order to make use of the structural information the alignment of each rigid unit in the molecule with respect to the magnetic field must be determined. 5 independent elements of the alignment tensor must be known. Providing 5 experimental RDC for each rigid unit the alignment tensor can determined. Since it is known that oligosaccharides are often flexible around the glycosidic bonds, therefore every monosaccharide unit must be regarded as rigid unit for which separate alignment tensor must be determined. This requirement leads to several problems during the interpretation of RDCs in oligosaccharides. For a pyranose ring 5 one-bond heteronuclear RDCs can be measured. The distribution of C,H bond vectors is, however, not isotropic due to the geometry of the

pyranose rings. To increase the number of experimental dipolar couplings H,H dipolar couplings must be measured as well. With the additional homonuclear residual dipolar couplings, it is possible to obtain an alignment tensor for each monosaccharide. (183, 184)

4.4 Results and discussion

NMR investigations

Solvent accessibilities were studied by temperature coefficients for the hydroxide and amide protons to identify possible H bonding sites, ^{1}H-^{1}H NOE were measured in order to reveal interannular NOEs between protons of the sugar rings and finally one-bond residual dipolar ^{1}H-^{13}C couplings were measured in weakly oriented media.

NMR studies of exchangable protons of carbohydrates in aqueous solution are severely hampered by the presence of fast chemical exchange of labile groups with water. DMSO as a solvent were used to circumvent chemical exchange of OH and NH protons with the residual water where NMR signals of hydroxide and amide protons can readily be observed and provide useful additional source of interresidual NOE contacts and temperature coefficients. Measurement of RDCs, however, involves dissolving the substance to be studied in an aqueous dilute liquid crystal media. Potential conformational changes induced by the different solvent were examined by comparing ^{1}H and ^{13}C chemical shifts.

Full ^{1}H and ^{13}C assignments of the substances in DMSO-d_6 and aqueous liquid crystal medium were achieved by conventional 1D and 2D NMR experiments. Assignments of ^{1}H and ^{13}C resonances are listed in Table 4.1 and 4.2.

Conformational changes induced by solvent effects as evaluated by chemical shifts

^{1}H nuclei located at peripheral positions of molecules are in direct contact with the solvent molecules, while the ^{13}C atoms in the interior of the skeleton of molecules are influenced by solvation effects to a smaller extent. As a result, variations in ^{13}C chemical shifts more reliably reflect possible alteration in conformation than changes in the ^{1}H chemical shifts. Although differences in ^{1}H chemical shifts between DMSO and the aqueous liquid crystal solvent range up to ca. 0.9 ppm (4th and 6th column of Table 4.1), but this change incorporate effects of the difference in solvation and that of the possible structural

changes. The ^{13}C chemical shift changes are <1 ppm (4th and 6th column of Table 4.1) suggest no extensive conformational differences in the two media.

Table 4.1 Chemical shifts for Glc-S-S-Man in DMSO and in D_2O - DMPC/CHAPSO at isotropic sample conditions

Assignment	**δ_{1H}**		**$\Delta\delta$**	**δ_{13C}**		**$\Delta\delta$**
	DMSO-d_6	**D_2O - DMPC/CHAPSO**		**DMSO-d_6**	**D_2O - DMPC/CHAPSO**	
G1	4.241	4.679	0.438	87.63	88.05	0.87
G2	3.421	3.915	0.494	70.20	70.78	0.58
G3	3.213	3.732	0.519	77.65	77.54	-0.11
G4	3.017	3.581	0.564	69.64	69.96	0.32
G5	3.169	3.671	0.502	81.13	80.81	-0.32
G6a	3.691	4.058	0.889	61.15	61.55	0.40
G6b	3.368	3.868	0.500	61.15	61.55	0.40
M1	4.786	5.110	0.324	92.15	91.99	-0.16
M2	3.832	4.343	0.498	71.27	72.05	0.78
M3	3.283	3.799	0.516	73.94	74.61	0.67
M4	3.28	3.756	0.476	66.42	67.02	0.78
M5	3.090	3.597	0.303	81.69	81.47	-0.22
M6a	3.691	4.103	0.412	61.15	61.69	0.54
M6b	3.423	3.914	0.491	61.15	61.69	0.54

Table 4.2 Chemical shifts for Glc-S-S-Gal in DMSO and in D_2O - DMPC/CHAPSO at isotropic sample conditions

Assignment	**δ_{1H}**		**$\Delta\delta$**	**δ_{13C}**		**$\Delta\delta$**
	DMSO-d_6	**D_2O - DMPC/CHAPSO**		**DMSO-d_6**	**D_2O - DMPC/CHAPSO**	
G1	4.311	4.491	0.180	89.65	88.76	-0.89
G2	3.285	3.580	0.295	71.57	70.95	-0.62
G3	3.173	3.451	0.278	78.00	77.16	-0.84
G4	3.072	3.347	0.275	69.55	69.34	-0.31
G5	3.131	3.405	0.274	81.19	80.38	-0.81
G6a	3.660	3.819	0.159	61.08	60.85	-0.23
G6b	3.441	3.645	0.204	61.08	60.85	-0.23
Ga1	4.323	4.464	0.141	91.51	90.84	-0.67
Ga2	3.512	3.682	0.170	69.11	69.08	0.03
Ga3	3.330	3.608	0.278	74.66	73.92	-0.74
Ga4	3.642	3.882	0.240	68.43	69.04	0.97
Ga5	3.400	3.662	0.262	79.55	79.74	0.19
Ga6a	3.504	3.700	0.196	60.62	61.14	0.78
Ga6b	3.504	3.663	0.159	60.62	61.14	0.78

Investigations in DMSO solution

Temperature coefficients for labile protons are listed in Table 4.3. Large upfield shifts are observed as the temperature is increased since the values are in the range of - 6-8 ppb/K demonstrating appreciable solvent exposure. The only exception is NAcGlc-2NH displaying an intermediate value of -3.8 ppb/K.

Table 4.3 Temperature coefficients of labile (OH and NH) protons

Glc-S-S-Man		**Glc-S-S-Man**		**Glc-S-S-NAcNH**	
assignment	Δδ/ΔT (ppb/K)	assignment	Δδ/ΔT (ppb/K)	assignment	Δδ/ΔT (ppb/K)
Glc-2OH	-6.5	Glc-2OH	-6.6	Glc-2OH	-6.9
Glc-3OH	-7.1	Glc-3OH	-7.2	Glc-3OH	a
Glc-4OH	-6.6	Glc-4OH	-6.4	Glc-4OH	-6.4
Glc-6OH	-6.8	Glc-6OH	-6.7	Glc-6OH	-8.6
Man-2OH	-7.9	Gal-2OH	-6.6	NAcGlc-NH	-3.8
Man-3OH	-7.0	Gal-3OH	-7.8	NAcGlc-3OH	-6.3
Man-4OH	-6.4	Gal-4OH	-6.5	NAcGlc-4OH	a
Man-6OH	-7.3	Gal-6OH	-5.9	NAcGlc-6OH	-6.6

a) Not determined due to mutual overlap

The important glycosyl NOEs are summarized in Table 4.4. As expected, only a few conformationally relevant contacts were found for all three derivatives.

Table 4.4 Interannular contacts observed as NOESY crosspeaks in Glc-S-S-NAcGlc

peracetylated Glc-S-S-Man		
1	Glc-2	Man-2
2	Glc-4	Man-2
3	Glc-6a	Man-2
Glc-S-S-Gal		
4	Glc-2OH	Gal-6CH_2
Glc-S-S-NAcGlc		
5	Glc-2	NAcGlc-Me
6	Glc-4	NAcGlc-Me
7	Glc-6OH	NAcGlc-Me
8	Glc-6OH	NAcGlc-2NH

For the Glc-S-S-Man in particular, no interresidual NOE were detected at all. Exploratory $^{1}H–^{1}H$ NOE measurements on the peracetylated Glc-S-S-Man, however, disclosed significant interannular NOEs between H-2 of the mannose residue and various glucose ring protons as illustrated in Figure 4.3 left side, these connectivities cannot, however, be observed for the deacetylated derivative. Inspection of qualitative molecular

models indicated that in the conformation required by NOEs the ω $_{C1\text{-}S\text{-}S\text{-}C1}$ torsion angle is ca. -80° to -90°; this value is virtually identical with that observed in unconstrained disulfides (174). Partial map of the NOE experiment showing the above mentioned connectivities can be seen on Figure 4.3 right side.

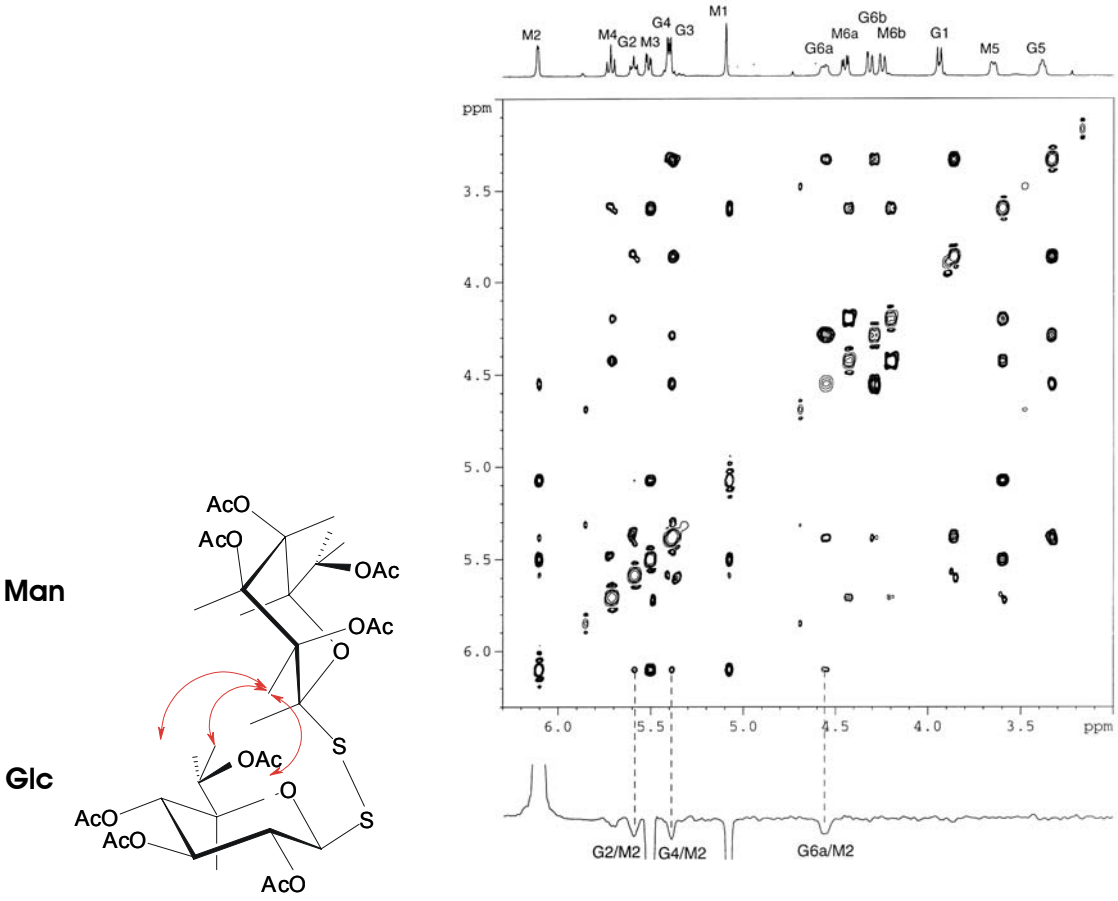

Figure 4.3 Interannular NOE connectivities observed for the peracetylated Glc-S-S-Man derivative and the NOESY map of peracetylated Glc-S-S-Man showing interannular connectivities

Only one weak NOE crosspeaks were detected for Glc-S-S-Gal (Figure 4.4) and a series of NOEs involving the N-acetyl moiety were observed for the Glc-S-S-NAcGlc (Figure 4.5 and 4.6).

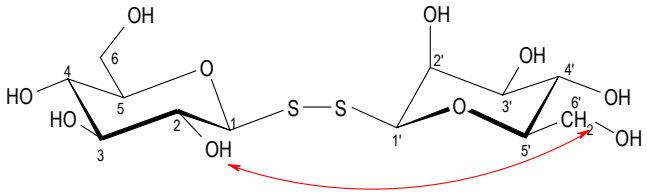

Figure 4.4 Interannular NOE detected on Glc-S-S-Gal

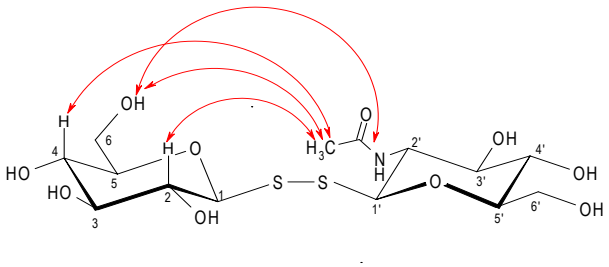

Figure 4.5 ^{1}H-^{1}H interannular connectivities in Glc-S-S-NAcGlc

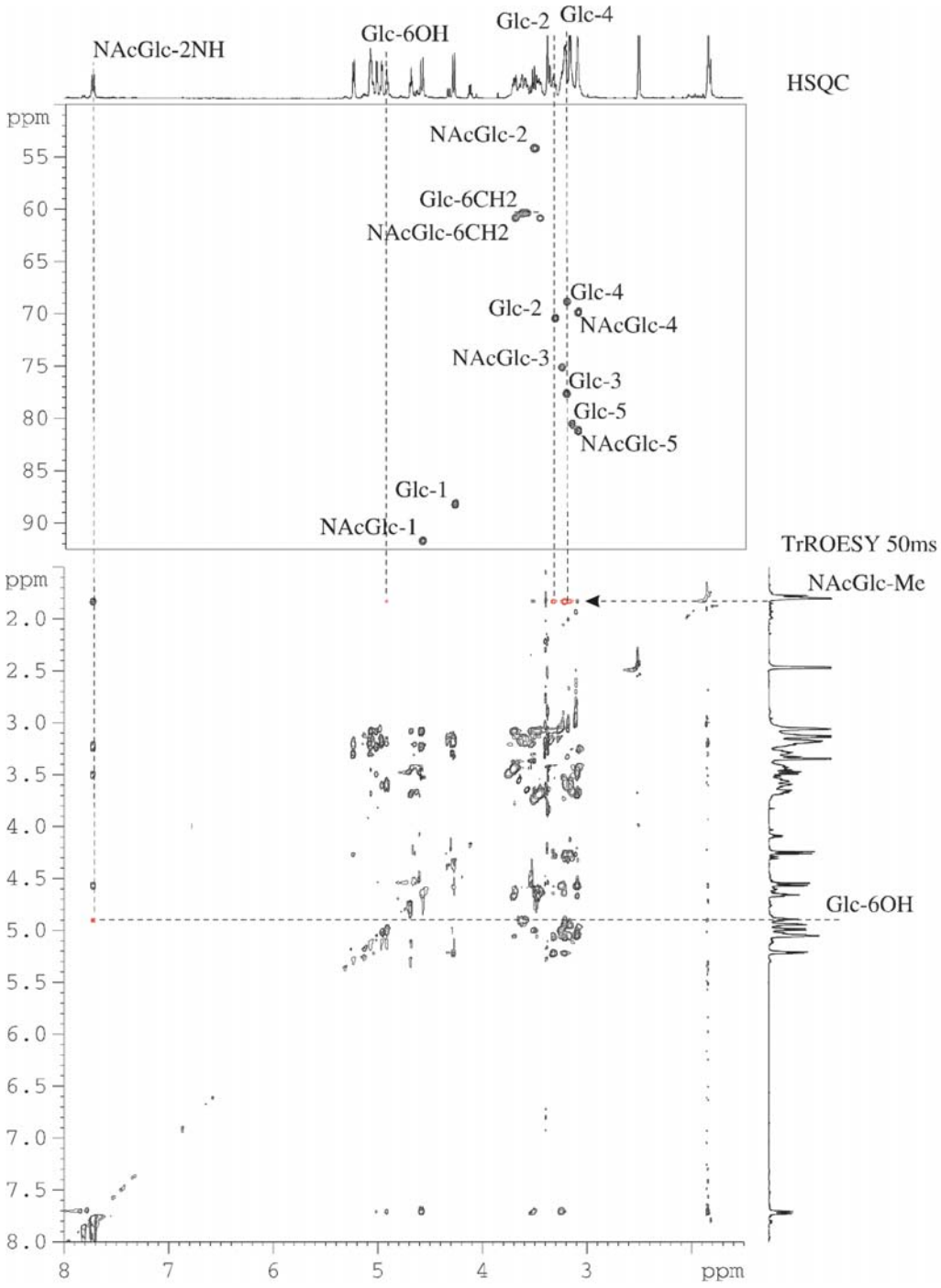

Figure 4.6 T-ROESY map of Glc-S-S-NAcGlc showing interannular connectivities

In conclusion, considerable conformational flexibility of the disaccharides studied in DMSO-d_6 solutions can be assumed from the large temperature coefficients and the sparse number or the complete lack of any interannular interresidue NOE/ROE interactions.

Residual dipolar couplings measured in dilute liquid crystalline media

One-bond ^{1}H-^{13}C RDCs measured for the Glc-S-S-Man and the Glc-S-S-Gal derivatives at various liquid crystal concentrations are listed in Table 4.5 and 4.6, respectively.

Table 4.5 One-bond heteronuclear RDCs (Hz) in Glc-S-S-Man at different liquid crystal concentrations

Assignment	7.5%	15%	30%
G1	3.2	4.9	10.5
G2	1.2	4.5	7.2
G3	4.7	6.5	8.1
G4	2.3	8.5	12.6
G5	1.7	3.4	7.9
M1	5.3	8.6	18.0
M3	5.5	7.6	15.8
M4	5.3	14.3	20.3
M5	7.3	12.4	20.5
M2	0.6	0.8	2.2

.

Table 4.6 One-bond heteronuclear RDCs (Hz) in Glc-S-S-Gal at different liquid crystal concentrations

Assignment	7.5%	15%	30%
G1	3.2	5.0	10.0
G2	2.2	3.6	6.8
G3	2.5	3.1	6.5
G4	2.8	5.2	9.1
G5	2.1	4.4	9.0
Ga1	2.9	4.5	8.3
Ga2	2.2	3.7	7.9
Ga3	1.5	2.8	6.4
Ga5	2.1	3.4	6.5
Ga4	-2.5	-5.5	-12.1

A random error of ca. 1-2Hz in the RDCs were observed using the modified F1 coupled HSQC technique described in chapter 5. The error was estimated by repeating the measurement. This error is hardly smaller than the effect measured at 7.5% total amphiphile concentration which is in agreement with the observation of Tjandra et al. (185). Martin-Pastor and Bush (186-187) also reported ±0.5Hz and ±0.8Hz error for the precision of the

original F1 coupled HSQC. In order to increase the effect to be measured, the liquid crystal concentration was increased to 15% and 30%. The RDCs are clearly showing an increasing tendency with the same random error of 1-2Hz as can be seen on Figure 4.7 and 4.8.

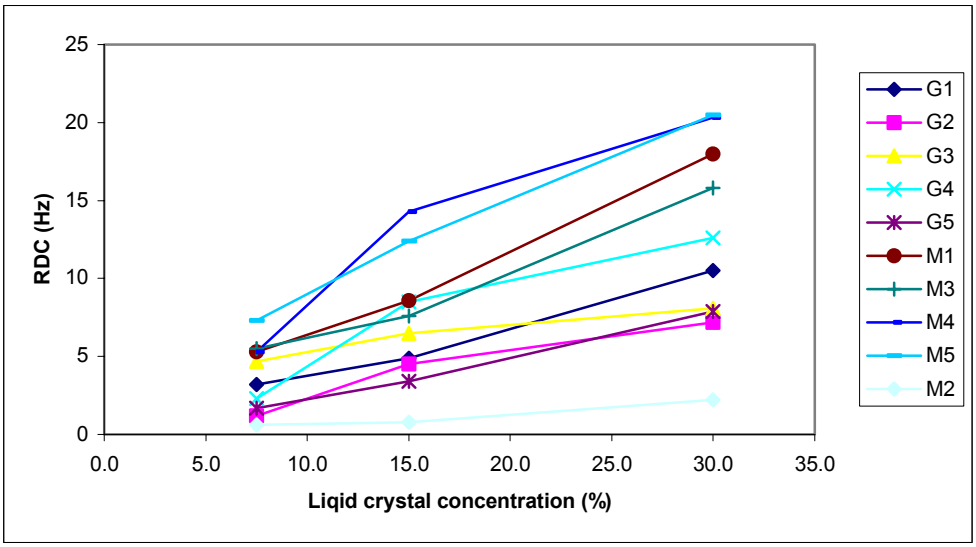

Figure 4.7 Changes of RDCs with the liquid crystal concentration for the Glc-S-S-Man derivative

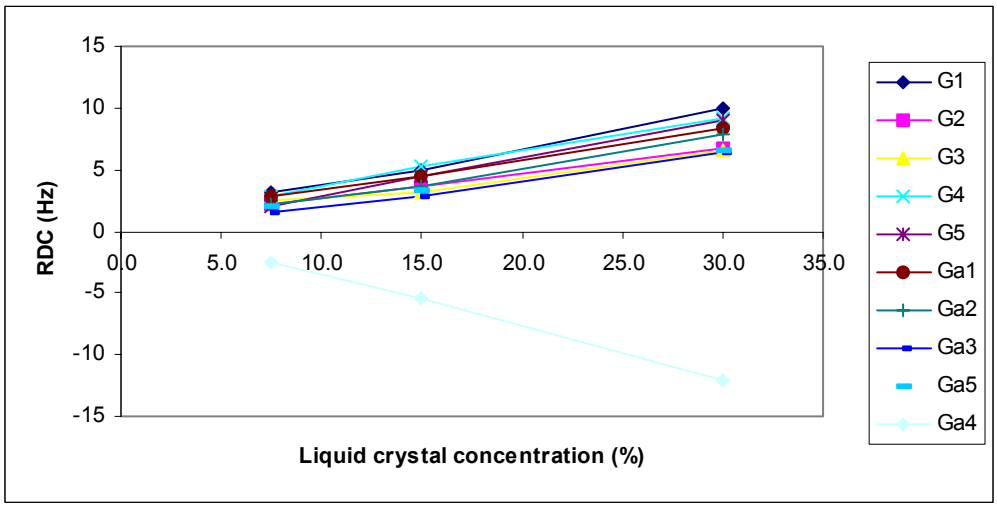

Figure 4.8 Changes of RDCs with the liquid crystal concentration for the Glc-S-S-Gal derivative

Relative magnitudes of the intraresidue RDCs reflect the stereochemistry at each carbon centre, since the ring geometries of the constituent monosaccharide residues in the oligosaccharide can be considered as rigid. The RDCs for the C1-H1, C2-H2, C3-H3, C4-H4 and C5-H-5 bond vectors of the glucose residue in Glc-S-S-Man and Glc-S-S-Gal are comparable at a given liquid crystal concentration reflecting a similar (axial) orientations of the ring protons (Figure 4.9). The RDCs for the glucose residue in the Glc-S-S-Man and in the Glc-S-S-Gal are plotted on Figure 4.10, respectively. The absolute values of the respective RDC are different for the glucose residue in the two molecules due to different alignments.

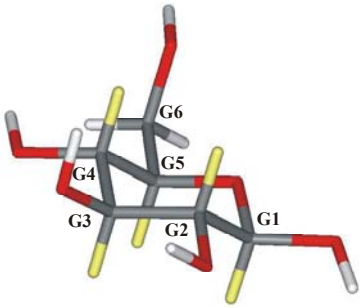

Figure 4.9 Axial orientation of the ^{1}H-^{13}C bond vectors in glucose highligthed in yellow

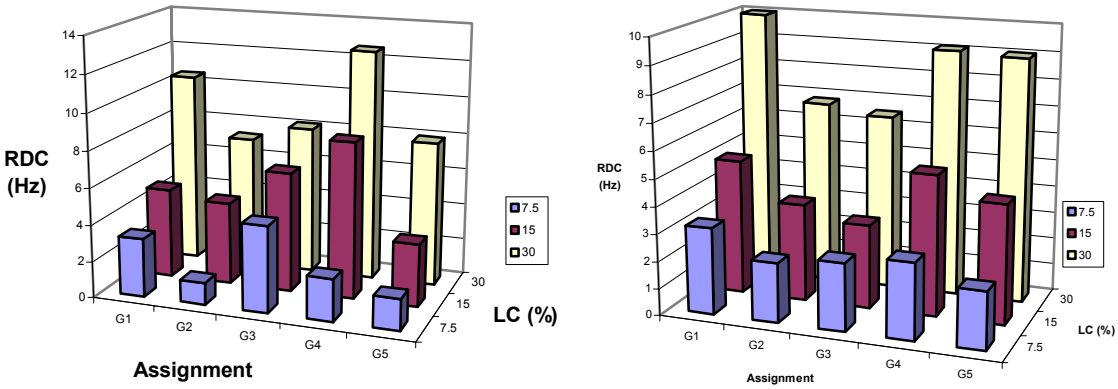

Figure 4.10 Distribution of RDCs belonging to axially aligned ^{1}H-^{13}C bond vectors in the glucose unit in Glc-S-S-Man (left) and in Glc-S-S-Gal (right) derivative at various liquid crystal concentrations

Similarly, the axial bond vectors of the mannose (C1, C3, C4, C5 in Figure 3.11) and galactose (C1, C2, C3, C5 in Figure 3.12) residues display fairly similar values when compared at the same liquid crystal concentration. In contrast, the RDC for the C2-H2 bond vector in mannose is very small and for the C4-H4 in galactose is a negative value, reflecting the equatorial orientation of the respective protons.

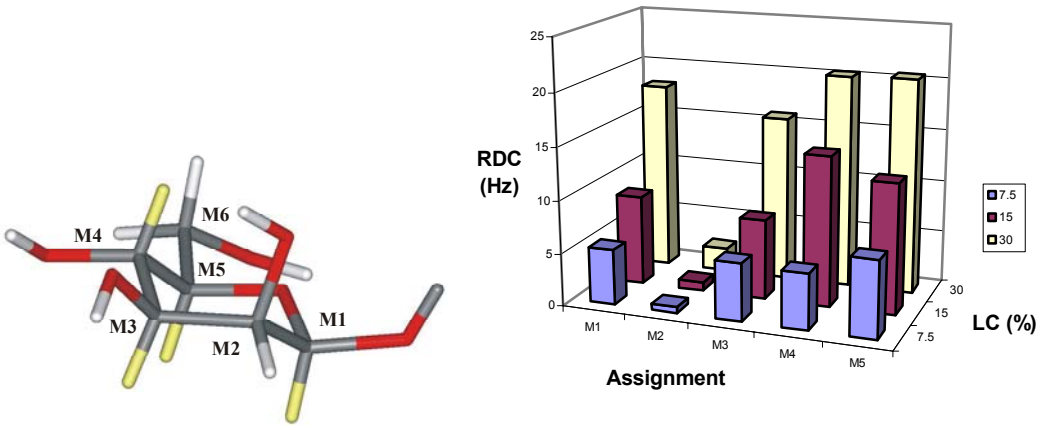

Figure 4.11 Orientation of the ^{1}H-^{13}C bond vectors in mannose and the distribution of RDCs for ^{1}H-^{13}C bond vectors in the mannose unit in Glc-S-S-Man derivative at various liquid crystal concentrations

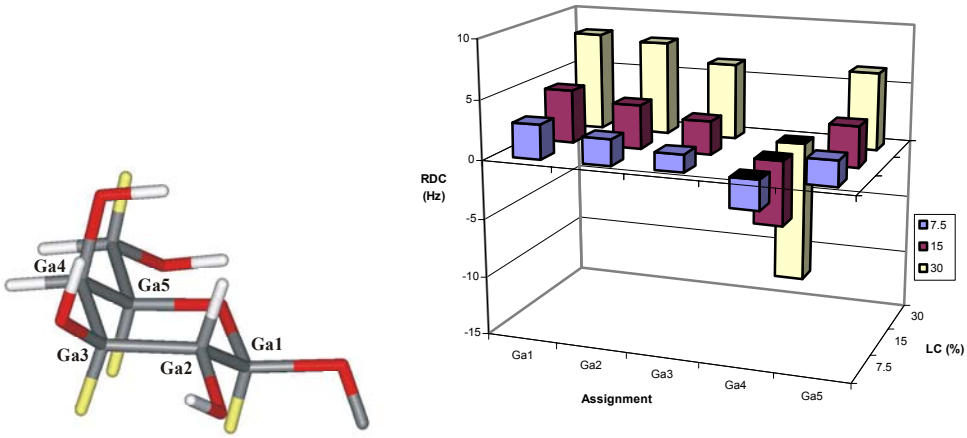

Figure 4.12 Orientation of the ^{1}H-^{13}C bond vectors in galactose and the distribution of RDCs for ^{1}H-^{13}C bond vectors in the galactose unit in Glc-S-S-Gal derivative at various liquid crystal concentrations

Since on the basis of the results obtained in DMSO solution no single conformer can be assumed for the disulfide disaccharides studied, hence alignment of each rigid unit must be determined. This requires 5 independent data for each monosaccharide ring. The 5 one-bond ^{1}H-^{13}C RDCs measured for the derivatives provide 1 independent data for the glucose residue and 2 independent data for the mannose and galactose residue. With lack of ^{1}H-^{1}H RDC data structure determination was not attempted thus far.

Computer aided conformational analysis

Since 3D structure determination of carbohydrates using NMR data is complicated by the time-averaged nature of the NMR observables, it is therefore necessary to rely more heavily upon modelling methods to calculate potential energy surfaces as an aid to interpretation of NMR data. In order to explore the conformational space available to the compounds conformational searches were carried out. The searches included systematic as well as stochastic searches. The molecular mechanics calculations were performed using the AMBER force field (188, 189) extended with Homans' carbohydrate parameters (190).

Calculations utilizing carbohydrate force-fields implicitly assume the existence of the exo-anomeric effect via incorporation into the parameter set of the force-field. The conformational behaviour of alpha and beta-anomeric linkages for C-, N- and S-glycosyl compounds were studied by Tvaroska et. al. (191). Ab-initio calculations were carried out on axially and equatorially 2-ethyl, 2-methylamino, 2-thiomethyl, and 2-methylammonio substituted derivatives of tetrahydropyran as model compounds. The exo-anomeric effect was found to decrease in the methoxy > methylamino > thiomethyl order, while the

methylammonio group did not show an exo-anomeric effect. For the equatorial form of the 2-thiomethyl tetrahydropyran derivative, the deepest rotational minimum appeared at -63.5° and the next deepest is at 58.3° and the third minimum is in the antiperiplanar region at 192.1°. Steric interactions in 2-thiomethyl tetrahydropyran conformers were found to be reduced, due to the larger C-S bond lengths resulting in smaller relative energies and barriers of rotation. Comparison of the differences between the bond lengths and bond angles for different conformers of 2-thiomethyl tetrahydropyran revealed clear and important structural changes characteristic of the exo-anomeric effect.

The calculations have been carried in vacuum. Simulations conducted in vacuum are usually dominated by conformations stabilized by intramolecular H bonds. In order to prevent formation of extensive H bonds that are not observed in polar solvents, a high dielectric constant is used to scale down electrostatic terms.

The flexible geometry systematic search (GS) was conducted around the interglycosidic linkage to obtain relaxed energy maps. The three glycosyl angles have been systematically rotated by 10^o increments that were followed by an energy minimization.

Simulated annealing (SA) procedure has been applied to obtain an ensemble of structures. 1000 structures were generated for analysis.

The conformers obtained by the procedures were analysed by identifying low energy conformational families by creating isoenergetic three dimensional surfaces according to the three interglycosidic angles. The interglycosidic torsion angles and potential energies of the structures were summarized and analysed.

Flexible geometry systematic search or grid search (GS)

Systematic search around the Φ_A, Φ_B and ω angles resulted in 18 minima in the conformational space for each three disaccharides investigated. In general, the two Φ angles (Figure 4.2) indicate staggered conformations around the C1-S bond ($+60^o$ and 300^o (or -60^o) for synclinal and 180^o for antiperiplanar arrangements, respectively), whereas the conformation around the disulfide bond, ω, was found to be close to $\pm 90^o$. The conformations are listed in Table 4.7. A simplified scheme of the conformational space with the location of the 18 conformational families is depicted as an illustration in Figure 4.13.

The interglycosidic torsional angles of low energy conformations identified by the flexible geometry search are listed in Table 4.8. The Φ angles have a $\pm 10^o$ deviation from the staggered conformations around the C1-S bond, while the spread of ω angle with a range of

±30° around ±90° were found. The potential energies listed in Table 4.8 were obtained by subtracting the lowest E_{pot} from the higher ones since the absolute value of the force-field potential energy has no physical meaning.

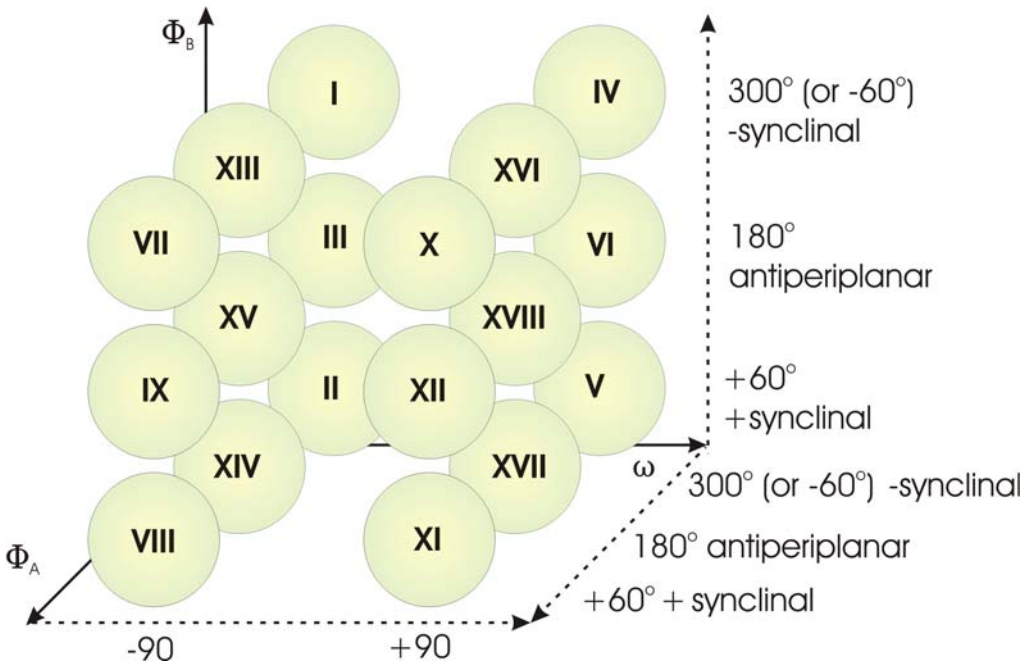

Figure 4.13 Simplified scheme of the conformational hyperspace

Table 4.7 The 18 conformational family resulting from the combination of the three torsion angles where the Φ angles are arranged in staggered conformations around the C1-S bond, that is ±60° for synclinal arrangements and 180° for antiperiplanar arrangement, whereas the ω angle is close to ±90°.

#	$\Phi_{Glc(O-C-S-S)}$	$\omega_{C-S-S-C}$	$\Phi_{(S-S-C-O)}$
I	- synclinal	-90	- synclinal
II	- synclinal	-90	+ synclinal
III	- synclinal	-90	antiperiplanar
IV	- synclinal	+90	- synclinal
V	- synclinal	+90	+ synclinal
VI	- synclinal	+90	antiperiplanar
VII	+ synclinal	-90	- synclinal
VIII	+ synclinal	-90	+ synclinal
IX	+ synclinal	-90	antiperiplanar
X	+ synclinal	+90	- synclinal
XI	+ synclinal	+90	+ synclinal
XII	+ synclinal	+90	antiperiplanar
XIII	antiperiplanar	-90	- synclinal
XIV	antiperiplanar	-90	+ synclinal
XV	antiperiplanar	-90	antiperiplanar
XVI	antiperiplanar	+90	- synclinal
XVII	antiperiplanar	+90	+ synclinal
XVIII	antiperiplanar	+90	antiperiplanar

Table 4.8 Low energy conformations resulting from flexible geometry systematic conformational search

Glc-S-S-Man					Glc-S-S-Gal					Glc-S-S-NAcGlc				
	Φ_A	ω,	Φ_B	E_{pot} (kcal/mol)		Φ_A	ω,		E_{pot} (kcal/mol)		Φ_A	ω,	Φ_B	E_{pot} (kcal/mol)
IV	300	109	300	0.0	**II**	300	270		0.00	**VII**	70	280	300	0.00
I	300	280	300	0.2	**I**	309	280		0.30	**I**	300	280	290	0.05
VII	60	270	300	0.3	**IV**	300	109		0.33	**II**	300	270	60	0.57
VI	300	90	190	0.4	**VII**	60	270	300	0.44	**IV**	291	109	300	1.37
	51	110	300	0.8	**V**		110	51	0.93	**V**	310	111		1.53
III	300	260	189		**X**	51	110	300	0.98	**VIII**		251	60	1.69
IX	60		190	0.9	**VI**	300	90	200		**VI**	300	81	190	1.73
II	300	270	50	1.1	**VIII**	60		51	1.37	**X**	51	110	300	
XII	60	99	190	1.3		200	90	300	1.79	**XII**	51		200	2.61
XVI	181	89		2.0	**XVII**	200	99	60	2.42		181	90	60	2.64
VIII		259	50	2.1	**XII**	60	91		2.66	**XVI**	181	90	300	2.71
	301	110	60	2.7	**XIII**		259	290	2.98	**XIII**	180	260		2.93
XVIII	200	80	190	2.8	**III**	300	259	189	3.01	**XI**	59	129	59	3.63
XIII	181	260	300	3.1	**IX**	59	251	180	3.23	**IX**	50	249	190	
XIV	181	251	50	4.3	**XI**	60	121	60	3.27	**XIV**	181	250	60	3.92
XVII	200	100	60	4.6	**XIV**	181	250	60	3.30	**III**	300	260	180	4.47
XI	50	121	60	5.5	**XVIII**	200	80	200	3.56	**XVIII**	182	70	190	4.55
XV	180	239	190	5.8	**XV**	190	239	190	6.00	**XV**	181	239	190	7.32

Table 4.9 Low energy conformations resulting from simulated annealing sorted according to decreasing potential energy. N stands for the number structures generated.

Glc-S-S-Man						Glc-S-S-Gal						Glc-S-S-NAcGlc					
#	Φ_A	ω,	Φ_B	N	E_{pot} (kcal/mol)	#	Φ_A	ω,	Φ_B	N	E_{pot} (kcal/mol)	#	Φ_A	ω,	Φ_B	N	E_{pot} (kcal/mol)
IV	301	103	303	76	0	**IV**	300	104	301	76	0.00	VII	56	269	290	117	0.00
I	300	277	301	269	0.98	**II**	298	271	58	98	1.04	IV	301	104	301	85	0.47
VII	59	271	300	119	1.00	**VII**	58	270	298	102	1.14	II	296	270	58	112	0.85
VI	299	90	187	112	1.12	**I**	300	277	300	207	1.33	I	303	280	296	266	0.94
X	56	109	302	27	1.58	**V**	301	110	56	36	1.92	VIII	57	255	58	35	1.42
XVI	203	89	301	85	1.61	**VIII**	57	256	55	36	1.96	VI	299	83	188	87	1.78
III	301	263	185	62	1.73	**VI**	301	90	199	109	2.14	X	56	110	301	40	1.84
II	297	271	49	67	1.77	**XVI**	203	89	301	105	2.16	XVI	202	89	300	86	2.14
IX	60	252	189	23	2.14	**X**	55	109	299	41	2.20	XVII	189	92	56	28	2.24
XII	59	97	185	44	2.22	**XVII**	198	95	59	37	3.39	V	302	113	54	17	2.78
VIII	58	254	53	10	2.81	**XII**	59	95	194	38	3.48	XII	59	94	196	25	3.26
XVIII	195	82	186	42	3.22	**XIII**	187	260	297	31	3.69	XIII	187	260	296	44	3.49
V	305	109	60	15	3.44	**III**	297	260	187	27	3.82	XI	55	121	51	7	3.71
XIII	187	260	298	41	3.63	**IX**	54	253	185	15	4.03	XIV	185	252	56	8	4.17
XVII	198	100	56	10	5.09	**XI**	54	120	54	11	4.37	III	304	259	181	26	4.23
XIV	186	254	46	6	5.58	**XIV**	185	252	54	11	4.42	XVIII	195	81	197	26	4.63
XV	183	237	189	4	6.41	**XVIII**	195	81	195	32	4.65	IX	53	250	188	7	4.74
XI	52	123	58	6	6.45	**XV**	190	237	190	6	7.43	XV	188	237	190	2	11.73

Three dimensional potential energy surfaces of the derivatives are presented for each derivative. The dimensions are generated by the three torsion angles of the interglycosidic linkage, the colours changing from blue to green to yellow to red and finally to black indicate the magnitude of the E_{pot} for a particular conformation. The PES was further characterized by creating 2 dimensional cross-sections (see in Appendix E, F and G). The energy barriers between conformers can also be investigated by examining at E_{pot} values at the saddle points. The widths and the shapes of the minimum energy wells can be assessed by studying the 3D conformational space.

The relative thermodynamic stability of the conformational families is reflected by the differences in conformational energies. It should be noticed, however, that the accuracy of the E_{pot} values corresponding to conformer families generated by the grid search (GS) is limited, since the minimum conformers are calculated at the grid points, not at the precise location of the minima.

Simulated annealing (SA)

The simulated annealing calculations consistently resulted in a similar set of 18 minima in the conformational space (Figure 4.19) for each three disaccharides investigated. The torsion angles of the lowest energy conformers are listed in Table 4.9 in the order of decreasing potential energy. The number of structures generated in the family is also listed. The Φ angles range from $\pm 50^{o}$ to $\pm 60^{o}$ for synclinal arrangements and between 180^{o} and 200^{o} for antiperiplanar conformation, while the ω angle is spread over larger range of $\pm 30^{o}$ around $\pm 90^{o}$.

Relative thermodynamic stability of the 18 conformations as reflected by the E_{pot} is compared with the values resulting from the grid search in the following discussion for each three disaccharide. The relative magnitude E_{pot} corresponding to the conformation families calculated by simulated annealing are more reliable for accessing relative thermodynamic stability since the minimum is precisely located by the simulation.

The conformational families are also characterized by comparing the number structures generated by the SA. The family with the highest number of structures and lowest energy conformer does not necessarily coincide. The number of structures generated for a given family is more determined by the shape or width of the minimum energy well than its potential energy.

Analysis

The E_{pot} difference between the highest and lowest energy conformer is only ca. 4-6 kcal/mol indicating the presence of multiple conformers (not considering the last high energy structures). The largest range of E_{pot} is observed for Glc-S-S-Man, while the smallest for Glc-S-S-Gal, which is roughly the same as for Glc-S-S-NAcGlc according to the SA.

Table 4.9 E_{pot} difference between the highest and lowest energy conformers for the derivatives

	E_{pot} of the highest energy conformer	
	GS	**SA**
Glc-S-S-Man	5.8	6.45
Glc-S-S-Gal	3.56	4.65
Glc-S-S-NAcGlc	4.55	4.77

The 3D PES's of the derivatives as calculated by the GS is depicted in the left hand side in Figure 4.14 (2D cross-section4 at Appendix E, F and G). The structures generated by the SA are shown in the right side of Figure 4.14.

4 wider and another 5 medium sized energy well as denoted on the left side of Figure 4.14 is observed in the conformational surface of Glc-S-S-Man (I, VII, IV, VI and III, II, IX, X, XII)) and Glc-S-S-Gal (II, I, VII, IV and VIII, X, VI, V, XVI). The former group of structures correspond to the first 4 lowest energy conformational family, whereas the latter match low energy conformations from the 5th to 9th. As opposed to the other two molecules there is only 3 wider minima (VII, I, II as denoted on the left side of Figure 3.14c) detected on the 3D hyperspace for the Glc-S-S-NAcGlc derivative with others of significantly smaller sizes. This group of structures correspond to the first 3 lowest energy conformational family in the GS.

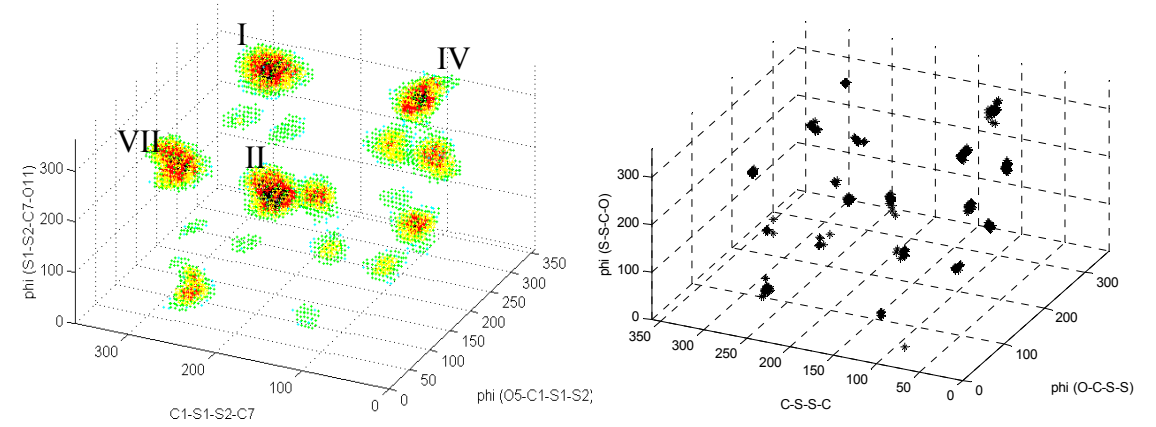

a) Glc-S-S-Man

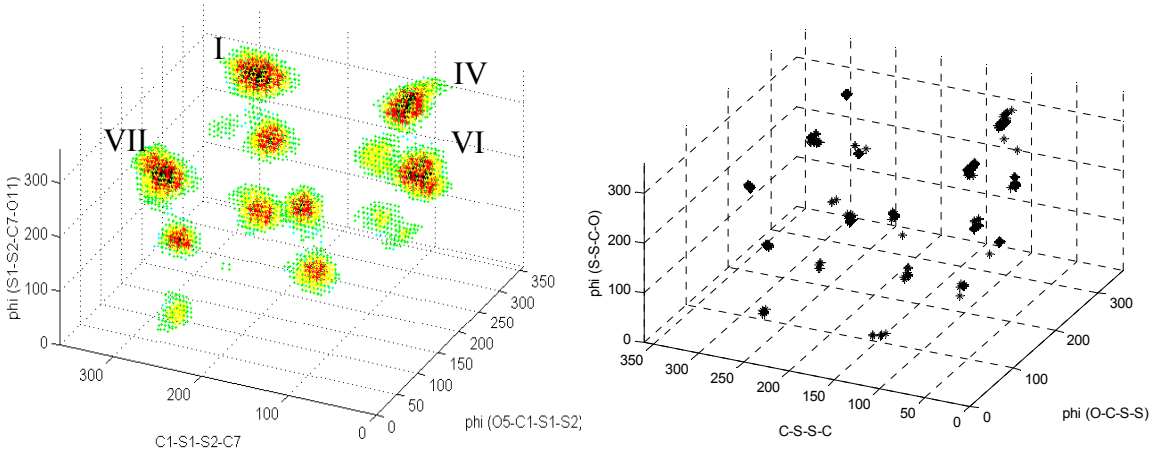

b) Glc-S-S-Gal

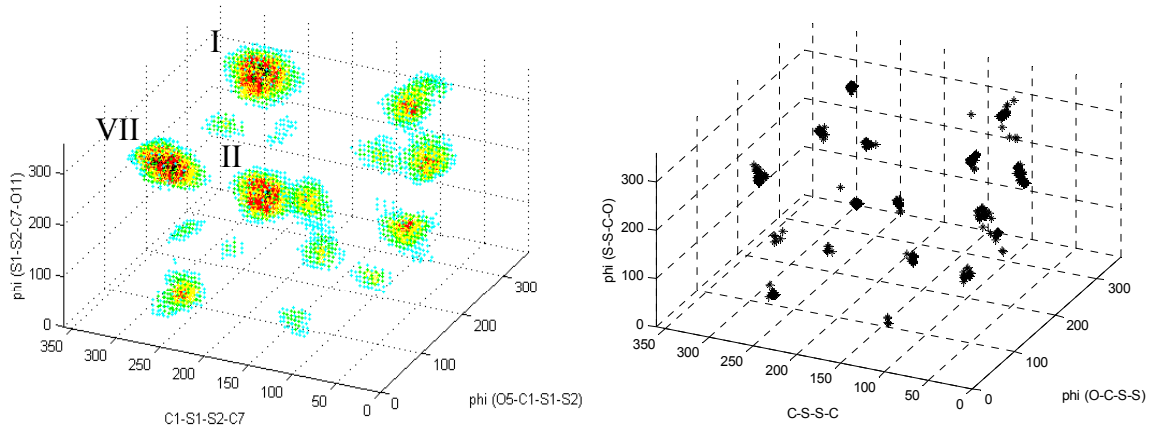

c) Glc-S-S-NAcGlc

Figure 4.14 Left: 3D PES resulting from flexible geometry conformational search by plotting energies of conformers versus interglycosidic torsion angles, Right: Structures from simulated annealing plotting interglycosidic torsion angles of the structures generated.

In order to visualize the tendencies in thermodynamic stability within the conformational families, the potential energies computed by the GS and the SA and the number of structures generated by the SA have been plotted with decreasing values in Figure 4.15, 4.17 and 4.19 for Glc-S-S-Man, Glc-S-S-Gal and Glc-S-S-NAcGlc, respectively. In all cases an overall steady decline is observed in the change of the E_{pot} with somewhat larger stepwise alterations at the positions indicated by arrows. These changes are more pronounced for Glc-S-S-Gal and Glc-S-S-Man, whereas the E_{pot} smoothly, gradually changes for Glc-S-S-NAcGlc. These changes suggest existence of subgroups of low energy of conformations for Glc-S-S-Gal and Glc-S-S-Man. For instance, the 1st low energy conformer (IV) is ca. 1 kcal/mol more stable than the 2nd. Then from the 2nd to 4th low energy conformations have similar energies within ca. 1.1 kcal/mol (see Table 4.10). These first 4 low energy structures also belong to the wider energy wells on the 3D PES. An analogous cluster is observed from the 5th to the 9th low energy structures (within ca. 2.2 kcal/mol). Furthermore, the last conformations are of considerably higher E_{pot} for Glc-S-S-Gal and Glc-S-S-NAcGlc.

Table 4.10 Subgroup of conformers characterized by the energy of the last conformation.

	E_{pot} of the last conformer (kcal/mol)		
	Glc-S-S-Man	**Glc-S-S-Gal**	**Glc-S-S-NAcGlc**
first 4 lowest energy conformation	1.12	1.33	0.94
first 9 lowest energy conformation	2.14	2.20	2.24

Structures II and IV are in agreement with the NOE found between Glc2-OH/Gal6-OH observed for Glc-S-S-Gal as indicated by straight lines in Figure 4.18.

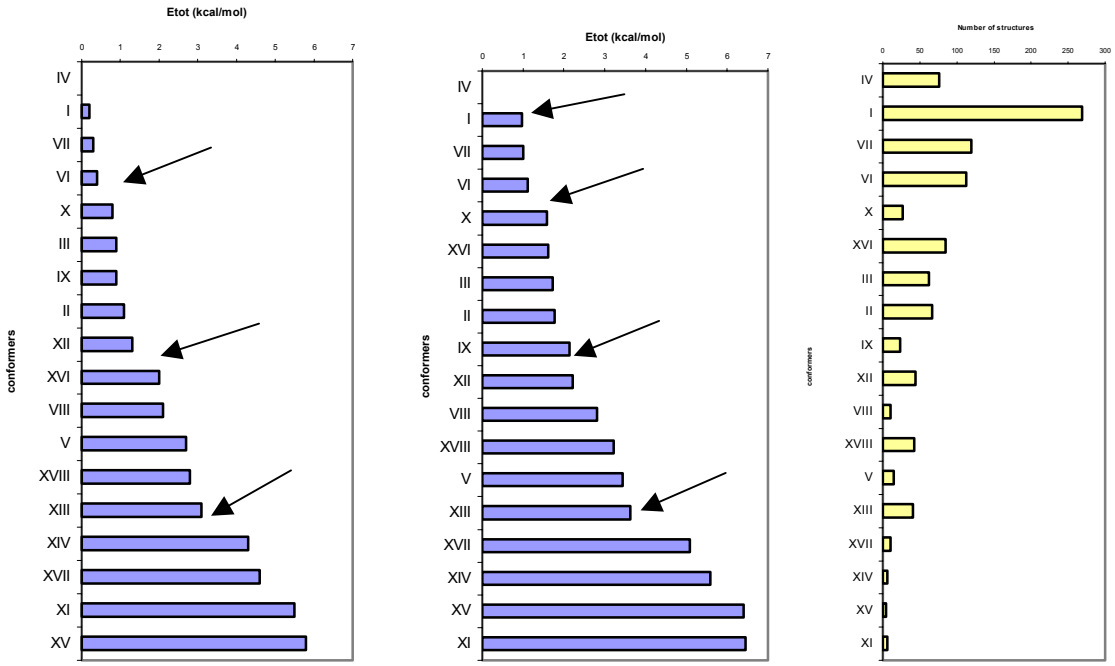

a **b** **c**

Figure 4.15 Thermodynamic stability according to the distribution of the conformational energy within the 18 families for Glc-S-S-Man (a) in grid search, b) simulated annealing, and c) shows the number of structures generated in simulated annealing

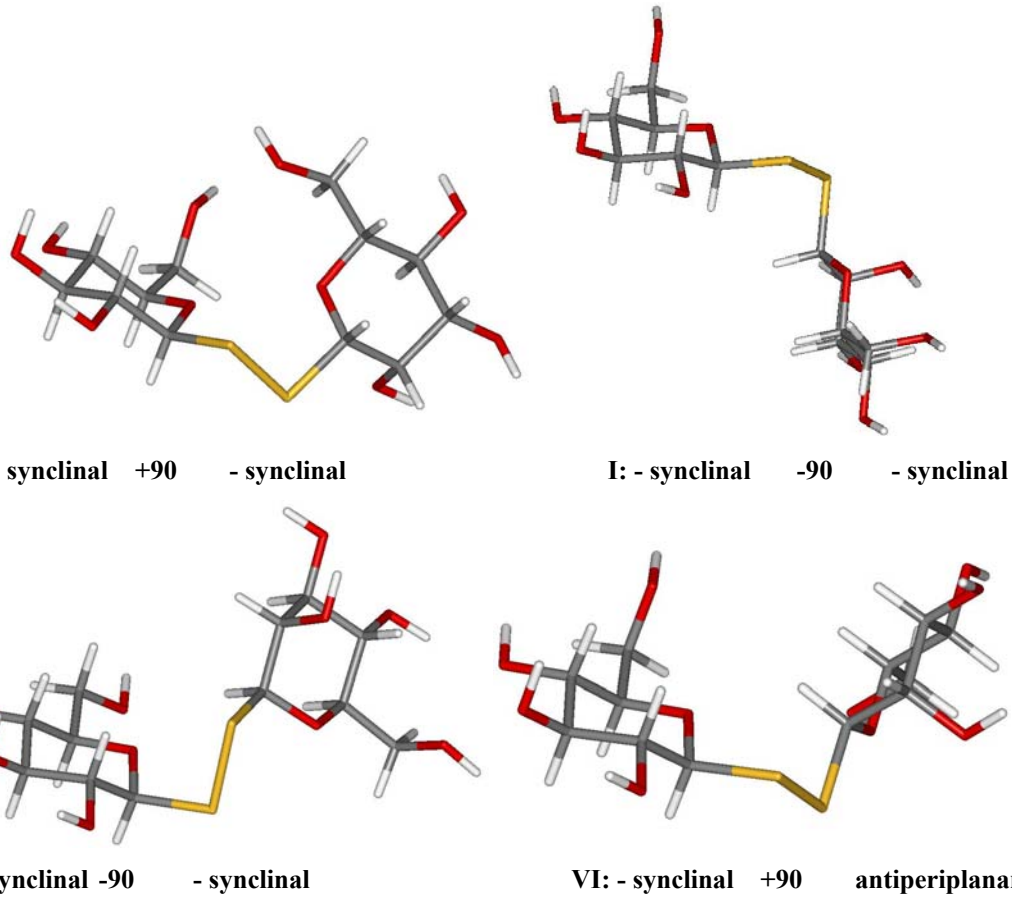

IV: - synclinal +90 - synclinal **I: - synclinal -90 - synclinal**

VII: + synclinal -90 - synclinal **VI: - synclinal +90 antiperiplanar**

Figure 4.16 The structures of the conformations VI and I for Glc-S-S-Man with the glucose residue aligned at the same orientation.

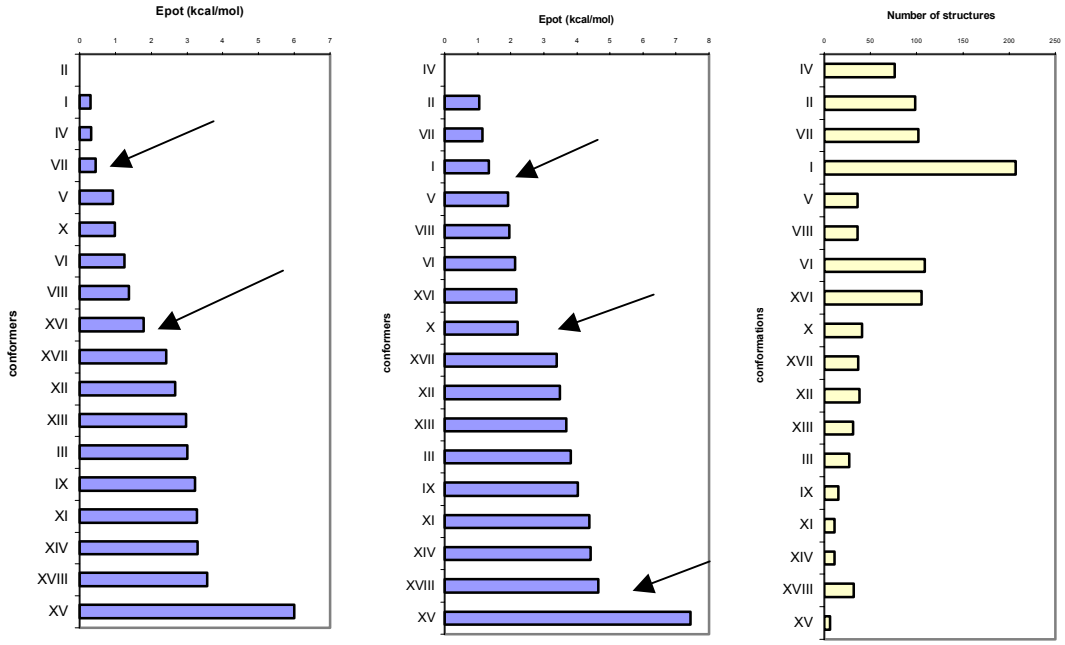

a **b** **c**

Figure 4.17 Thermodynamic stability according to the distribution of the conformational energy within the 18 families for Glc-S-S-Gal (a) in the grid search, b) simulated annealing, and c) shows the number of structures generated in the simulated annealing

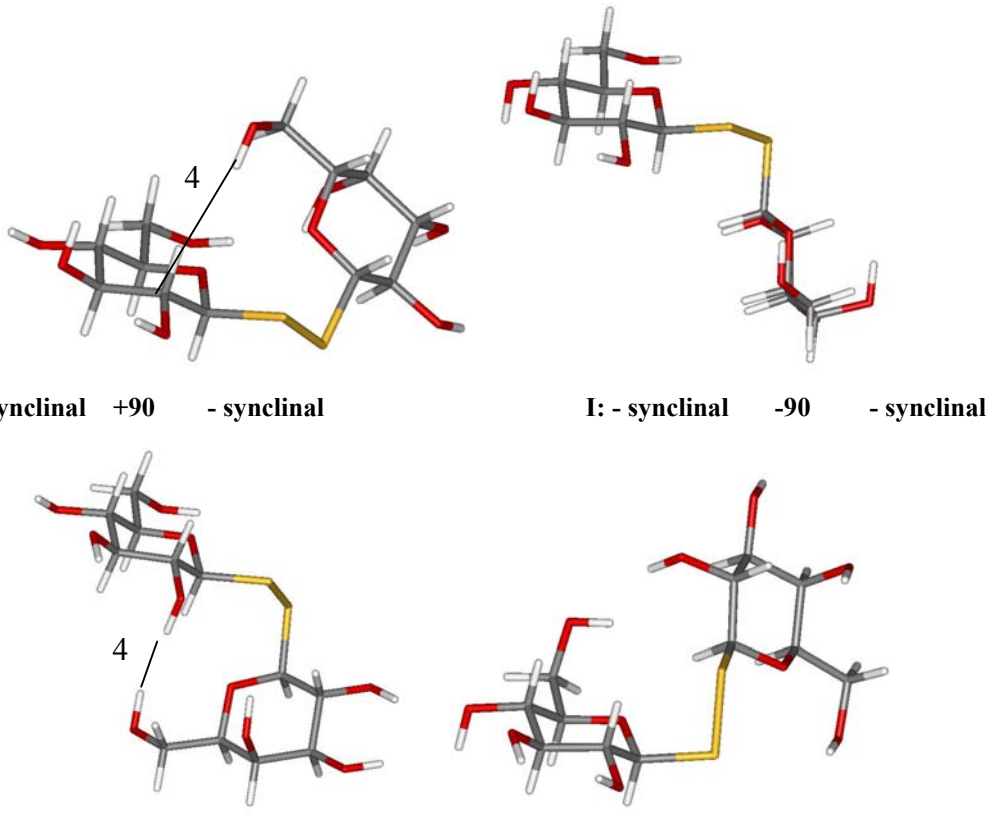

IV: - synclinal +90 - synclinal **I: - synclinal -90 - synclinal**

II: - synclinal -90 + synclinal **VII: + synclinal -90 - synclinal**

Figure 4.18 The structures of conformations I, VI, II, and VII for Glc-S-S-Gal with the glucose residue aligned at the same orientation. ^{1}H-^{1}H distances observed experimentally are highligthed.

Structure VII satisfies all of the NOEs found, while conformer I satisfies spatial proximity between Glc6-OH/NAcGlc2-Me and Glc6-OH/NAcGlc2-NH detected for Glc-S-S-NAcGlc as indicated by the lines in Figure 4.20. It is important to note this structure is only the 3rd and 4th lowest energy conformer for the other two derivatives, whereas it is the 1st one for Glc-S-S-NAcGlc. The temperature coefficient for the NAcGlc-2NH was observed to be -3.8 ppb/K, while all the others are in the range of - 6-8 ppb/K. All these facts can be rationalized if we examine conformer VII and realize the possibility of an interresidual H bond between the NAcGlc-2NH and Glc-6OH. The corresponding distance between the NH hydrogen and the oxygen is 2.03A, while the angle formed by the O - H - N atoms is 171.3^{o}. This conformation is also very probable for the other two derivatives as well where there is an OH group in the place of the amide group. The hydrogen of the OH group is, however, much more polarized due to higher electronegativity of the oxygen and therefore more likely to be involved in exchange with the solvent. Furthermore, the assumed H bond is further stabilized by a steric hinderance between the acetyl methyl group and the hydrogens of the sugar ring. The intermediate value of the NH temperature coefficient is likely the result of fast exchange with other conformations where this interaction is not present.

This grouping of structures is supported by the tendencies observed in the changes of the number of structures generated by the SA. The first 4 low energy conformer accounts for ca. 58% of the total number of structures generated by the SA for Glc-S-S-Man and Glc-S-S-NAcGlc and only for 48.3% for Glc-S-S-Gal (data listed in Table 4.11). The first 9 conformational families in the E_{pot} listing sum upto ca. 85% of the total 1000 structures for Glc-S-S-Man and Glc-S-S-NAcGlc, and only for 81% in the case of Glc-S-S-Gal.

3 conformer within the first 4 lowest energy structures are identical for all three derivatives with small variations in the E_{pot}: IV, I and VII. The structures of first 4 lowest energy are shown in Figure 4.16, 4.18 and 4.20 for Glc-S-S-Man, Glc-S-S-Gal and Glc-S-S-NAcGlc, respectively.

Table 4.11 Subgroup of conformers characterized by the fraction of structures accounted for and the energy of the last conformation.

	Fraction of structures represented by the subgroup		
	Glc-S-S-Man	**Glc-S-S-Gal**	**Glc-S-S-NAcGlc**
first 4 lowest energy conformation	57.6%	48.3%	58.6%
first 9 lowest energy conformation	84.0%	81.0%	85.6%

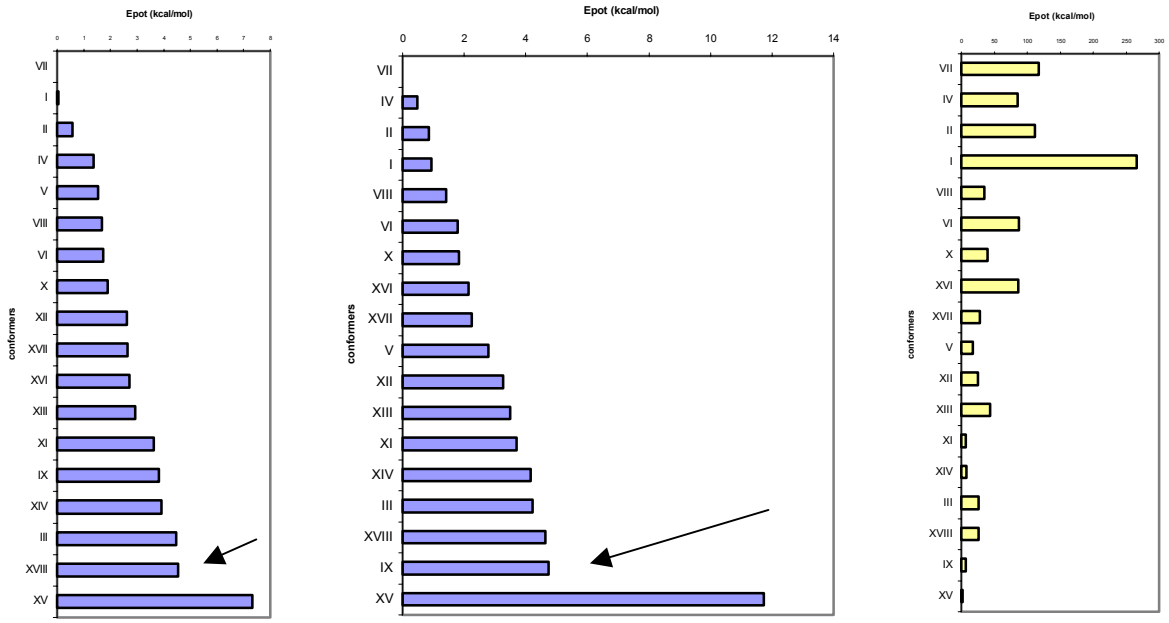

a **b** **c**

Figure 4.19 Thermodynamic stability according to the distribution of the conformational energy within the 18 families for Glc-S-S-NAcGlc (a) in grid search, b) simulated annealing, and c) shows to the number of structures generated in simulated annealing

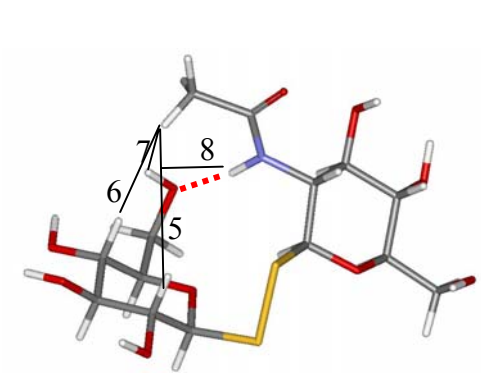

VII: + synclinal +90 - synclinal

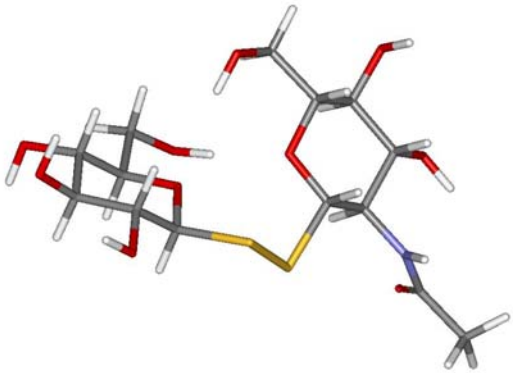

IV: - synclinal +90 - synclinal

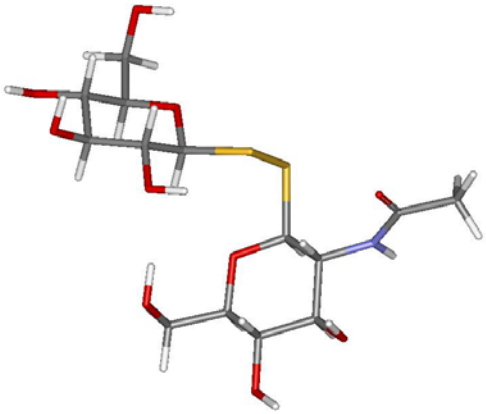

II: - synclinal -90 + synclinal

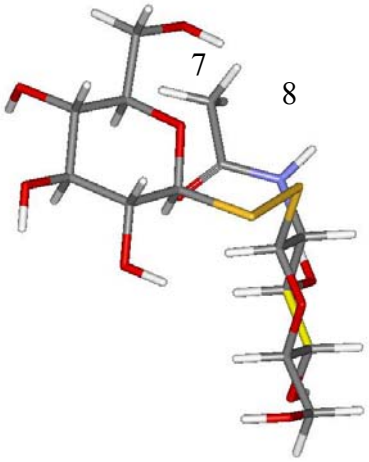

I: - synclinal -90 - synclinal

Figure 4.20 The structures of conformations VII, IV II and I for Glc-S-S-NAcGlc with the glucose residue aligned at the same orientation. ^{1}H-^{1}H distances observed experimentally are highligthed.

Both conformer I and VI feature double exo-anomeric effects possessing -synclinal arrangements at the Φ angles close to the sugar residues, whereas most of the conformers among the first 9 low energy structures incorporate at least one exo-anomeric effect as listed in Table 4.12. Conformations with exo-anomeric effects are marked with bold font in Table 4.12.

#	$\Phi_{Glc(O-C-S-S)}$	$\omega_{C-S-S-C}$	$\Phi_{Man(S-S-C-O)}$
IV	**- synclinal**	+90	**- synclinal**
I	**- synclinal**	-90	**- synclinal**
VII	+ synclinal	-90	**- synclinal**
VI	**- synclinal**	+90	antiperiplanar
X	+ synclinal	+90	**- synclinal**
XVI	antiperiplanar	-90	+ synclinal
III	**- synclinal**	-90	antiperiplanar
II	**- synclinal**	-90	+ synclinal
IX	+ synclinal	-90	antiperiplanar

#	$\Phi_{Glc(O-C-S-S)}$	$\omega_{C-S-S-C}$	$\Phi_{Gal(S-S-C-O)}$
IV	**- synclinal**	+90	**- synclinal**
II	**- synclinal**	-90	+ synclinal
VII	+ synclinal	-90	**- synclinal**
I	**- synclinal**	-90	**- synclinal**
V	**- synclinal**	+90	+ synclinal
VIII	+ synclinal	-90	+ synclinal
VI	**- synclinal**	+90	antiperiplanar
XVI	antiperiplanar	+90	**- synclinal**
X	+ synclinal	+90	**- synclinal**

#	$\Phi_{Glc(O-C-S-S)}$	$\omega_{C-S-S-C}$	$\Phi_{NAcGlc(S-S-C-O)}$
VII	+ synclinal	-90	**- synclinal**
IV	**- synclinal**	+90	**- synclinal**
II	**- synclinal**	-90	+ synclinal
I	**- synclinal**	-90	**- synclinal**
VIII	+ synclinal	-90	+ synclinal
VI	**- synclinal**	+90	antiperiplanar
X	+ synclinal	+90	**- synclinal**
XVI	antiperiplanar	+90	**- synclinal**
XVII	antiperiplanar	+90	+ synclinal

Table 4.12 Most probable conformers listed in the order of increasing E_{pot} calculated by SA for Glc-S-S-Man (first table), for Glc-S-S-NAcGlc (second table) and for Glc-S-S-Gal (third table)

4.5 Conclusion

Temperature coefficients for the hydroxide and amide protons indicate that labile protons were exposed to the solvent and not involved in hydrogen bonding. Only a few conformationally relevant interannular NOEs contacts were found for all three derivatives. Relative magnitudes of the intraresidue RDCs were interpreted in terms of the stereochemistry at each carbon centre. The 5 one-bond ^{1}H-^{13}C RDCs measured for each sugar ring provide 1 independent data for the glucose residue and 2 independent data for the mannose and galactose residue. Since determination of alignment tensor for the individual monosaccharide units which is required for flexible oligosaccharides were not possible with lack of ^{1}H-^{1}H RDC data, therefore structure determination on the basis of RDCs was not attempted thus far.

Systematic search around the Φ_A, Φ_B and ω angles as well as simulated annealing calculations consistently resulted in 18 minima in the conformational space for each of the 3 disaccharides investigated. The Φ angles close to the sugar residues are featuring the angles of the staggered conformations around the C1-S bond, that is $+60^o$ and -60^o) for synclinal arrangements and 180^o for antiperiplanar arrangement, whereas the conformation around the disulfide bond, ω, were found to be close to $\pm 90^o$.

On the basis of the distribution of the E pot and the number of structures generated by SA conformational families were divided into subgroups of low energy of conformations. The larger subgroup includes the first 9 lowest energy conformations. Within these, separate subgroup incorporating the first 4 lowest energy structures can be distinguished. 3 conformers IV, I and VII within the latter group were found to be identical for all three derivatives with insignificant variation in the E_{pot}.

Conformers featuring exo-anomeric effect at their Φ angles dominate among the low energy conformers. The conformations with double exo-anomeric effect are among the first 3 lowest energy conformers with conformer IV being the lowest energy conformer in the listing of SA (with the exception for Glc-S-S-NAcGlc where VII is more stable by 0.47 kcal/mol) and conformer I being the most abundant one in SA.

None of the minimum conformation can be used as 'single state model' to satisfactorily account for the experimental data observed. It is shown the interglycosidic linkage in the disulfide disaccharide derivatives must be treated as a flexible entity to account for the experimental data. Intraresidual NOEs were found to be in agreement with conformations among low energy structures.

Existence of H bonding interaction can be assumed in conformer VII in derivative Glc-S-S-NAcGlc between with NAcGlc-2NH being the H donor and the acceptor provided by the oxygen in the Glc-6OH group. This assumption is based on the intermediate value of the temperature coefficient for NAcGlc-2NH, comparison of the E_{pot} energy order between derivatives, the presence of 4 interresidual NOEs which are satisfied by conformer VII and finally by the arrangement of the three atoms involved which is characteristic of the geometry of a H bond.

Experimental data suggested the presence of several different, time-averaged conformations, however the computational results were indicative of definite conformational preferences in these novel disulfide disaccharide mimics. Thus, the increase of the degrees of motional freedom, expected a priori upon extension of the interglycosidic linkage, gets largely offset by stereoelectronic effects, such as the exo-anomeric effect and the preference of the disulfide torsion angle towards 90^{o}.

IMPROVING METHODS

FOR DETERMINATION OF NMR PARAMETERS

5. ACCURATE DETERMINATION OF SMALL ONE-BOND HETERONUCLEAR RESIDUAL DIPOLAR COUPLINGS WITH A MODIFIED F1 COUPLED HETERONUCLEAR CORRELATION EXPERIMENT

5.1 Measurement one-bond heteronuclear scalar and residual dipolar couplings by conventional NMR techniques

Measurement of the residual dipolar contributions presents a considerable experimental challenge for small flexible molecules whereas the RDCs are often small due to the effects of dynamics (192). Spherical shape of the molecules may also result in low degree of alignment yielding only small RDCs (193-194).

One-bond heteronuclear coupling constant can be measured by various well-established NMR methods ranging from coupled heteronuclear spectra as the simplest approach, heteronuclear *J* resolved spectra, or coupled heteronuclear correlation spectra. The coupling constant information is obtained as a frequency difference between splittings for these experiments. In choosing the best method one should consider issues regarding sensitivity which is directly connected to the required measurement time, various factors influencing the straightforwardness of the coupling constant extraction. The extraction of the coupling constant may be complicated by spectral overlap, strong coupling effects and the presence of additional splittings apart from the desired coupling to be measured. The various experimental problems will be demonstrated on saccharose depicted on Figure 5. 1.

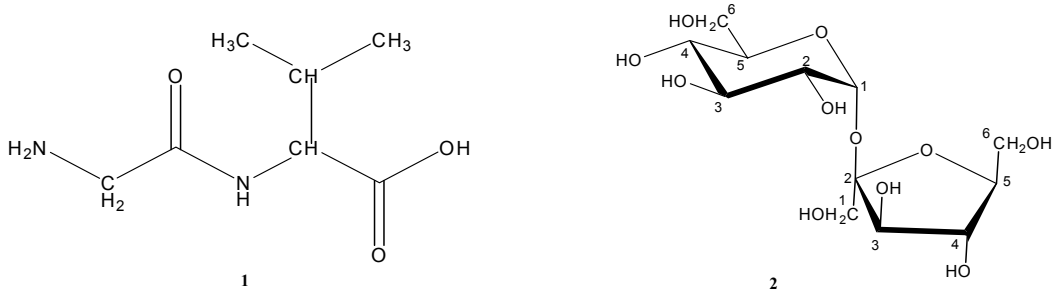

Figure 5.1 Formula of GlyVal and saccharose

The most widely used approach is the HSQC experiment (60) without the 180° ^{1}H refocusing pulse in the middle of the heteronucleus frequency labelling period (*F1* coupled HSQC) (89). The result is a X-^{1}H chemical shift correlation spectrum with peaks split in the indirect dimension by the $^{1}J_{X,H}$ coupling. Spectral crowding due to the increase of the number of crosspeaks is a difficulty for macromolecules. To circumvent this problem the IPAP approach (195), spin-state selective methods (196-202), TROSY technique (203, 204) and the E-COSY principle (205) were proposed. Measurement in the indirect dimension is desirable due to reduction of additional splittings caused by homonuclear ^{1}H,^{1}H couplings in the acquisition dimension and also because of favourable heteronuclear relaxation characteristics for macromolecules. Extraction of coupling constants from an HSQC experiment non-decoupled during the acquisition (*F2* coupled HSQC) may also be complicated by strong coupling effects (10) resulting in asymmetric multiplets as can be seen on Figure 5.2. In these cases simulations have to be used to extract accurate values of coupling constants.

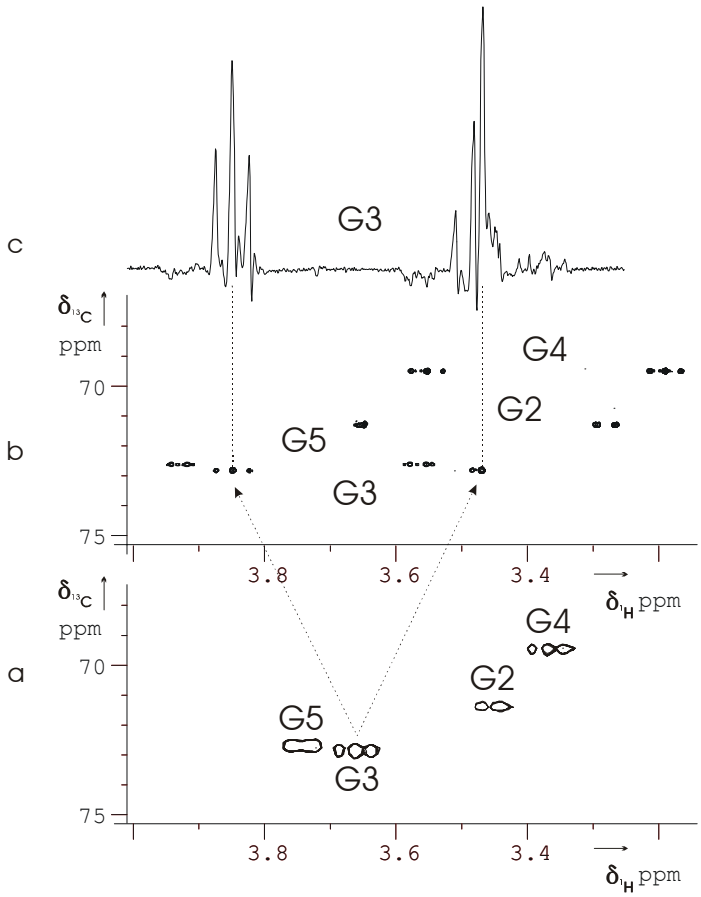

Figure 5.2 Expansions of decoupled (a) and coupled (b) gradient enhanced, sensitivity improved HSQC spectra for saccharose (**2**) in liquid crystal medium. The inlet (c) is a ^{13}C satellite subspectrum of Glc-H3 extracted as a row from the HSQC spectrum coupled during acquisition. In trace (c) the Glc-H3 multiplet becomes asymmetric due to strong coupling in the ^{13}C-isotopomer spin system and cannot be analysed as a first order spectrum in order to extract the value of the one-bond heteronuclear coupling constant.

In order to achieve optimum precision, data must be collected for a period of time on the order of the proton transverse relaxation time. Heteronuclear correlation experiments coupled in the indirect *F1* dimension are limited by the necessity of acquiring large number of t_1 points to achieve high digital resolution in a spectral window determined by the large chemical shift dispersion of the heteronucleus, therefore making the experiment rather time-consuming. *J* resolved spectroscopy can be employed to reduce the frequency span of the indirect dimension and also to improve precision as field inhomogenity effects are refocused, this is however, often compromised by overlap in the acquisition dimension even in case of medium sized molecules.

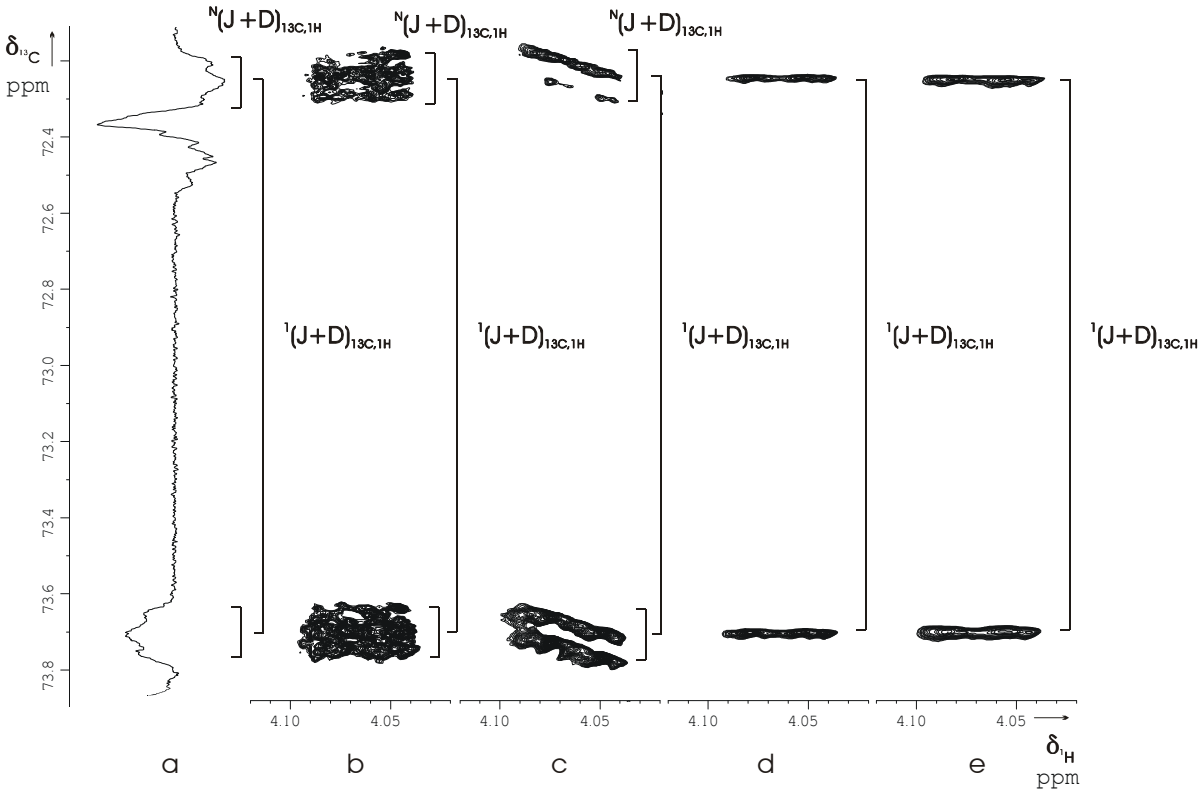

Figure 5.3 Comparison of Glc-5 carbon multiplet of saccharose (**2**) in a liquid crystalline phase in non-refocused, non-decoupled ^{13}C INEPT (a), and in various gradient enhanced F1-coupled HSQC spectra without sensitivity improvement (b), with sensitivity improvement (c), with G-BIRD$^{(r)}$ module in the t_1 period (d), and with both sensitivity improvement and G-BIRD$^{(r)}$ module (e). In a), b), and c) the carbon signal is split by the one-bond $^{1}J_{13C,1H}$ coupling and by many long-range couplings resulting in a broad multiplet. The insertion of the G-BIRD$^{(r)}$ element (d, e) effectively removes the splittings caused by the long-range interactions.

Cross correlation effects also influence frequency difference between multiplet components via differential linebroadening and second order dynamic frequency shifts. This problem has been solved by the introduction of the CE-HSQC (89) in which the evolution period has been divided into two distinct parts. During the first part both chemical shift and coupling is allowed to evolve, while in the second part only coupling evolution occurs. During the pure coupling evolution period field inhomogenity contributions are refocused and cross relaxational effects are cancelled.

Appearance of any coupling different from the desired one-bond interaction further complicates the extraction of RDCs and reduces signal intensity. As mentioned before, this is in part the reason why *F2* coupled HSQC is preferably not used. There are additional splittings, however, in *F1* coupled HSQC spectra as well. The antiphase X magnetization during t_1 evolves not only according to the one-bond couplings, but also due to the long-range heteronuclear couplings. In case of small molecules these couplings can readily be detected in high-resolution spectra as splittings, or as line broadening for macromolecules. Sensitivity is also degraded by splitting the resonance lines into multiplets. This is especially severe in the presence of several long-range couplings as can be seen for instance for Glc-5 in saccharose on Figure 5.3b and c. The remote nuclei which is the source of these additional splittings, may also be directly coupled to the heteronucleus, yielding additional dipolar contributions of unknown magnitude to the multiplets in anisotropic media as demonstrated in Figure 5.4. Multiplet patterns detected in isotropic and anisotropic media hence are different. For the precise value of coupling constants frequency difference has to be measured between multiplet centers, but not between peak maxima.

SCE HSQC (89) was suggested for proteins to decouple multiple bond heteronuclear couplings of backbone N to α and β protons by the application of selective pulses. The G-BIRD module has also been employed by Pham et al. (206) for decoupling long-range couplings in *J* modulated experiments.

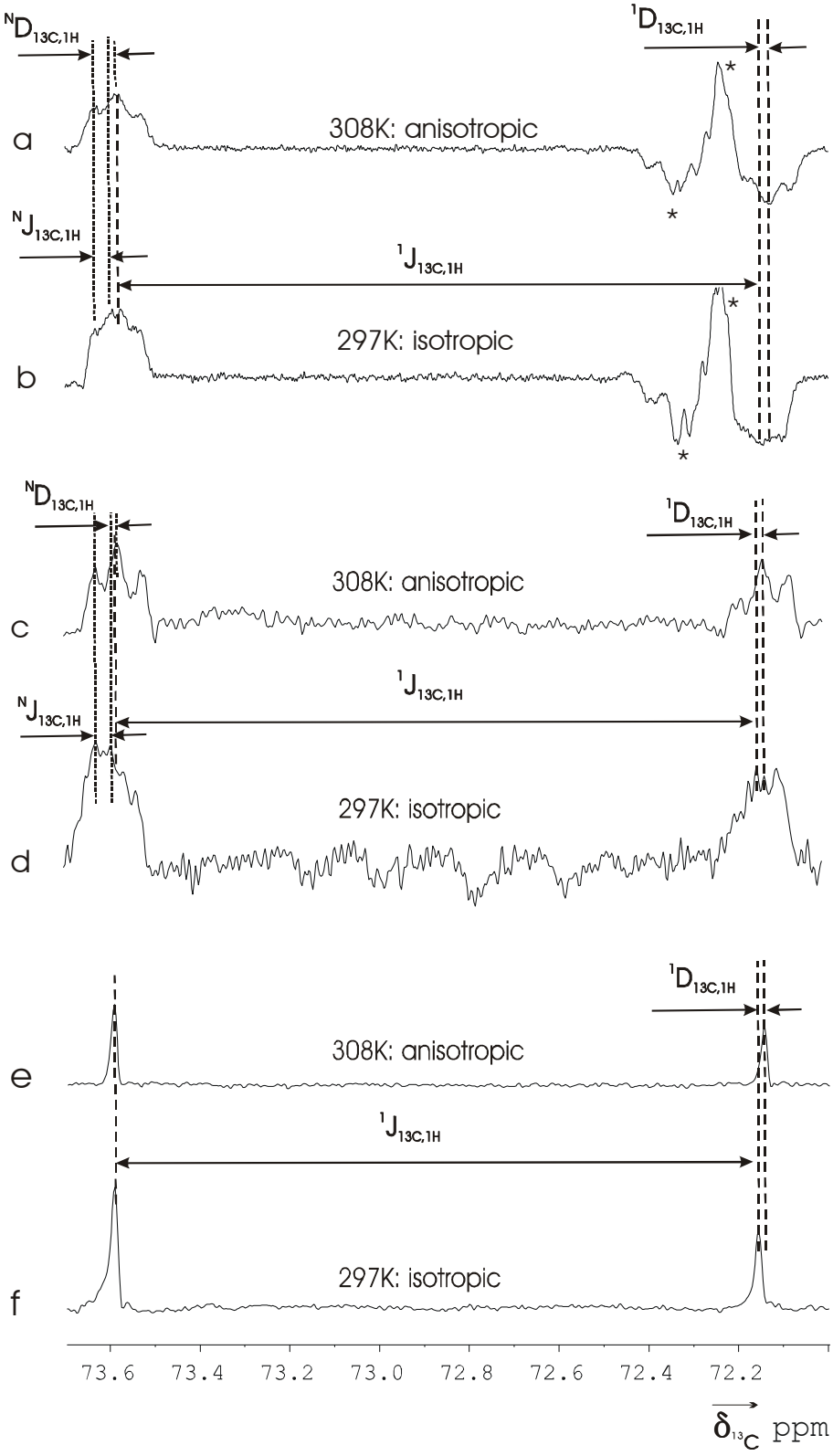

Figure 5.4 Glc-5 carbon resonance of saccharose in non-refocused, non-decoupled ^{13}C INEPT spectra (a and b) and the corresponding columns from gradient enhanced, sensitivity improved F1-coupled HSQC without (c and d) and with G-BIRD$^{(r)}$ module (e and f). Lower traces (b, d and f) are from spectra acquired in isotropic and upper traces (a, c and e) in anisotropic liquid crystalline media. Employing the G-BIRD$^{(r)}$ sequence long-range splittings disappear (e, f) allowing accurate and simple measurement of the one-bond dipolar contribution. Signals denoted with * are due to other overlapping carbons.

5.2 F1 coupled HSQC with G-BIRD$^{(r)}$

For the problem of the line splittings caused by multiple bond couplings an F1 coupled HSQC sequence with an inserted G-BIRD$^{(r)}$ (90, 91) element is suggested here. The pulse sequence as depicted on Figure 5.5 is actually/in fact/essentially a variation of the sensitivity enhanced, gradient selected HSQC experiment originally introduced by Kay et al. (62). In place of the 180^{o} ^{1}H refocusing pulse a G-BIRD$^{(r)}$ (90, 91) sequence is inserted at midway of t_1. The G-BIRD$^{(r)}$ pulse inverts only the remote protons, and neither the directly attached nor the X nuclei are inverted. As a result, the chemical shift and heteronuclear one-bond coupling evolution of X nuclei are not affected during t_1, so as they continue to evolve; whereas effective refocusing of heteronuclear long-range coupling evolution is achieved by the end of t_1 interval. The resulting correlation spectra have simplified crosspeaks with splittings due to only the desired one-bond couplings and with higher intensities. This allows the accurate determination of the scalar coupling constant and subsequently the dipolar contribution. Note that the two gradients of opposite signs purge out the fraction of magnetization that does not experience perfect rotation by the BIRD$^{(r)}$ pulse.

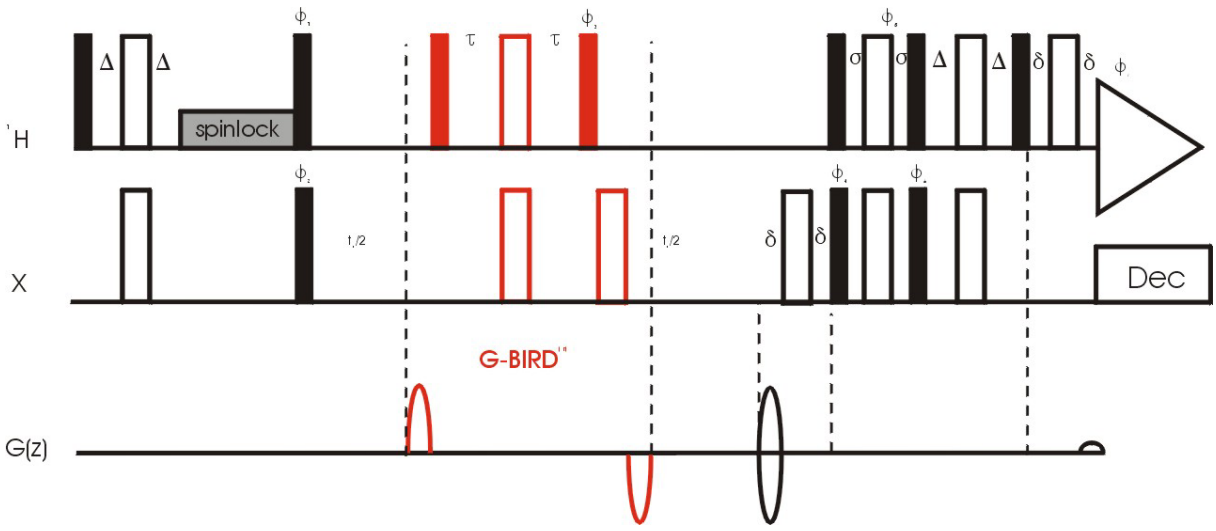

Figure 5.5 Gradient enhanced, sensitivity improved HSQC sequence with G-BIRD$^{(r)}$ element in the t_1 interval to eliminate long-range coupling modulation of the evolving antiphase heteronucleus magnetization. Thin, filled bars represent 90^{o} hard pulses, while thick, non-filled bars 180^{o} hard pulses. Phase cycling is as follows: phases for pulses without phase notation correspond to x, φ_1 = y, -y φ_2 = x, x, x, x, -x, -x, -x, -x; φ_3 = -x φ_4 = x, x, -x, -x; φ_5 = y; φ_6 = y, y, -y, -y; φ_r = x, -x, -x, x, -x, x, x, -x . The delay Δ is adjusted to ¼ $^{1}J_{X,H}$, τ is to ½ $^{1}J_{X,H}$, σ is to 1/8 $^{1}J_{X,H}$ and δ is the duration of the shaped gradient pulses. Echo-antiecho selection is achieved by the gradients.

The method has been tested on isotropic samples of a model dipeptide glicine-valine (GlyVal) and partially oriented anisotropic sample of saccharose, both of them are depicted on Figure 5.1. In case of the peptide there is one single long-range coupling to the amide ^{15}N resulting in a clear doublet of doublet that can be seen on Figure 5.6a and b.

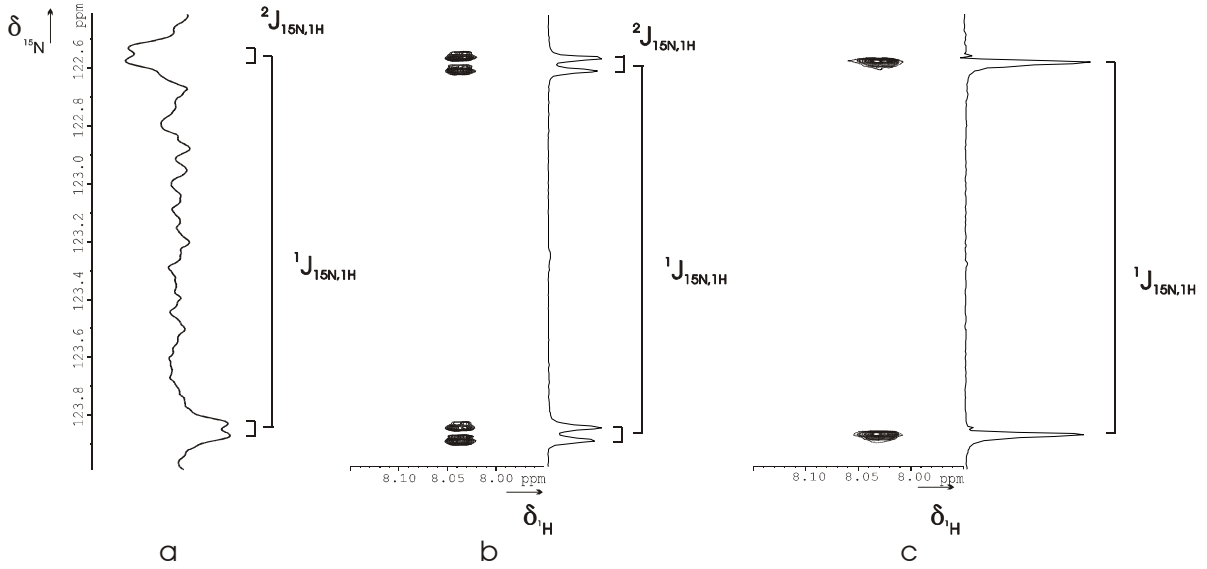

Figure 5.6 Comparison of multiplicity and intensity of backbone ^{15}N in a model dipeptide, GlyVal 1 in a) non-refocused, non-decoupled ^{15}N INEPT, b) gradient enhanced F1-coupled HSQC, and c) gradient enhanced F1-coupled HSQC with G-BIRD$^{(r)}$ module in the t_1 period. In a and b the ^{15}N signal is split by the one-bond $^1J_{15N,1H}$ coupling and by long-range coupling to Hα resulting in a well-resolved doublet. The insertion of the G-BIRD$^{(r)}$ element (c) effectively removes the splitting caused by the long-range interaction. Comparing the peak intensities in columns extracted from 2D spectra demonstrates that the decoupling of long-range interactions considerably improves the sensitivity.

For a carbohydrate on the other hand, there are many long-range heteronuclear interactions that yield an unresolved, broad multiplet (Figure 5.3.a,b,c). The one-bond coupling constant is therefore extracted by measuring frequency difference between the multiplet centers which is a relatively easy task in case of the peptide, but problematic for the broad multiplet of the carbohydrate (see Figure 5.4). As seen on Figure 5.4 the Glc-5 carbon signal is split by the one-bond coupling to the directly bonded proton (an antiphase splitting in INEPT and an in-phase splitting in HSQC) and by the long-range couplings to all the multiple bonded protons. Small increase of the one-bond coupling due to the dipolar contribution can be detected in partially oriented phase by measuring differences between multiplet centers. The multiplet patterns caused by the long-range couplings are also changing due to small dipolar interaction between the relevant spins resulting in long-range RDCs ($^1D_{13C,1H}$). For

example, the “doublet of doublet" observed in isotropic medium (d) becomes a "triplet" in the presence of partial alignment (c). Note that multiplicities are difficult to assess because of the large number of possible multiple bond coupling interactions. Although the multiplets are in principle symmetric the center of the multiplet is, however, quite undetermined. This is especially severe on the multiplet of F1 coupled HSQC column in isotropic solution as shown on Figure 5.4d. The uncertainty of the multiplet center in the case of the Glc-5 multiplet was ±1Hz (three data points for 0.33 Hz resolution). Furthermore, as the signal intensity is halved with each coupling partner, sensitivity gets degraded especially in carbohydrates. With the insertion of the G-BIRD$^{(r)}$ element to decouple the long-range interactions, sensitivity can significantly be improved. This is demonstrated in Figure 5.6 by comparing signal intensities of the columns extracted from the 2D spectra obtained with the conventional *F1* coupled HSQC and the *F1* coupled HSQC employing G-BIRD(r) experiments.

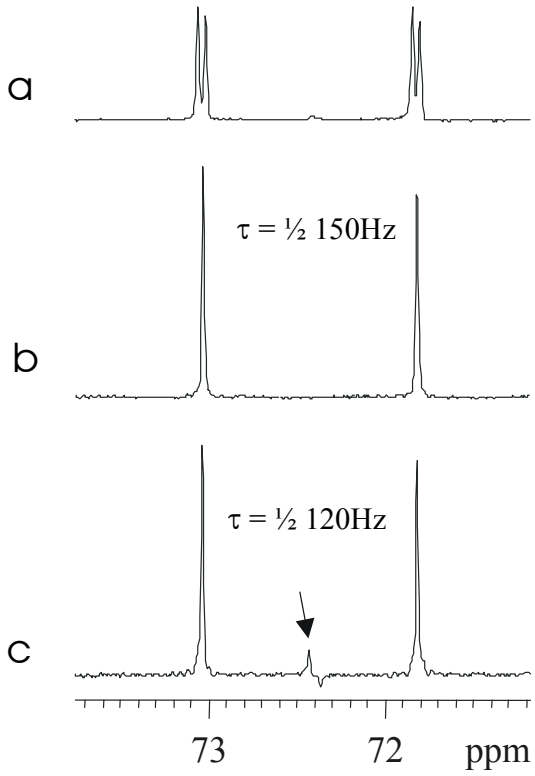

Figure 5.7 Influence of the variation in coupling constants on the effect G-BIRD module. Trace a) shows the column from F1 coupled HSQC with 152.3Hz heteronuclear one-bond splitting and a small long-range coupling. Trace b) is the column of the same multiplet from F1 coupled HSQC incorporating the G-BIRD module with delay τ tuned to 150Hz yielding perfect decoupling of the long-range coupling. Trace c) shows of the effect of the mismatch between delay τ (tuned to 120Hz) and the value of the one-bond coupling constant (152.3Hz). A decoupled signal can be seen in the middle of the multplet as a result of the partial inversion of the directly bonded protons.

The effect of the BIRD module in case of variations in the one-bond heteronuclear coupling has been examined by setting the delay used in the G-BIRD module (τ) to a value 30 Hz smaller than the true value of ^{1}J of a specific multiplet. As a result of the mismatch the direct proton is partially inverted and hence decoupled by the BIRD yielding an ordinary HSQC signal in the middle of the multiplet as can be seen on Figure 5.7. The intensity of the decoupled signal depends on the deviation of the delay from the true value of the coupling constant.

5.3 Conclusion

Small residual dipolar contributions between directly bonded nuclei can accurately be measured by means of an HSQC sequence modified with a G-BIRD$^{(r)}$ module which decouples all the long-range couplings of the heteronucleus while retaining the one bond coupling to the directly bonded proton. Summarizing the advantages of the proposed sequence: i) allows simple frequency difference extraction between peak maxima, ii) accurate measurement of small one-bond heteronuclear dipolar couplings without complications arising from other dipolar contributions or strong couplings, iii) improved sensitivity due to simplification of multiplets, iv) easy implementation of the G-BIRD$^{(r)}$ module in any variant of HSQC sequence.

6. BANDSELECTIVE SUPPRESSION OF UNWANTED SIGNALS IN OLIGOSACCHARIDE SPECTRA

6.1 Signal overlap in the NMR spectra of oligosaccharides

Signal overlap in 1D NMR spectroscopy is a common obstacle to the analysis of all but the simplest spectra. ^{1}H NMR spectra of oligosaccharides notoriously feature narrow ranges of chemical shifts for the ring protons (with the exception of the anomeric ones) even at lower molecular masses (e.g., di- or trisaccharides). Anomeric proton signals tend to stand out downfield of the bulk of resonances and can therefore be utilized as structure "reporter" signals in cases where no detailed assignments are available (207). They are, on the other hand, natural starting points for resonance assignments by 2D methods.

The synthesis of a specific carbohydrate molecule (e. g. an oligosaccharide) is often a multistep procedure which require application of protecting groups. Regioselectivity and stereochemistry of the product after each reaction step is most often monitored by NMR. Difficulties arise when anomeric signals get buried by low-field shifted resonances arising from protecting groups, such as benzylic methylenes or others used in oligosaccharide synthesis (208, 209). It was shown recently that signals from protons not J-coupled to the spin system of interest, e.g. those constituted by sugar backbone protons, can be selectively purged from 1D spectra even in the case of severe overlap (210). The method is based on band-selective suppression of all signals, including the "useful" ones, from one region of the spectrum, followed by a TOCSY transfer to recover resonances of protons J-coupled to the non-suppressed ones. For instance, signals of anomeric protons overlapped by OCH_2's in carbohydrate benzyl ethers could be cleanly recovered while eliminating the latter disturbing resonances (210).

Overlap is much less of a problem with 2D NMR but not uncommon even with smaller molecules having unfavourable spectral properties such as compressed chemical shift range. Signals originating from the protecting groups could further complicate NMR investigations by causing severe overlap with signals of interest. This is exemplified by the pseudo-tetrasaccharide depicted on Figure 6.1, bearing eight benzylic groups whose CH_2

signals overlap with anomeric resonances (H1', H1") and with quite a few of the backbone proton signals (H3, H4, H6, H3").

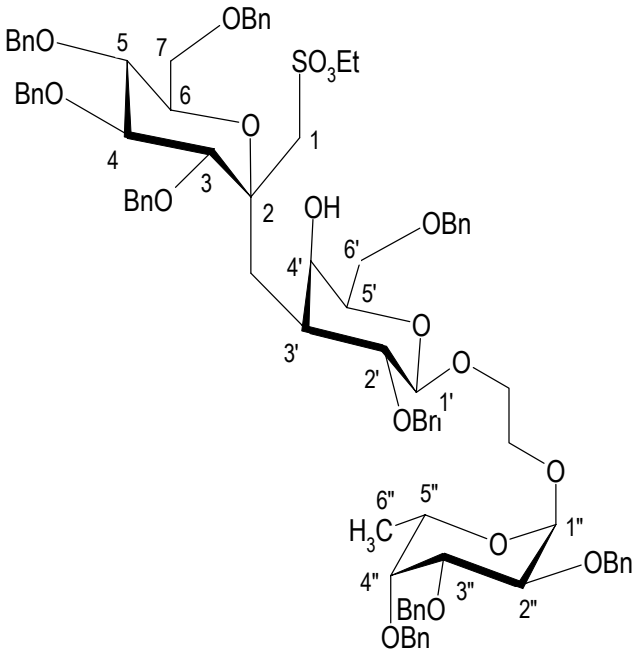

Figure 6.1 Structure of model pseudo-tetrasaccharide

In the course of the assignments of ^{1}H and ^{13}C spectra of this molecule it turned out furthermore that one of the backbone cross peaks (later identified as H6) got completely buried by those from benzylic CH_2's in the ^{1}H, ^{13}C HSQC map (Figure 6.2a) as well.

6.2 Bandselective DPFGSE-TOCSY as a preparation period

In order to selectively eliminate disturbing cross peaks arising from the latter, a modification to the original HSQC sequence was introduced (62). This consists of a preparation step whereby band-selective suppression of signals in the "benzylic" region (ca. 4.1 to 5.2 ppm, including the shift of H6) is followed by restoration of the suppressed backbone resonances using MLEV17 transfer (54) (Figure 6.3). Suppression is effected by the DPFGSE sequence or "excitation sculpting" (93, 94) wherein the band-selective 180^{o} pulses are implemented as pulse width modulated DANTE trains (211). Using the DANTE employing hard pulses was found to be robust and more convenient in terms of calibration and bandwidth adjustment than using shaped pulses (212) or RE-BURP (213).

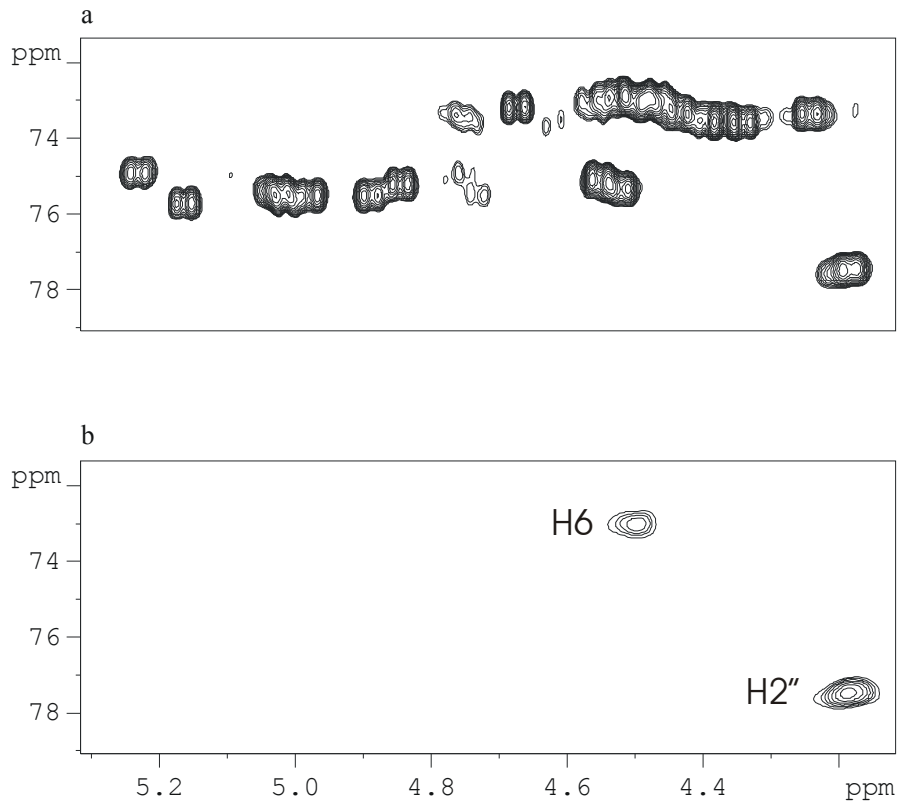

Figure 6.2 Partial plots of gradient-enhanced $^{1}H,^{13}C$ HSQC spectra of 1 displaying the spectral region characteristic for benzylic CH_2 resonances; without (a) and with (b) insertion of the band-selective suppression element of Figure 3 before the HSQC sequence.

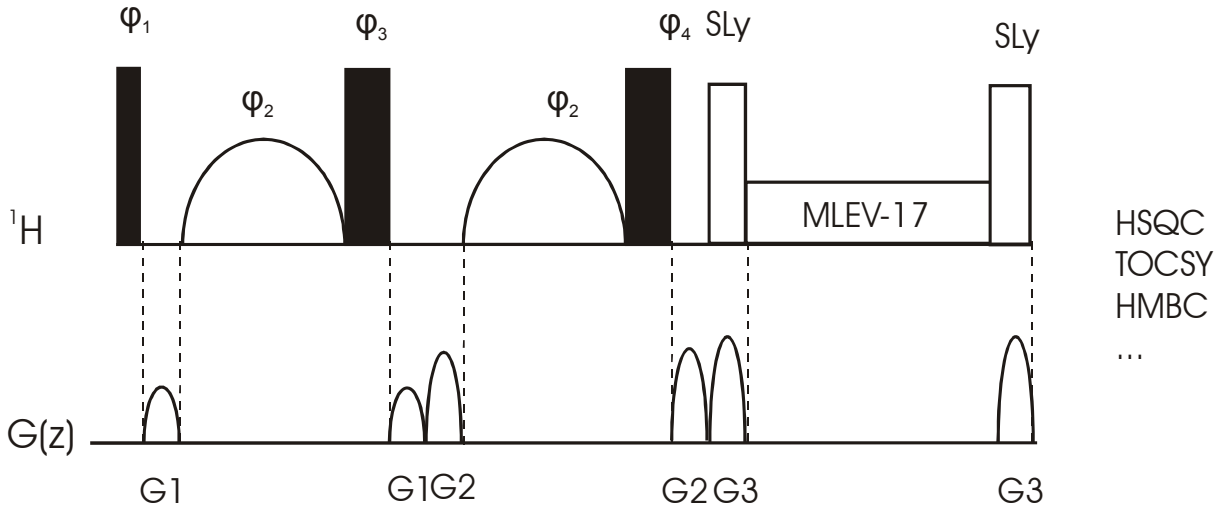

Figure 6.3 Band-suppressive excitation scheme serving as a preparation pulse in regular 2D experiments. Thin and thick filled bars represent ^{1}H 90° and 180° pulses, respectively. Shaped bars indicate band-selective inversion pulses. The MLEV17 scheme is flanked by simultaneously switched gradient (G3) and spin-lock (Sly) pulses in order to achieve pure phase excitation. The strengths of sine-bell shaped gradient pulses of 1 ms duration were: G1=5 G/cm, G2=9 G/cm and G3= 10 G/cm. The phase cycling was set as $\phi1$ = x, –x; $\phi2$ = x, –x; $\phi3$ = x, –x; and $\phi4$ = x, –x, y, –y.

The effect of the band-selective excitation scheme is shown in Figure 6.4. where the ^{1}H spectra containing all overlapping signals (upper trace) and the outcome right after the preparation period (lower trace) are compared. All signals of benzyilic methylene protons are removed from the spectra whereas the sugar proton resonaces (H1", H3, H1, H1', H4, H3") are restored by the isotropic mixing period.

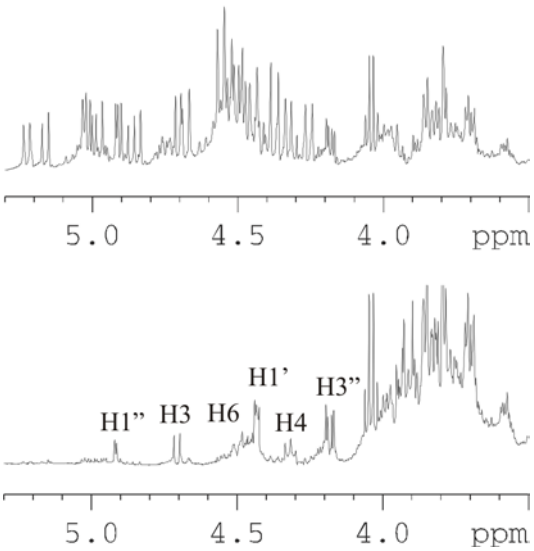

Figure 6.4 Suppression of the benzylic methylene protons detected by reading out ^{1}H magnetisation immediately after the preparation period as described in ref. 4 (lower trace) as compared to regular ^{1}H spectra (upper trace)

6.3 Applications

The result of the modified HSQC experiment incorporating the band-suppressive element, evident from Figure 6.2b, is to clear all benzylic CH_2 cross peaks while retaining that of H6 (with somewhat decreased intensity).

Prerequisitive for the application of the proposed method is the existence of coupling partners outside the region influenced by the band-selective suppression from where magnetisation is transferred back to ring protons by the subsequent isotropic mixing period. Efficiency of the back-transfer depends on the magnitude of the corresponding coupling constant, which it should preferably be larger than ca. 4Hz. In general, not only protecting group methylene proton signals, but any isolated spin system can be suppressed if the signals of interest resonating in the same spectral region can be recovered by transferring magnetisation back from coupling partners outside the suppressed zone.

The proposed purging scheme is not limited to the modified HSQC experiment shown; it is, in fact, quite general and can be utilized as a preparation step preceding other homo- or heterocorrelated 2D sequences like HMBC or TOCSY. As an example, Figure 6.5 shows COSY and CH_2-suppressed 2D TOCSY maps of **1**.

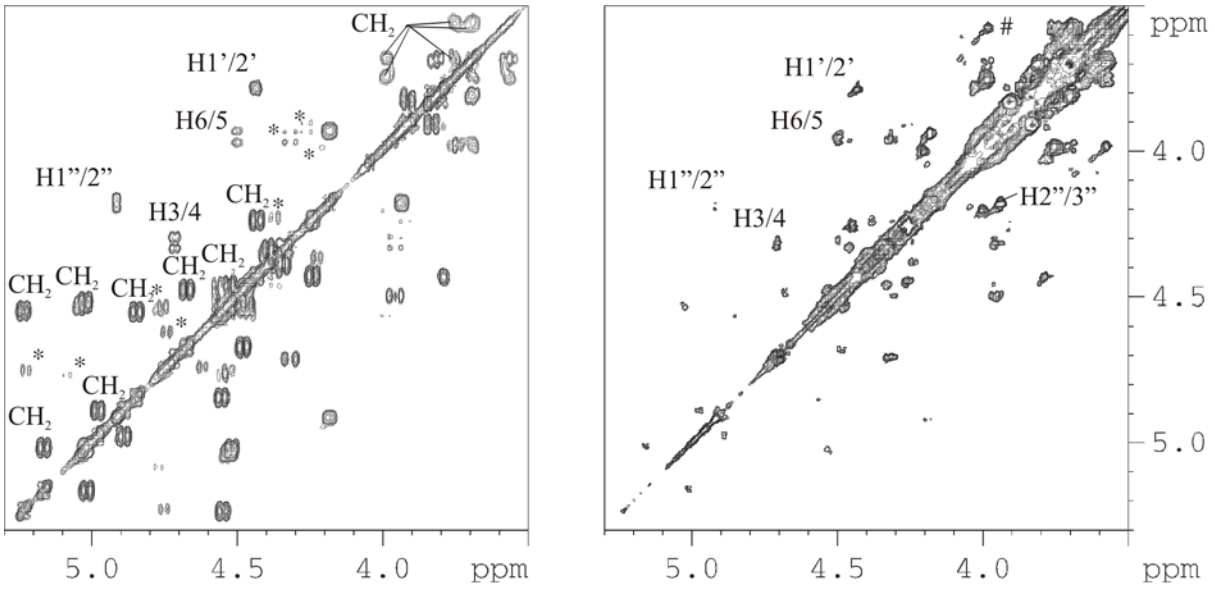

Figure 6.5 Partial TOCSY map (left side) of 1 showing selective suppression of the cross peaks from benzylic CH_2 protons (denoted by CH_2) achieved with the modified sequence (Fig. 3) as compared with the result obtained using regular, gradient COSY (right side). Signals denoted by stars belong to an unidentified impurity in the sample. The mixing time in the TOCSY experiment was 15 ms resulting in cross peaks arising from one step magnetisation transfer, whereas the one denoted by # originates from a two step transfer due to the large value of the corresponding coupling constant.

Suppression of the disturbing methylene crosspeaks is not as perfect in the case of the TOCSY as for the HSQC. Residual geminal crosspeaks are still detected with significantly reduced signal intensity, however. Appearance of the residual crosspeaks is due to the longer duration of the sequence where relaxation restores magnetisation belonging to protons previously selectively suppressed by the preparation scheme. It also should be considered that the original intensity of HSQC crosspeaks are more or less identical due to the more homogeneous distribution of the values of the one-bond heteronuclear coupling constants whereas the TOCSY crosspeaks to be suppressed arise from large geminal couplings giving rise to strong signals, while the ones to be kept are of smaller intensity due to smaller coupling constant values.

Application of CH_2 suppressed HMBC for determining regioselectivity of glycosylation reaction is presented in Figure 6.6 and 6.7. The reaction (Figure 6.6) was

carried out using a glycosyl donor bearing two unprotected hydroxyl groups. The glycosylation proceeded to both sites producing regioisomers 2-4' and 2-3' with, however, significantly different yields. As a result only one of the isomers could be isolated in an amount sufficient for NMR investigation. Determination of interglycosidic bond location was first attempted by regular long-range heteronuclear correlation (spectra not shown) where crosspeak between C2 and H4' or H3' was sought. The C2/H3' crosspeak was not found which could be due to the small value of the corresponding coupling constant. Identification of the C2/H4' crosspeak is complicated by the overlap of H4' with CH_2-1b which is a neighbouring site to C2. Both of the CH_2-1 protons gave a strong intraresidual crosspeak to C2 compromising the verification of the interglycosidic connection.

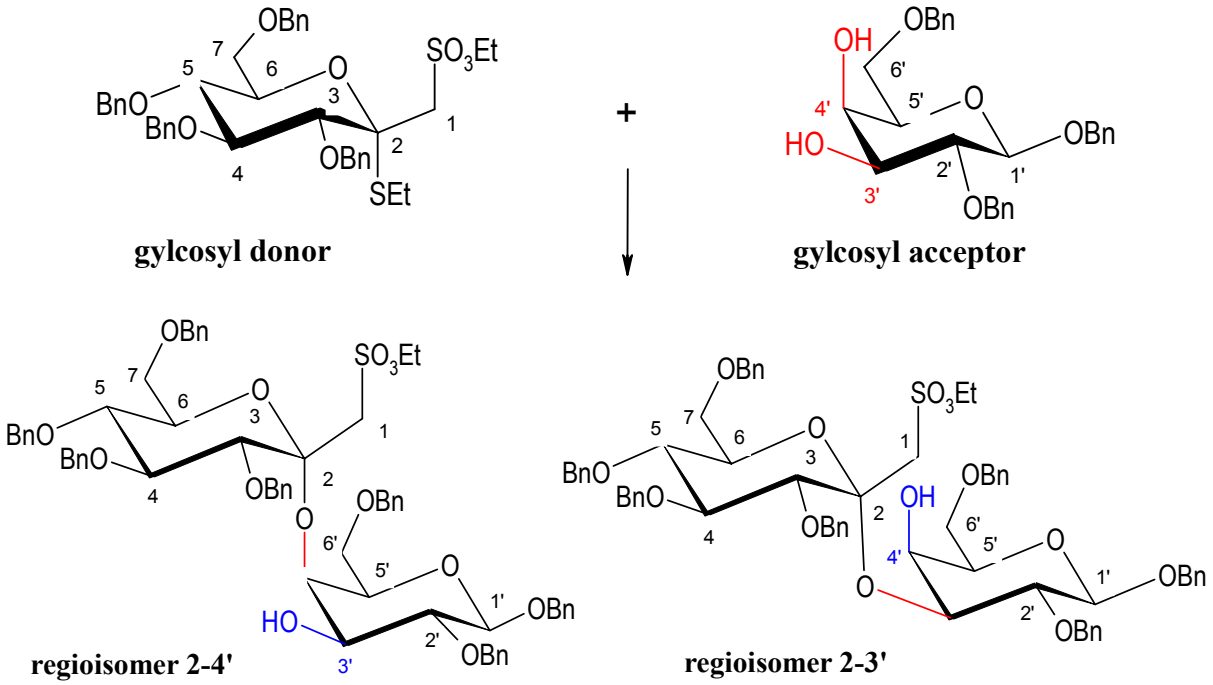

Figure 6.6 The glycosylation reaction with a glycosyl donor bearing two unprotected hydroxil group yielding two regioisomers with interglycosidic linkage 2-4' and 2-3'.

The HMBC combined with the band-selective DPFGSE-TOCSY element efficiently purged out the disturbing C2/CH_2-1b crosspeak revealing the C2/H4' interresidual signal (highligthed in red on lower spectra in Figure 6.7), thus proving the interglycosidic connection. The fact that the trivial crosspeaks to CH2-1b as well as CH2-1a were both completely suppressed (indicated with dashed lines in Figure 6.7) may be considered as an evidence that the a detected crosspeak is not a residual signal of the initial strong peak, but a true correlation over the interglycosidic linkage.

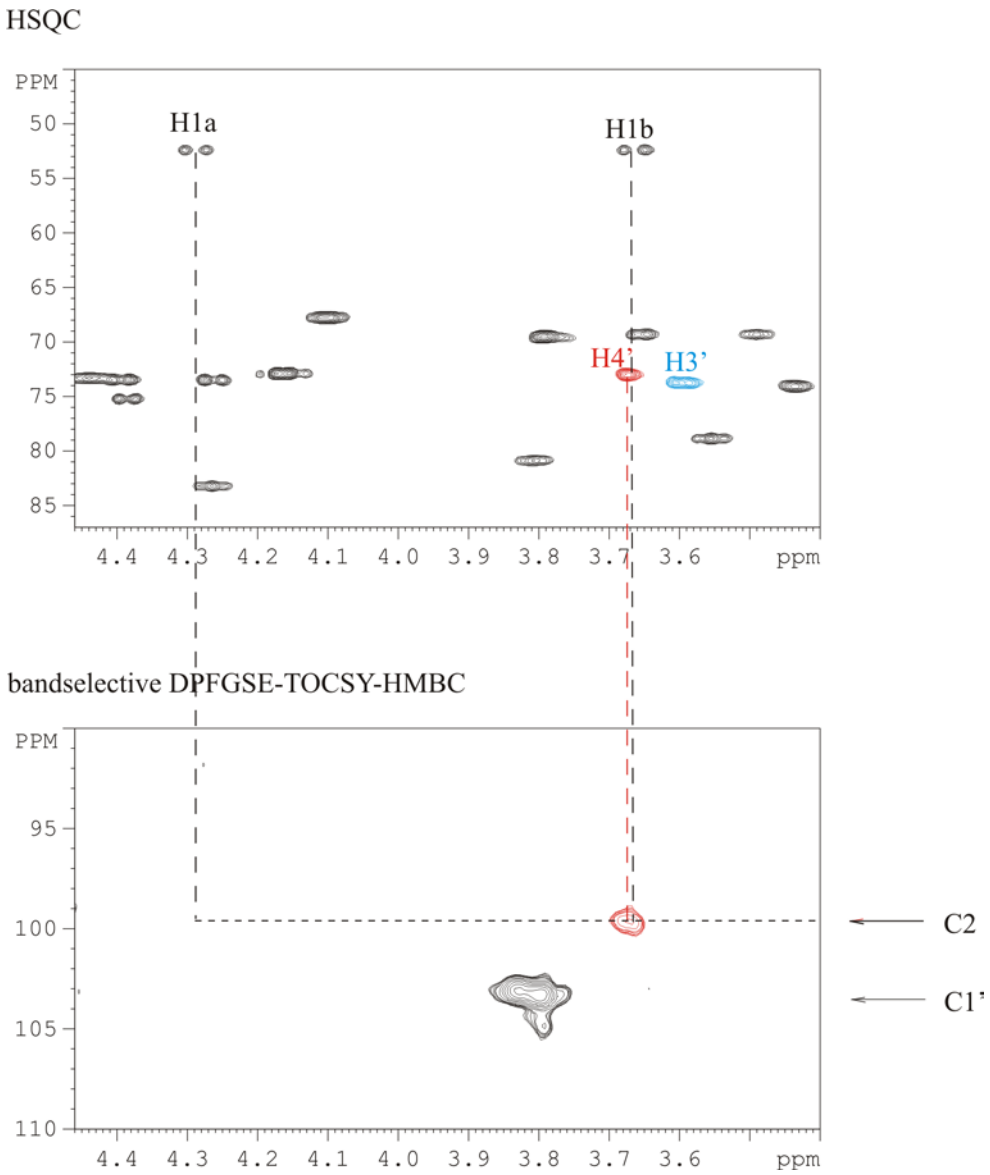

Figure 6.7 HSQC (upper spectra) and CH_2 suppressed HMBC (lower spectra) proving 2-4' connection between monosaccharide units.

Finally it is interesting to note that, as another extension, the MLEV17 restoration scheme can, in principle, be replaced by other sequences, like NOESY or ROESY, to recover signals in the suppressed spectral region. NOESY or ROESY will, however, revive resonances that are coupled by dipolar (or through-space), rather than by scalar-J (or through-bond), mechanism to the spins in the unsuppressed region(s). This may offer a viable alternative when through-bond transfer (by MLEV17) becomes inefficient because the relevant scalar couplings are small.

7. EXPERIMENTAL

7.1 NMR measurements of the peptidoglycan derivatives

Samples

PGM was obtained from a penicillin-treated mutant of *Brevibacterium divaricatum.* (114, 214) Derivatives Ad-PGM and BocTyr-PGM were synthesized from PGM according to published procedures (138, 139). The NMR samples contained 4-8 mg of material dissolved in 0.5ml of 99.9% DMSO-d_6.

NMR measurements

NMR measurements have been carried out on a Bruker DRX-500 spectrometer using a 5 mm broad-band inverse probehead equipped with z-gradient coil. Spectra were recorded at a temperature where the chemical shift distribution was dispersed optimally in the amide proton region, that is at 300K for Ad-PGM and BocTyr-PGM and at 293K for PGM. Proton and carbon chemical shift scales were calibrated to the DMSO-d_6 solvent signal at 2.500 ppm for ^{1}H and 39.95 ppm for ^{13}C. The raw datasets typically consisted of 1-2K x 512 complex data points.

NMR Assignments

In solution all three compounds exist as equilibrium mixtures of the α- and β anomeric forms at the reducing MurNAc end of these molecules. Partial ^{1}H NMR assignments have been reported for the α anomeric form of PGM in DMSO solution (124) whereas tentative ^{13}C assignments were deduced, by comparison with model compounds, for the same in D_2O solution.(122) We have now achieved unambiguous full assignments of ^{1}H- and ^{13}C- signals of the major α-anomeric forms, relying on various 2D measurements, for PGM, Ad-PGM and BocTyr-PGM. ^{1}H NMR assignments have been based on gradient COSY (52) and 2D TOCSY experiments (56) recorded with different mixing times (50 and 80 ms). The doublet signals of the anomeric protons served as starting points to derive assignments for the disaccharide moiety. Individual side chain resonances for the peptide part have been identified by characteristic cross peak patterns in the TOCSY maps. For the assignment of some of the sugar ring protons HSQC-TOCSY measurements (59) were necessary. These assignments have been cross-checked through 1D TOCSY measurements (71). Three-bond Hα/CO correlations in the gradient HMBC spectra (65) and Hα/NH sequential cross peaks between

two Ala residues in the NOESY maps helped to establish sequential assignments for the three Ala residues. Hε of *m*-Dap exhibited a four-bond coupling to εCONH$_2^Z$ in the COSY/TOCSY maps; this was further confirmed by appropriate HMBC cross peaks. HSQC measurements (62) have furnished assignments for protonated carbons whereas ^{13}C HMBC experiments provided identification for the CO signals. The NMR chemical shift data are shown in Table 3.1 while Table 3.4 lists ^3J(NH,Hα) values and temperature dependence of amide NH chemical shifts.

NMR parameters

^{1}H chemical shifts and conformationally important homonuclear coupling constants were extracted from a resolution enhanced 1D spectrum or, in case of signal overlap, from selective TOCSY experiments. Amide ^{1}H chemical shift temperature coefficients have been determined over a temperature range between 293K and 308K using 5K increments. ^{1}H/^{1}H distance information was obtained using phase sensitive NOESY spectra. ROESY and T-ROESY (215) have also been recorded to crosscheck for peaks resulting from coherent or mixed magnetization transfer. NOE buildup curves were constructed from experiments with mixing times of 50, 100, 150 and 300 ms; values up to 100 ms were found to be in the linear regime. The cross peak intensities were determined by volume integration from the baseplane corrected NOESY or ROESY spectra recorded with 100 ms mixing time.

Computational Procedures.

The cross-peaks obtained from NOESY and/or ROESY spectra were converted to NOE distance restraints and used in distance geometry calculations followed by energy minimization in the classical force field *cvff* (216) employing the DGII and DISCOVER modules of InsightII (Accelrys Inc., 9685 Scranton Road, San Diego, CA), respectively. The NOE distance restraints were divided in strong, medium and weak with upper limits of 2.6, 3.6 and 5 Å, respectively. The number of distance restraints used for the structure calculations was: 64 for PGM, 67 for Ad-PGM and 76 for BocTyr-PGM. Only *inter*residual experimental contacts are listed in Table 3.2. For pro-chiral protons or proton groups a pseudoatom correction was applied.[16] 100 structures were calculated for each of the molecules and divided in clusters of conformations according to values of the dihedral angles GlcNAc-φ', GlcNAc-ψ, MurNAc-ψ', Lac-φ', Lac-ψ', Ala^1-φ, Ala^1-ψ, *i*Gln^2-φ, *i*Gln^2-ψ, *i*Gln^2-χ_1 and *i*Gln^2-χ_2 with a tolerance of 30° [GlcNAc-φ', C2–C1–O1–C4(MurNAc); GlcNAc-ψ, C1–O1–C4(MurNAc)–C3(MurNAc); MurNAc-φ', C4–C3–O3–Lac-α; Lac-φ', C3–O3–Lac-α–Lac-C'; Lac-ψ', O3–

Lac-α–Lac-C'–Ala[1]-N; the definition of the *i*Gln dihedral angles is used irrespective of the *i*Gln[2]-Cγ–Dap[3]-N linkage]. The most populated cluster with low energy was chosen to represent the preferred conformations. (217)

7.2 NMR measurements on isotropic diglycoside disulfide samples

Samples

Samples for the NOE and temperature coefficient measurements were prepared by dissolving 10 mg of the respective diglycoside disulfide in 500ul DMSO-d_6 solvent containing TMS as a reference material.

Assignments

Complete and unambiguous assignment of ^{1}H and ^{13}C resonances was achieved by the combined use/analysis of COSY (52), phase sensitive pure absorption 2D TOCSY (56), selective TOCSY (71) (isotropic mixing times of 15 and 50ms), edited HSQC (62) and HMBC (65). The raw datasets typically consisted of 2K × 512 complex data points.

NMR parameters

^{1}H chemical shift temperature coefficients for labile protons were obtained over a temperature range between 298K and 318K using 5K increments. $^{1}H/^{1}H$ distance information was obtained using T ROESY experiments (215) with 1.5KHz spinlock field strength. The duration of the spin-lock pulse was 50ms.

7.3 Sample preparation and NMR measurements on partially oriented samples

Diglycoside disulfide samples

For determination of residual dipolar couplings ~10 mg of the respective derivative were used. NaN_3 were used to prevent bacterial growth and DSS as a reference material. For the alignment, bicelles were formed from CHAPSO/DMPC (218) at mass ratio of 1/3.5 and total liqiud cryssatl concentrations 7.5%, 15% and 30%). CHAPSO (3-[(3-cholamidopropyil) dimethylammonio]-2-hidroxy-1-propanasesulfonate) and DMPC (Dimyristoyl-DL-α-

phosphatidylcholine 1,2-ditetradecanoyl-rac-glycerol-3-phosphocholine) was purchased from Sigma (Sigma-Aldrich) as dry powders and used without further purification.

Samples for testing F1 coupled HSQC with GBIRD$^{(r)}$ technique

The isotropic sample of dipeptide of glycine-valine used as model compound for testing the proposed method described in chapter 5 was prepared by dissolving 25mg of GlyVal in 700ul of D_2O resulting in 205mM solution.

The use of the proposed technique for the extraction of RDCs was demonstrated on liquid crystal sample of 100mM saccharose in 700µl anisotropic media.

Sample preparation procedure

The substance to be investigated was dissolved in 0.7ul D_2O. Concentration of the dissolved substance should lower than mol/l. The temperature region where the liquid crystal phase exist considerably shrink at higher concentration of the dissolved substance. 1mg NaN_3 and 1mg DSS has been added to the solution. Weigthed amount of DMPC were dissolved in the previous solution resulting in a milky, but still easily flowing liquid. The solution was carefully homogenized by vortexing, then premeasured amount of CHAPSO were added to the solution. By adding the detergent the consistency changes giving a semi-transparent, opalescent gel which practically does not flow. The mixture was homogenized by vortexing. Thorough homogenization is crucial for obtaining a stable liquid crystal phase, however mixing using ultrasound should be avoided. The presence of microscopic inhomogeneities was checked by centrifuging at 4000G for 5 min. If centrifugation yielded phase separation, additional cycles of vortexing/centrifuging were repeated. If the sample formed one, homogeneious, semi-transparent, slightly opalescent phase, then it was cooled on ice which reduces viscosity and makes it easier to transfer to the tube by a Pasteur pipette. Viscosity can only be reduced by cooling the media, while warming up increases the viscosity. Warming the mixture should anyway be avoided because above 325K irreversible disruption of the phase has been observed in several cases. A stable media is perfectly clear, but extremely viscosous under 299K (it practically does not flow, not even if the tube is turned up-side down), and becomes milky above 299K where thermal induced phase transition from to gel to liquid crystal occur.

NMR measurements on partially oriented samples

All experiments were performed on Bruker DRX-400, 600 and 700 spectrometers (Bruker AG, Rheinstetten, Germany) equipped with TBI z-grad probes. All spectra were processed with XWINNMR 3.1 (Bruker AG, Karlsruhe, Germany).

The temperature for measurements under isotropic conditions was set to 297 K while for anisotropic conditions to 308K.

The deuterium signal of the solvent is split by the residual quadrupolar coupling. Locking was performed using one signal component by manually optimizing parameters of the lock channel. Magnetic field homogenizing was executed by shimming on ^{1}H FID integral.

For the measurement of $^{1}H,^{13}C$ residual dipolar couplings F1 coupled gradient selected, sensitivity enhanced HSQC spectra modified with a G-BIRD module (219) described in chapter 5 were used. The spectral window in the indirect dimension were typically 20ppm giving a frequency span of 2000Hz at 400MHz, 2500Hz at 600MHz and 3500MHz at 700MHz. Acquiring 4K t1 experiment yielded ca. 0.49Hz, 0.61Hz and 0.85Hz spectral resolution, respectively. Columns of the 2D map were extracted and inverse Fourier transformed. Linear prediction and zero filling were used to increase digital resolution, then time domain data were apodised with squared squared cosine window function prior to 2D Fourier transformation to yield a digital resolution of 0.25Hz, 0.30Hz and 0.42Hz. Each 1D trace was individually phased corrected. Peak maxima were identified using the peak picking utility of the XWINNMR 3.1 program. MHz). In order to estimate the precision/random error of the measurements, each spectrum was recorded twice.

Methods for conformational analysis

Conformational search has been carried out including systematic as well as stochastic searches. The molecular mechanics calculations were carried out with the DISCOVER program implemented in the InsightII 2000 (MSI, San Diego, CA). All calculations were performed using the AMBER force field (188, 189) extended with Homans' carbohydrate parameters (190). The calculations have been carried out in vacuum, a distance dependent dielectric constant was used and 1-4 interactions were scaled by a factor of 0.5. All hydrogen atoms were explicitly included into the calculations.

Systematic search

Flexible geometry systematic searches were carried out by optimising the structures with fixed interglycosidic torsion angles. All three interglycosidic torsion angles were systematically rotated in 10^o increments. Conformations were forced to adopt the target geometry by applying a biharmonic forcing potential. The sugar rings were constrained to the $^4C_1$ conformation until the gradient reached 1 kcal/mol.Å and then released. The structures were further optimised to a final gradient of < 0.001 kcal/mol.Å by the quasi-Newton-Raphson (VA09A) minimization method. The next rotation has been done on the unminimized structure not to bias the calculation by the geometry optimised towards the previous conformer. InsightII DISCOVER input file for executing the simulation is attached in Appendix C.

Simulated annealing

An initial minimization was applied to remove high strains from the starting structure using a steepest descent algorithm until the gradient reached 10 kcal/mol.Å followed by a quasi-Newton-Raphson minimization until 1 kcal/mol.Å. The system was then heated to 1000K in 1ps, equilbirated at high temperature for 5ps, then the temperature exponentially decreased to 300K in 5ps. The resulting structures were energy minimized to 0.001 kcal/mol.Å as above. 1000 structures were generated for analysis. InsightII DISCOVER input file for executing the simulation is attached in Appendix D.

7.4 NMR measurements on protected oligosaccharides

Samples

Samples for the measurements were prepared by dissolving 30-70 mg of the respective protected oligosaccharide in 500ul benzene-d_6 solvent containing TMS as a reference material.

NMR measurements

The specifications of the equipment are described in paragraph 7.1. The temperature was set to 300K. The pulse-width modulated DANTE train (92, 211) consisted of 32 pulse elements of 20.6us, whereas the duration of the interpulse delay was 50us resulting in ca. +/- 2 ppm band-width.

8. SUMMARY

Two important classes of molecules, namely, new lipophilic derivatives of cell-wall glycopeptides and novel disaccharide derivatives featuring disulfide interglycosidic linkage were investigated by means of NMR spectroscopy and model calculations to reveal conformational features of possible biological relevance. The results obtained can be summarized as follows.

Conformational investigations of modified cell wall peptides

Polymeric peptidoglycans of bacterial cell walls, and smaller glycopeptides derived from them, exhibit versatile biological activities including immunomodulating properties. Peptidoglycan monomer (PGM) isolated from *Brevibacterium divaricatum* cell wall has the following chemical structure:

D-GlcNAc - β(1→4) - D-MurNAc - L-Ala^{1} - D-*iso*Gln^{2} - *meso*Dap(εNH$_2$)^{3} - D-Ala^{4} - D-Ala^{5}

The parent PGM molecule and novel lipophilic derivatives of PGM bearing either (adamantyl-1-yl)-acetyl or Boc-Tyr substituents (Ad-PGM and BocTyr-PGM, respectively) were investigated by NMR and molecular modelling methods.

Full assignments of the ^{1}H and ^{13}C spectra, using 2D NMR techniques, were obtained for all three compounds in DMSO solutions. NOESY/ROESY experiments have provided interproton distance restraints that were used in distance geometry modelling calculations to derive conformational preferences for each of these molecules. These data were supplemented with information available from chemical shifts, temperature dependence of amide proton shifts and proton-proton scalar couplings.

Analyses of the results suggest that the lipophilic substituents attached to the Dap^{3}-ε amino group of the parent PGM molecule introduce changes to the conformational preferences of the peptide moiety. In PGM electrostatic interactions between charged end groups apparently promote folded conformations with participation of the long Dap side chain. Derivatives wherein such interactions are suppressed by acylation of the Dap^{3}-ε amino group are characterized by more extended conformations of the peptide chain. The new synthetic derivatives exhibit biological properties similar to those of the parent PGM. This may indicate that peripheral parts of the peptide chain such as the C-terminal and end groups

of the long Dap side chain do not significantly contribute to the binding to receptors or enzymes under physiological conditions.

Conformational preferences of diglycosyl disulfides

Conformational preferences of a novel class of glycomimetics, non-symmetric oligosaccharides containing a three-bond disulfide linkage in place of the interglycosidic oxygen were investigated by conformational analysis based on the comparison of NMR data and modelling calculations.

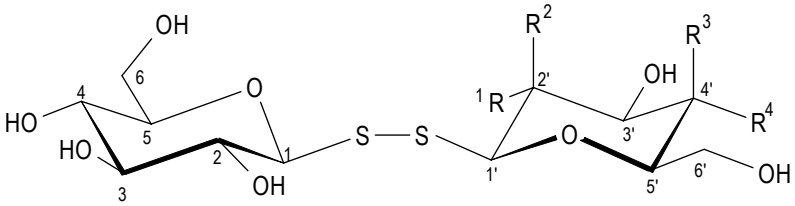

	R^1	R^2	R^3	R^4
Glc-S-S-Man	H	OH	H	OH
Glc-S-S-Gal	OH	H	OH	H
Glc-S-S-NAcGlc	NAc	H	H	OH

Temperature coefficients for the hydroxide and amide protons indicate that majority of the labile protons was exposed to the solvent and not involved in hydrogen bonding. The exchange with the solvent was found to be somewhat restricted in the case of the amide proton in Glc-S-S-NAcGlc. Only a few conformationally relevant interannular NOEs contacts were found for all three derivatives. Relative magnitudes of the intraresidue residual dipolar couplings were interpreted only in terms of the stereochemistry at each carbon centre, but structure determination on the basis of residual dipolar couplings was not attempted thus far.

Experimental NMR data were supplemented by force-field calculations. Systematic search around the Φ_A, Φ_B and ω angles as well as simulated annealing calculations resulted in 18 minima in the conformational space for each of the 3 disaccharides investigated. The Φ angles around the bond connecting the anomeric carbon and the sulfur indicate staggered conformations around the C1-S bond, that is $+60^o$ (+ synclinal) and 300^o (- synclinal or -60^o) for synclinal arrangements and 180^o for antiperiplanar arrangement. Conformers featuring exo-anomeric effect at their Φ angles dominate among the low energy conformers. The conformation around the disulfide bond, ω, was found to be close to $\pm 90^o$. The kinetic energy

(kT) available for the molecules at room temperature is sufficient to overcome the low conformational barriers. Consequently these data suggest the presence of several different, time-averaged conformations.

On the basis of the distribution of the E_{pot} and the number of structures generated by SA conformational families were divided into subgroups of low energy of conformations. The larger subgroup includes the first 9 lowest energy conformations. Within these, a separate subgroup incorporating the first 4 lowest energy structures can be distinguished. 3 conformers within the latter group were found to be identical for all three derivatives with insignificant variation in the E_{pot}.

None of the minimum conformation can be used as 'single state model' to satisfactorily account for the experimental data observed. The intraresidual NOEs observed were found to be in agreement with conformations among low energy structures. A H bonding interaction was found to exist/identified in the lowest energy conformer satisfying all the interresidual NOEs for derivative Glc-S-S-NAcGlc.

Experimental data suggested the presence of several different, time-averaged conformations, however the computational results were indicative of definite conformational preferences in these novel disulfide disaccharide mimics. Thus, the increase of the degrees of motional freedom, expected a priori upon extension of the interglycosidic linkage, gets largely offset by stereoelectronic effects, such as the exo-anomeric effect, the preference of the disulfide torsion angle towards $\pm 90^{o}$ and the existence of interresidual H bonding interactions.

The second part of the dissertation describes modifications of known NMR techniques to aid/for measurements of residual one-bond ^{1}H-^{13}C dipolar couplings and assignment of oligosaccharides featuring strong overlap in their NMR spectra.

Accurate determination of small one-bond heteronuclear residual dipolar couplings

A modification of the F1-coupled HSQC experiment was proposed for the accurate determination of one-bond heteronuclear residual dipolar couplings. The modification consists of inserting a G-BIRD$^{(r)}$ module which has been employed to refocus the long-range coupling evolution of the heteronucleus during the t_1 frequency labelling period. As a result, the crosspeaks obtained are split only by the direct one-bond coupling that can be extracted by

measuring simple frequency differences between singlet maxima. Additionally the decoupling of long-range multiple bond splittings leads to considerable sensitivity enhancement.

Bandselective suppression of unwanted signals in oligosaccharide spectra

Finally a general scheme was proposed for eliminating disturbing signals of some protecting groups from the 2D NMR spectra of oligosaccharides by making use of a band-selective suppression – restoration sequence that serves as a preparation step to various 2D NMR experiments. This consists of a preparation step whereby band-selective suppression of unwanted signals is followed by a TOCSY transfer to recover useful resonances in the spectral region of interest. When the element is inserted in the place of the initial 90^{o} ^{1}H pulse of any sequence, it yields a transverse magnetisation arising from the useful signals that is further manipulated by the remaining parts of the specific sequence. Modified versions of 2D methods commonly used for assignment (such as COSY, TOCSY, HSQC, HMBC) yielded spectra dsiplaying signals of useful anomeric and sugar ring protons without disturbing signals arising from protecting groups, thus, unambiguous assignments of the substances become possible.

ÖSSZEFOGLALÁS

Az értekezés első része sejtfal glikopeptidek és diszulfid interglikozidos hidat tartalmazó diszacharidok konformációs sajátságainak vizsgálatával foglalkozik. NMR és molekula modellezési módszerek kapcsolt alkalmazásával vizsgáltuk a molekulák konformációs jellemzőit, amelyek biológiai kölcsönhatásokban is jelentős szerepet játszhatnak.

Módosított sejtfal glikopeptidek konformációs vizsgálata

A bakteriális sejtfal polimer peptidoglikánjai valamint a belőlük származó kisebb fragmensek változatos biológiai tulajdonságokkal rendelkeznek. A *Brevibacterium divaricatum* baktérium törzsből izolált peptidoglikán monomer a következő szerkezettel rendelkezik:

D-GlcNAc - β(1→4) - D-MurNAc - L-Ala^{1} - D-*iso*Gln^{2} - *meso*Dap(εNH$_2$)^{3} - D-Ala^{4} - D-Ala^{5}

Tanulmányoztuk a peptidoglikán monomer és két új lipofil származék szerkezetét, amelyek adamatil-1-acetil- illetve BocTyr- csoportokat tartalmaznak.

Elvégeztünk a származékok ^{1}H és ^{13}C spektrumainak teljes jelhozzárendelését DMSO oldatban. NOESY és ROESY kísérletekből nyert proton-proton távolság kényszerfeltételek alapján távolság-geometria számításokkal meghatároztuk a molekulák konformációs jellemzőit. A model számításokon kívül felhasználtuk a kémiai eltolódásból, az amid protonok kemiai eltolódásásnak hőmérséklet függéséből és a proton-proton skaláris csatolásokból származó szerkezeti információkat is. Az adatok elemzése azt mutatta, hogy az eredeti PGM molekulához a Dap^{3}-ε amino csoporton keresztül kapcsolt lipofil szubstituensek konformációs változásokat idéznek elő a molekulák peptid részén. Az elektrosztatikus kölcsönhatások a Dap oldallánc az elektromos töltéssel rendelkező végcsoportok (DAla^{5}-COO^{-}) között ezen csoportok térközelségével jellemzett konformációkat hoznak létre a PGM molekulában. Nyújtottabb konformációk jellemzők a két származékra, ahol a Dap^{3}-ε amino csoport acilezve van. Az új szintetikus származékok az eredeti PGM molekulához hasonló biológiai tulajdonságokkal bírnak. Ez a tény arra utal, hogy a peptid lánc periferális részei és a hosszú Dap oldallánc végcsoportjai fiziológiás körülmények között feltehetőleg nem játszanak szerepet a receptorokhoz és enzimekhez kötődés során.

Diglikozil diszulfidok konformációs jellemzői

Új tipusú glikomimetikumok konformációjanak analízisét végeztük el NMR vizsgálatok és a molekula modellezés eredményeinek összehasonlításával. A vizsgált glikomimetikumok az interglikozidos oxigén helyett három kötéses diszulfid hidat tartalmazó asszimmetrukus oligoszacharidok voltak.

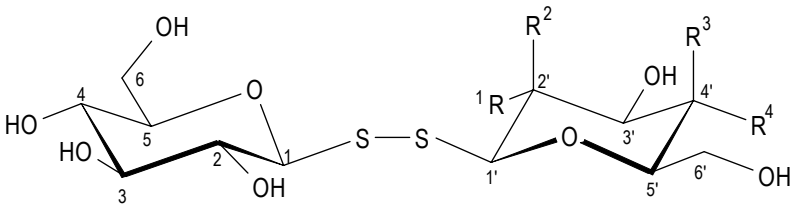

	R^1	R^2	R^3	R^4
Glc-S-S-Man	H	OH	H	OH
Glc-S-S-Gal	OH	H	OH	H
Glc-S-S-NAcGlc	NAc	H	H	OH

A hidroxil és amid protonok hőmérsekleti együtthatói azt mutatták, hogy a cserélhető protonok többsége az oldószerrel áll kölcsönhatásban és nincs hidrogén kötésben. Az oldószerrel való gyors cserélődés némiképpen gátolt az amid proton esetén a Glc-S-S-NAcGlc molekulában. Mindhárom származék esetén csak néhány, monoszaccharid egységek közötti NOE-t észleltünk. A gyengén orientálódó folyadékkristályos közegben mért maradék dipoláris csatolások értékeinek nagyságát a ^{1}H-^{13}C kötésvektorok a cukor gyűrűre jellemző irányítotttsága szempontjából elemeztük. A maradék dipoláris csatolások alapján szerkezetszámolásokat egyenlőre nem végeztünk.

Az NMR kísérleti adatokat molekula mechanika számításokkal egészítettük ki. A Φ_A, Φ_B és ω szögek körül végzett szisztematikus keresések és a szimulált hűtést alkalmazó számítások egyaránt 18 minimumot eredményeztek a konformációs térben. A monoszaccharid gyűrűkhöz közeli Φ szögek a C1-S kötés körül a nyitott konformációra jellemző értékeket vettek fel, azaz, $+60^o$ (+ szinklinális) és 300^o (- szinklinális or -60^o) értékeket szinklinális és 180^o antiperiplnáris elrendeződés esetén. Az alacsony energiájú konformerek között dominálnak az exo-anomer effektusnak megfelelő Φ szöggel bíró szerkezetek. A diszulfid híd körüli ω szög $\pm 90^o$ körül változott.

A konformációs családok potenciális energia sorrendje és szimulált hűtés által létrehozott szerkezetek száma alapján a konformációs családokat alcsoportokba soroltuk. A

legnagyobb alcsoport az első 9 legalacsonyabb energiájú konformert foglalja magába. Ezen belül egy külön alcsoportot alkot az első 4 legkisebb energiájú szerkezet. Ez utóbbi csoporton belül három konformer - némiképpen eltérő potenciális energiával - megjelenik mindhárom származék esetén.

Noha az önmagában a minimum energiájú konformációk egyike sem elegendő az észlelt kísérleti adatok értelmezéséhez, azonban az észlelt egységek közötti NOE-kat kielégítik a alacsony energiájú konformerekben mérhető ^{1}H-^{1}H távolságok. A Glc-S-S-NAcGlc legalacsonyabb energiájú konformációját, amely egyszerre teljesíti valamennyi NOE távolságfeltételt, valószínűleg H hidas kölcsönhatás stabilizálja.

Noha a kísérleti adatok számos időátlagolt konformáció jelenlétét mutatja, azonban a konformációs analízis határozott konformációs preferenciákat eredményezett mindhárom diszulfid diszaccharid származék esetén. A hosszabb interglikozidos kötés esetén várható megnövekedett mozgási szabadságot tehát korlátozzák a sztereoelektronikus effectusok, mint az exo-anomer effektus, diszulfid torziós szög $\pm 90^{o}$ felé irányuló preferenciája és a feltételezhető H kötés jelenléte.

A disszertáció második része ismert NMR mérési módszerek módosításaival foglalkozik, az egykötéses heteronukleáris maradék dipoláris csatolások pontos mérése, illetve erősen átfedő jeleket tartalmazó NMR spektrumok jelhozzárendelésének elősegítése céljából.

Egykötéses heteronukleáris maradék dipoláris csatolási állandók pontos meghatározása

Az egykötéses heteronukleáris maradék dipoláris csatolások pontos meghatározása érdekében javasoltuk az F1 dimezióban csatolt HSQC szekvencia módosítását. A módosítás során egy G-BIRD$^{(r)}$ elemet illesztettünk a szekvencába, amely refókuszálja távolható heteronukláris csatolások evolúcióját a t_1 idő alatt. Ennek eredményeképpen a spektrumban kapott keresztcsúcsok csak a kívánt egykötéses csatolás szerint hasadtak fel, amely a szingulett csúcsok közötti frekvencia különbség meghatározása révén pontosan és egyszerűen mérhető. A távolható csatolások ily módon történő eltávolítása jelentős érzékenység növekedést is eredményezett.

Sávszelektív jelelnyomás alkalmazása zavaró jelek kiszűrésésre

Végezetül, egy általánosan alkalmazható sémát javasoltunk oligoszaccharidok védőcsoportjaitól származó zavaró jelek elnyomására, amelyek megnehezítik a 2D spektrumok analízisét. A módszer sávszelektív elnyomáson majd azt követő szelektív mágnesezettség átvitelen alapszik, és bármely 2D NMR kísérletben előkészítő perióduskénti alkalmazható. Első lépésben a zavaró jelek teljes sávszelektív elnyomása történik amelyet egy izotróp keverési periódus követ. Ez utóbbi segítségével visszanyerjük az ugyanazon spektrális tartományban levő a hasznos jeleket. A jelhozzárendelésre általánosan használt NMR módszerek, mint pl. COSY, TOCSY, HSQC, HMBC kísérletek módosításai által elértük, hogy az anomer és más cukorváz protonok rezonancia jelei zavaró jelektől mentesen jelenjenek meg, lehetővé téve ezáltal az egyértelmű hozzárendelést.

9. REFERENCES

1. Lewitt M. H. *Spin Dynamics: Basics of Nuclear Magnetic resonance* John Wiley & Sons; (**2001**)

2. Gaemers, S. and A. Bax, Morphology of three lyotropic liquid crystalline biological NMR media studied by translational diffusion anisotropy. *J. Am. Chem. Soc.* 123, 12343-12352 (**2001**).

3. Buckingham AD and Lovering EG, **1962**, Tans. Faraday Soc. 58:2077,

4. Ruessink, B. H. and C. Maclean, Electric-Field NMR - a Method to Measure the Molecular Polarizability. *Mol. Phys.* 60, 1059-1066 (**1987**).

5. Prestegard JH, Tolman JR, Al-Hachimi HM, Andrec M Protein structure and dynamics from field induced residual dipolar couplings. In Biological Magnetic Resonance, Vol 17, Structure Computation and Dynamics in Protein NMR, (Eds Krishna NR, Berliner LJ) Chapter 8, 311-355. Plenum, New York (**1996**)

6. H. C. Kung, K. Y. Wang, I. Goljer, and P. H. Bolton, Magnetic alignment of duplex and quadruplex DNAs. *J. Magn. Reson. B* 109**,** 323 (**1995**).

7. Tjandra, N., J. G. Omichinski, A. M. Gronenborn, G. M. Clore and A. Bax, Use of dipolar H-1-N-15 and H-1-C-13 couplings in the structure determination of magnetically oriented macromolecules in solution. *Nat. Struct. Biol.* 4, 732-738 (**1997**).

8. Tolman, J. R., J. M. Flanagan, M. A. Kennedy and J. H. Prestegard, Nuclear Magnetic Dipole Interactions in Field-Oriented Proteins - Information for Structure Determination in Solution. *Proc. Natl. Acad. Sci. U. S. A.* 92, 9279-9283 (**1995**).,

9. Tolman, J. R., J. M. Flanagan, M. A. Kennedy and J. H. Prestegard, NMR evidence for slow collective motions in cyanometmyoglobin. *Nat. Struct. Biol.* 4, 292-297 (**1997**).

10. Tjandra, N., S. Grzesiek and A. Bax, Magnetic field dependence of nitrogen-proton J splittings in N- 15-enriched human ubiquitin resulting from relaxation interference and residual dipolar coupling. *J. Am. Chem. Soc.* 118, 6264-6272 (**1996**).

11. Van zijl, P. C. M., C. Maclean and A. A. Bothnerby, Angular-Correlation and Diamagnetic Susceptibilities Studied by High-Field Nmr. *J. Chem. Phys.* 83, 4410-4417 (**1985**).

12. Saupe, A. and G. Englert, High-Resolution Nuclear Magnetic Resonance Spectra of Orientated Molecules. *Phys. Rev. Lett.* 11, 462-& (**1963**).

13. Emsley JW, Lindon JC, NMR Spectroscopy Using Liquid Crystal Solvents Pergamon New York, (**1975**),

14. Diehl P in Nuclear Magnetic Resonance of Liquid Crystals Emsley JW, Ed. Reidel, Dordrecht, Netherlands, 147-180. (**1985**)

15. Bax, A. and N. Tjandra, High-resolution heteronuclear NMR of human ubiquitin in an aqueous liquid crystalline medium. *J. Biomol. NMR* 10, 289-292 (**1997**).

16. Prestegard, J. H., New techniques in structural NMR - anisotropic interactions. *Nat. Struct. Biol.* **5**, 517-522 (**1998**).

17. Bax, A. and N. Tjandra, Are proteins even floppier than we thought? *Nat. Struct. Biol.* 4, 254-256 (**1997**).

18. Tjandra, N. and A. Bax, Direct measurement of distances and angles in biomolecules by NMR in a dilute liquid crystalline medium. *Science* 278, 1111-1114 (**1997**).

19. Clore, G. M. and A. M. Gronenborn, New methods of structure refinement for macromolecular structure determination by NMR. *Proc. Natl. Acad. Sci. U. S. A.* 95, 5891-5898 (**1998**).

20. Sanders, C. R. and J. P. Schwonek, Characterization of Magnetically Orientable Bilayers in Mixtures of Dihexanoylphosphatidylcholine and Dimyristoylphosphatidylcholine by Solid-State Nmr. *Biochemistry **31***, 8898-8905 (**1992**).

21. Prosser, R. S., J. A. Losonczi and I. V. Shiyanovskaya, Use of a novel aqueous liquid crystalline medium for high- resolution NMR of macromolecules in solution. *J. Am. Chem. Soc.* 120, 11010-11011 (**1998**).

22. Barrientos, L. G., C. Dolan and A. M. Gronenborn, Characterization of surfactant liquid crystal phases suitable for molecular alignment and measurement of dipolar couplings. *J. Biomol. NMR* 16, 329-337 (**2000**).

23. Ruckert, M. and G. Otting, Alignment of biological macromolecules in novel nonionic liquid crystalline media for NMR experiments. *J. Am. Chem. Soc. **122***, 7793 (**2000**).

24. Clore, G. M., M. R. Starich and A. M. Gronenborn, Measurement of residual dipolar couplings of macromolecules aligned in the nematic phase of a colloidal suspension of rod- shaped viruses. *J. Am. Chem. Soc.* 120, 10571-10572 (**1998**).

25. Hansen, M. R., L. Mueller and A. Pardi, Tunable alignment of macromolecules by filamentous phage yields dipolar coupling interactions. *Nat. Struct. Biol.* 5, 1065-1074 (**1998**).

26. Sass, J., F. Cordier, A. Hoffmann, A. Cousin, J. G. Omichinski, H. Lowen and S. Grzesiek, Purple membrane induced alignment of biological macromolecules in the magnetic field. *J. Am. Chem. Soc.* 121, 2047-2055 (**1999**).

27. Koenig, B. W., J. S. Hu, M. Ottiger, S. Bose, R. W. Hendler and A. Bax, NMR measurement of dipolar couplings in proteins aligned by transient binding to purple membrane fragments. *J. Am. Chem. Soc.* 121, 1385-1386 (**1999**).

28. Fleming, K., D. Gray, S. Prasannan and S. Matthews, Cellulose crystallites: A new and robust liquid crystalline medium for the measurement of residual dipolar couplings. *J. Am. Chem. Soc.* 122, 5224-5225 (**2000**).

29. Fleming, K., D. G. Gray and S. Matthews, Cellulose crystallites. *Chem.-Eur. J.* 7, 1831-1835 (**2001**).

30. Tycko, R., F. J. Blanco and Y. Ishii, Alignment of biopolymers in strained gels: A new way to create detectable dipole-dipole couplings in high-resolution biomolecular NMR. *J. Am. Chem. Soc.* 122, 9340-9341 (**2000**).

31. Friebolin, H. *Basic One- and Two-dimensional NMR spectroscopy*, Wiley-VCH, Weinheim, Basel, p. 41-51 (**1993**).

32. Wehrli, FW and Wirthlin, T. *Interpretation of Carbon 13 NMR spectra*, Heyden, London, New York, p. 22-39 (**1976**) and references therein.

33. Soth, M. J. and J. S. Nowick, A peptide/oligourea/azapeptide hybrid that adopts a hairpin turn. *J. Org. Chem.* 64, 276-281 (**1999**).and references therein.

34. Thomas, W. A., Unravelling molecular structure and conformation - The modern role of coupling constants. *Prog. Nucl. Magn. Reson. Spectrosc.* 30, 183-207 (**1997**).
and references therein.

35. Edison, A. S., J. L. Markley and F. Weinhold, Calculations of One-Bond, 2-Bond and 3-Bond Nuclear Spin-Spin Couplings in a Model Peptide and Correlations with Experimental-Data. *J. Biomol. NMR* 4, 519-542 (**1994**).

36. Edison, A. S., F. Weinhold, W. M. Westler and J. L. Markley, Estimates of Phi-Torsion and Psi-Torsion Angles in Proteins from One-Bond, 2-Bond and 3-Bond Nuclear Spin-Spin Couplings - Application to Staphylococcal Nuclease. *J. Biomol. NMR* 4, 543-551 (**1994**).

37. Hansen, P. E., Carbon-Hydrogen Spin-Spin Coupling-Constants. *Prog. Nucl. Magn. Reson. Spectrosc.* 14, 175-296 (**1981**).

38. Bock, K. and C. Pedersen, Study of Ch-13 Coupling-Constants in Pentopyranoses and Some of Their Derivatives. *Acta Chemica Scandinavica Series B-Organic Chemistry and Biochemistry* B 29, 258-264 (**1975**).

39. Karplus, M. *J. Am. Chem. Soc.*, 85, 2870-2871 (**1963**).

40. Bystrov, V. F. Spin-Spin Coupling and the Conformational States of Peptide Systems. *Prog. NMR Spectrosc.*, 10, 41-81 (**1976**).

41. Derome, AE. *Organic Chemistry Series: Modern NMR Techniques for Chemistry Research*, Pergamon, Kidlington, Oxford, (**1995**).

42. Neuhaus, D and Williamson, MP. *The nuclear Overhauser effect in structural and conformational analysis*, VCH Publishers, New York,Weinheim, Cambridge, (**1989**).

43. Bax, A. and D. G. Davis, Practical Aspects of Two-Dimensional Transverse Noe Spectroscopy. *J. Magn. Reson.* 63, 207-213 (**1985**).

44. Wüthrich, K. *NMR of Proteins and Nucleic Acids*, Wiley and Sons, New York, (**1986**).

45. Prestegard, J. H., H. M. Al-Hashimi and J. R. Tolman, NMR structures of biomolecules using field oriented media and residual dipolar couplings. *Q. Rev. Biophys.* 33, 371-424 (**2000**).

46. Gronenborn, A. M., The importance of being ordered: improving NMR structures using residual dipolar couplings. *C. R. Biol.* 325, 957-966 (**2002**).

47. de Alba, E. and N. Tjandra, NMR dipolar couplings for the structure determination of biopolymers in solution. *Prog. Nucl. Magn. Reson. Spectrosc.* 40, 175-197 (**2002**).

48. Case, D. A. Calculations of NMR dipolar coupling strengths in model peptides. *J. Biomol. NMR* 15, 95-102. (**1999**).

49. Saupe, A. Recent results in the field of liquid crystals. *Angew. Chem. Int. Ed. Engl.* **7**, 97-112. (**1968**).

50. Claridge T. D. W. *High-Resolution NMR techniques in Organic Chemistry*, Pergamon, Amsterdam, p. 8-12, (**1999**)

51. J. Jeener, Ampere International Summer School, Basko Polje, **1971** (proposal)

52. von Kienlin, M., C. T. W. Moonen, A. Vandertoorn and P. C. M. van Zijl, Rapid Recording of Solvent-Suppressed 2d Cosy Spectra with Inherent Quadrature Detection Using Pulsed Field Gradients. *J. Magn. Reson.* 93, 423-429 (**1991**).

53. Braunschweiler, L. and R. R. Ernst, Coherence Transfer by Isotropic Mixing - Application to Proton Correlation Spectroscopy. *J. Magn. Reson.* 53, 521-528 (**1983**).

54. Bax, A. and D. G. Davis, Mlev-17-Based Two-Dimensional Homonuclear Magnetization Transfer Spectroscopy. *J. Magn. Reson.* 65, 355-360 (**1985**).

55. Davis, D. G. and A. Bax, Assignment of Complex H-1-Nmr Spectra Via Two-Dimensional Homonuclear Hartmann-Hahn Spectroscopy. *J. Am. Chem. Soc.* 107, 2820-2821 (**1985**).

56. Kövér, K. E., D. Uhrin and V. J. Hruby, Guadient- and sensitivity-enhanced TOCSY experiments. *J. Magn. Reson.* 130, 162-168 (**1998**).

57. Otting, G. and K. Wuthrich, Efficient Purging Scheme for Proton-Detected Heteronuclear Two- Dimensional Nmr. *J. Magn. Reson.* 76, 569-574 (**1988**).

58. Kövér, K. E., O. Prakash and V. J. Hruby, Z-Filtered Heteronuclear Coupled-Hsqc-Tocsy Experiment as a Means for Measuring Long-Range Heteronuclear Coupling-Constants. *J. Magn. Reson. Ser. A* 103, 92-96 (**1993**).

59. Kövér, K. E., V. J. Hruby and D. Uhrin, Sensitivity- and gradient-enhanced heteronuclear coupled/decoupled HSQC-TOCSY experiments for measuring long-range heteronuclear coupling constants. *J. Magn. Reson.* 129, 125-129 (**1997**).

60. Bodenhausen, G. and D. J. Ruben, Natural Abundance N-15 Nmr by Enhanced Heteronuclear Spectroscopy. *Chem. Phys. Lett.* 69, 185-189 (**1980**).

61. Palmer, A. G., J. Cavanagh, P. E. Wright and M. Rance, Sensitivity Improvement in Proton-Detected 2-Dimensional Heteronuclear Correlation Nmr-Spectroscopy. *J. Magn. Reson.* 93, 151-170 (**1991**).

62. Kay, L. E., P. Keifer and T. Saarinen, Pure Absorption Gradient Enhanced Heteronuclear Single Quantum Correlation Spectroscopy with Improved Sensitivity. *J. Am. Chem. Soc.* 114, 10663-10665 (**1992**).

63. Kontaxis, G., J. Stonehouse, E. D. Laue and J. Keeler, The Sensitivity of Experiments Which Use Gradient Pulses for Coherence-Pathway Selection. *J. Magn. Reson. Ser. A* 111, 70-76 (**1994**).

64. Bax, A. and M. F. Summers, H-1 and C-13 Assignments from Sensitivity-Enhanced Detection of Heteronuclear Multiple-Bond Connectivity by 2d Multiple Quantum Nmr. *J. Am. Chem. Soc.* 108, 2093-2094 (**1986**).

65. Willker, W., D. Leibfritz, R. Kerssebaum and W. Bermel, Gradient Selection in Inverse Heteronuclear Correlation Spectroscopy. *Magn. Reson. Chem.* 31, 287-292 (**1993**).

66. Ruizcabello, J., G. W. Vuister, C. T. W. Moonen, P. Vangelderen, J. S. Cohen and P. C. M. VanZijl, Gradient-Enhanced Heteronuclear Correlation Spectroscopy - Theory and Experimental Aspects. *J. Magn. Reson.* 100, 282-302 (**1992**).

67. Kessler, H., H. Oschkinat and C. Griesinger, Transformation of Homonuclear Two-Dimensional Nmr Techniques into One-Dimensional Techniques Using Gaussian Pulses. *J. Magn. Reson.* 70, 106-133 (**1986**).

68. Sklenar, V. and J. Feigon, Simplification of DNA Proton Nuclear-Magnetic-Resonance Spectra by Homonuclear Hartmann-Hahn Edited 2-Dimensional Nuclear Overhauser Enhancement Spectroscopy. *J. Am. Chem. Soc.* 112, 5644-5645 (**1990**).

69. Kessler, H., S. Mronga and G. Gemmecker, Multidimensional Nmr Experiments Using Selective Pulses. *Magn. Reson. Chem.* 29, 527-557 (**1991**).

70. Poppe, L. and H. Vanhalbeek, Noe Measurements on Carbohydrates in Aqueous-Solution by Double-Selective Pseudo-3d Tocsy-Roesy and Tocsy-Noesy - Application to Gentiobiose. *J. Magn. Reson.* 96, 185-190 (**1992**).

71. Facke, T. and S. Berger, Application of Pulsed-Field Gradients in an Improved Selective Tocsy Experiment. *J. Magn. Reson. Ser. A* 113, 257-259 (**1995**).

72. Jeener, J., B. H. Meier, P. Bachmann and R. R. Ernst, Investigation of Exchange Processes by 2-Dimensional NMR Spectroscopy. *J. Chem. Phys.* 71, 4546-4553 (**1979**).

73. reference **41.** at p.253-305

74. Wagner, R. and S. Berger, Gradient-selected NOESY - A fourfold reduction of the measurement time for the NOESY experiment. *J. Magn. Reson. Ser. A* 123, 119-121 (**1996**).

75. Parella, T., F. SanchezFerrando and A. Virgili, Quick recording of pure absorption 2D TOCSY, ROESY, and NOESY spectra using pulsed field gradients. *J. Magn. Reson.* 125, 145-148 (**1997**).

76. Bothnerby, A. A., R. L. Stephens, J. M. Lee, C. D. Warren and R. W. Jeanloz, Structure Determination of a Tetrasaccharide - Transient Nuclear Overhauser Effects in the Rotating Frame. *J. Am. Chem. Soc.* 106, 811-813 (**1984**).

77. Hwang, T. L. and A. J. Shaka, Cross Relaxation without Tocsy - Transverse Rotating-Frame Overhauser Effect Spectroscopy. *J. Am. Chem. Soc.* 114, 3157-3159 (**1992**).

78. Hwang, T. L., M. Kadkhodaei, A. Mohebbi and A. J. Shaka, Coherent and Incoherent Magnetization Transfer in the Rotating Frame. *Magn. Reson. Chem.* 30, S24-S34 (**1992**).

79. Bax, A. and D. G. Davis, Practical Aspects of Two-Dimensional Transverse Noe Spectroscopy. *J. Magn. Reson.* 63, 207-213 (**1985**).

80. reference **41.** at p. 312-327

81. Eberstadt, M., G. Gemmecker, D. F. Mierke and H. Kessler, Scalar Coupling-Constants - Their Analysis and Their Application for the Elucidation of Structures. *Angew. Chem.-Int. Edit. Engl.* 34, 1671-1695 (**1995**).

82. Montelione, G. T. and G. Wagner, Accurate Measurements of Homonuclear H-N-H-Alpha Coupling- Constants in Polypeptides Using Heteronuclear 2d Nmr Experiments. *J. Am. Chem. Soc.* 111, 5474-5475 (**1989**).

83. Billeter, M., D. Neri, G. Otting, Y. Q. Qian and K. Wuthrich, Precise Vicinal Coupling-Constants 3jhn-Alpha in Proteins from Nonlinear Fits of J-Modulated [N-15,H-1]-Cosy Experiments. *J. Biomol. NMR* 2, 257-274 (**1992**).

84. Vuister, G. W., F. Delaglio and A. Bax, The Use of ^{1}C-alpha-H-alpha Coupling-Constants as a Probe for Protein Backbone Conformation. *J. Biomol. NMR* **3**, 67-80 (**1993**).

85. Vuister, G. W. and A. Bax, Quantitative J Correlation - a New Approach for Measuring Homonuclear 3-Bond J(H(N)H(Alpha) Coupling-Constants in N-15-Enriched Proteins. *J. Am. Chem. Soc.* **115**, 7772-7777 (**1993**).,

86. Bax A, Vuister GW, Grzesiek S, Delaglio F, Wang AC, tschuldin R, Zhu G, Meth. Enzymol, 239:79, (**1994**)

87. Prestegard JH, Tolman JR, Al-Hachimi HM, Andrec M Protein structure and Dynamics from Field.induced residual Dipolar Couplings in Biological Magnetic Resonance, Vol 17, Structure, Computation and Dynamics in Protein NMR, Chapter 8, 311. (**1996**)

88. Abragam A *Principles of Nuclear Magnetism*, Caledron Press, Oxford, (**1961**)

89. Tolman, J. R. and J. H. Prestegard, Measurement of amide N-15-H-1 one-bond couplings in proteins using accordion heteronuclear-shift-correlation experiments. *J. Magn. Reson. Ser. B* 112, 269-274 (**1996**).

90. J. R. Garbow, D. P. Weitekamp, A. Pines, Bilinear Rotation Decoupling of Homonuclear Scalar Interactions. *Chem. Phys. Lett.* 93(5), 504-509 (**1982**).

91. D. Uhrin, T. Liptaj, K. E. Kövér, Modified Bird Pulses and Design of Heteronuclear Pulse Sequences. *J. Magn. Reson. Series A* 101(1), 41-46 (**1993**).

92. Morris, G. A. and R. Freeman, Selective Excitation in Fourier-Transform Nuclear Magnetic- Resonance. *J. Magn. Reson.* 29, 433-462 (**1978**).

93. Hwang, T. L. and A. J. Shaka, Water Suppression That Works - Excitation Sculpting Using Arbitrary Wave-Forms and Pulsed-Field Gradients. *J. Magn. Reson. Ser. A* 112, 275-279 (**1995**).

94. Stott, K., J. Stonehouse, J. Keeler, T. L. Hwang and A. J. Shaka, Excitation Sculpting in High-Resolution Nuclear-Magnetic- Resonance Spectroscopy - Application to Selective Noe Experiments. *J. Am. Chem. Soc.* 117, 4199-4200 (**1995**).

95. Leach A.R Molecular Modelling: Principles and Applications, 2nd edition, Prentice Hall, (2001)

96. *Forcefield-Based Simulations*, InsightII Manual, Acceryls Inc., San Diego, CA, (**1998)**

97. Homans, S. W., Oligosaccharide Conformations - Application of Nmr and Energy Calculations. *Prog. Nucl. Magn. Reson. Spectrosc.* 22, 55-81 (**1990**).

98. Perez, S., M. Kouwijzer, K. Mazeau and S. B. Engelsen, Modeling polysaccharides: Present status and challenges. *J. Mol. Graph.* 14, 307-& (**1996**).

99. Lemieux, R. U.; Pavia, A. A.; Martin, J. C.; Watanabe, K. A. *Can. J. Chem.*, *47*, 4427-2239, (**1969),**

100. Tvaroska, I. and T. Bleha, Anomeric and Exoanomeric Effects in Carbohydrate-Chemistry. *Adv. Carbohydr. Chem. Biochem.* 47, 45-123 (**1989**).

101. G.A. Jeffrey and W. Saenger. *Hydrogen Bonding in Biological Structures*. Springer Verlag, Heidelberg, (**1991**).

102. Kouwijzer, M. and P. D. J. Grootenhuis, Parametrization and Application of Cheat95, an Extended Atom Force-Field for Hydrated (Oligo)Saccharides. *J. Phys. Chem.* 99, 13426-13436 (**1995**).

103. Orozco, M., J. M. Lopez, C. Colomines, C. Alhambra, M. A. Busquets and F. J. Luque, Theoretical representation of solvation in biochemical systems: From discrete solute-solvent interactions to bulk solvation. *Int. J. Quantum Chem.* 60, 1179-1187 (**1996**).

104. Seidl, P. H., Schleifer, K. H. *Biological properties of peptidoglycans*; W.de Gruyter: Berlin, (**1986)**.

105. Ellouz, F., A. Adam, R. Ciorbaru and E. Lederer, Minimal structure requirement for adjuvant activity of peptidoglycan derivatives. *Biochem. Biophys. Res. Commun.* 59, 1317-1325 (**1974**).

106. Azuma, I., Synthetic immunoadjuvants: application to non-specific host stimulation and potentiation of vaccine immunogenicity. *Vaccine* 10, 1000-1006 (**1992**).

107. Stewart-Tull, D., Immunostimulation with peptidoglycan or its synthetic derivatives. *Prog. Drug Res* 32, 305-328 (**1988**).

108. Baschang, G., Muramylpeptides and lipopeptides: Studies towards immunostimulants. *Tetrahedron* 45, 6331-6360 (**1989**).

109. Roshni Mitra, Sarvjeet Singh and Ashok Khar Roshni Mitra, Sarvjeet Singh and Ashok Khar Antitumour immune response*s Expert Reviews in molecular medicine* Vol 5. at http://www.expertreviews.org/ (**2003)**,

110. Sava, G., S. Pacor, B. Vranesic, J. Tomasic and M. Cocchietto, Modification of the Growth of Mca Mammary-Carcinoma of Cba Mouse by New Adamantylpeptides. *Int. J. Oncol.* 2, 607-612 (**1993**).

111. Ladeçic, B., S. Perovic and I. Hrçak, Pharmacokinetics of an Immunomodulator Peptidoglycan Monomer in Mice After Intravenous Administration. *Int.J.Immunopharmac.* 15, 145-150 (**1993**).

112. Vraneçic, B., J. Tomaçic, D. Ljevakovic and I. Hrsak *Biological Activity of Novel Adamantyl Tripeptides with Emphasis on their Immunorestorative Effect*. New York Basel, Hong Kong, Marcel Dekker, Inc. (**1994**)

113. Keglević D., Ladešić B., Tomašić J., Valinger Z., Naumski R. Isolation procedure and properties of monomer unit from lysozyme digest of peptidoglycan complex excreted into the medium by penicillin-treated Brevibacterium divaricatum mutant. *Biochim. Biophys. Acta* 629 77-82. (**1979**),

114. Tomašić J., Sesartić Lj., Martin S.A., Valinger Z., Ladešić B. Comparative susceptibility of a peptidoglycan monomer from Brevibacterium divaricatum and its anhydromuramyl analogue to hydrolysis with N-acetylmuramyl-L-alanine amidase. *J. Chromatogr.* 440 405-414. (**1988**)

115. Tomašić J. and Hršak I. Peptidoglycan monomer originating from *Brevibacterium divaricatum* - its metabolism and biological activities in the host. In *Surface Structures of Microorganisms and Their Interaction with the Mammalian Host* (E. Schrinner, M.H. Richmond, G. Seidl and U. Schwartz, Eds.) 113-121. VCH Gesellschaft., (**1988**).

116. J. Tomašić, I. Hanzl-Dujmović, B. Špoljar, B. Vranešić, M. Šantak, A. Jovičić. Comparative study of the effects of peptidoglycan monomer and structurally related adamantyltripeptides on humoral immune response to ovalbumin in the mouse. *Vaccine* 18 1236-1243. (**2000**),

117. Sava, G., T. Giraldi, J. Tomasic and I. Hrsak, Immunotherapy of Lewis Lung-Carcinoma with Hydrosoluble Peptidoglycan Monomer (Pgm). *Cancer Immunol. Immunother.* 15, 84-86 (**1983**).

118. Hrsak, I., J. Tomasic and M. Osmak, Immunotherapy of B-16 Melanoma with Peptidoglycan Monomer. *European Journal of Cancer & Clinical Oncology* 19, 681-686 (**1983**).

119. Sava, G., J. Tomasic and I. Hrsak, Antitumor and Antimetastatic Activity of the Immunoadjuvant Peptidoglycan Monomer Pgm in Mice Bearing Mca Mammary-Carcinoma. *Cancer Immunol. Immunother.* 18, 49-53 (**1984**).

120. Martin, S. A., M. L. Karnovsky, J. M. Krueger, J. R. Pappenheimer and K. Biemann, Peptidoglycans as Promoters of Slow-Wave Sleep .1. Structure of the Sleep-Promoting Factor Isolated from Human-Urine. *J. Biol. Chem.* 259, 2652-2658 (**1984**).

121. Tomaçi†, J. and I. Hrçak, Peptidoglycan monomer originating from Brevibacterium divaricatum - its metabolism and biological activities in the host. *Preceedings of the Eigtheenh Workshop Conference Hoechst*, 113, (**1987**).

122. Klaić, B., ^{13}C NMR studies of a natural immunoadjuvant,peptidoglycan monomer and related compounds. *Carbohydr. Res.* 110, 320-325 (**1982**).

123. Klaić, B., B. Ljubi†, B. Metelko and M. Pongra†i†, NMR titration of a natural immonuadjuvant,disaccharide-pentapeptide,peptidoglycan monomer and related compounds. *Carbohydr. Res.* 123, 168-172 (**1983**).

124. Klaić, B., Domenick, R. L. ^{1}H-NMR Studies of a Natural Immunoadjuvant Peptidoglycan Monomer:Proposed Structure in Solution in Methyl Sulfoxide. *Carbohydr. Res.* 196, 19-27 (**1990**).

125. Matter, H., L. Szilágyi, P. Forgó, Z. Marinić and B. Klaić, Structure and dynamics of a peptidoglycan monomer i*hem. Soc.* 119, 2212-2223 (**1997**).

126. Halls, T. D. J., M. S. Raju, E. Wenkert, M. Zuber, P. Lefrancier and E. Lederer, The Anomeric Configuration of the Immunostimulant N- Acetylmuramoyl-Dipeptide and Some of Its Derivatives. *Carbohydr. Res.* 81, 173-176 (**1980**).

127. Chapman, B. E., M. Batley and J. W. Redmond, Proton N.M.R. of the Muramyl Dipeptide Adjuvant in Dimethyl Sulfoxide. *Aust. J. Chem.* 35, 489-493 (**1982**).

128. McFarlane, E. F. and C. Martinic, 400-MHz ^{1}H NMR of Adjuvant Muramyl Dipeptide in Dimethylsulfoxide. *Aust. J. Chem.* 36, 1087-1096 (**1983**).,

129. Fermandjian, S., B. Perly, M. Level and P. Lefrancier, A comparative ^{1}H-NMR study of MurNAc-L-Ala-D-DiGln (MDP) and its analogue Murabutide: evidence for a structure involving two successive beta turns in MDP. *Carbohydr. Res.* 162, 23-32 (**1987**).

130. Sizun, P., B. Perly, M. Level, P. Lefrancier and S. Fermandjian, Solution Conformations of the Immunomodulator Muramyl Peptides. *Tetrahedron* 44, 991-997 (**1988**).

131. Harb, V., J. Mavri, J. Kidric and D. Hadzi, Solution Conformation of the Immunomodulator Muramyl Dipeptide - Restrained Molecular-Dynamics Based on Nuclear-Magnetic- Resonance Data and Semiempirical Mo Study. *Croatica Chemica Acta* 64, 551-559 (**1991**).

132. Pristovsek, P., J. Kidric, J. Mavri and D. Hadzi, Nmr and Molecular-Dynamics Study of 4 Carbocyclic Muramyl Dipeptide Analogs. *Biopolymers* 33, 1149-1157 (**1993**).

133. Pristovsek, P. and J. Kidric, NMR and Molecular Dynamics Study of Muroctasin-Implications for the Bioactive Conformation. *Biopolymers* 42, 659-671 (**1997**).

134. Tonkovič, M., O. Had§ija, B. Ladeçič, B. Klaič and S. Musič, Preparation and Properties of the Complex of Fe(III) with Peptidoglycan Monomer. *Inorg. Chim. Acta* 161, 81-85 (**1989**).

135. Suskovic, B., Z. Vajtner and R. Naumski, Synthesis and Biological Activities of some Peptidoglycan Monomer Derivatives. *Tetrahedron* 47, 8407-8416 (**1991**).

136. Merser C, Sinay P, Adam A, Total synthesis and adjuvant activity of bacterial peptidoglycan derivatives. *Biochem. Biophys. Res. Commun.* 66:1316, (**1975**),

137. Adam A, Lederer E, Muramylpeptides as immunomodulators. *ISI atlas of Science: Immunology*. 1-205 (**1985**)

138. Levakovic, D., J. Tomasic, V. Sporec, B. H. Spoljar and I. Hanzl-Dujmovic, Synthesis of novel adamantylacetyl derivative of peptidoglycan monomer - Biological evaluation of immunomodulatory peptidoglycan monomer and respective derivatives with lipophilic substituents on amino group. *Bioorg. & Medic. Chem.* 8, 2441-2449 (**2000**).

139. Hršak, I.; Ljevaković, D.; Tomašić, J.; Vranešić, B. In *Immunotherapy of Infections;* Masihi, N., Ed.; Marcel Dekker, Inc.:; pp 249-257. (**1994**),

140. Vraneçic, B., D. C, J. Tomaçic and B. Ladeçic, A comperetive radioimmunoassay for peptidoglycan monomer. *Clin.Chim.A* 202, 23-38 (**1991**).

141. Dyson, H. J., G. Merutka, J. P. Waltho, R. A. Lerner and P. E. Wright, Folding of Peptide-Fragments Comprising the Complete Sequence of Proteins - Models for Initiation of Protein Folding .1. Myohemerythrin. *J. Mol. Biol.* 226, 795-817 (**1992**).

142. Malkin, V. G., O. L. Malkina, M. E. Casida and D. R. Salahub, Nuclear-Magnetic-Resonance Shielding Tensors Calculated with a Sum-over-States Density-Functional Perturbation-Theory. *J. Am. Chem. Soc.* 116, 5898-5908 (**1994**).

143. Weimar, T., U. C. Kreis, J. S. Andrews and B. M. Pinto, Conformational analysis of maltoside heteroanalogues using high-quality NOE data and molecular mechanics calculations. Flexibility as a function of the interglycosidic chalcogen atom. *Carbohydr. Res.* 315, 222-233 (**1999**). and the references cited therein

144. Jimenez-Barbero, J., J. F. Espinosa, J. L. Asensio, F. J. Canada and A. Poveda The conformation of C-glycosyl compounds. *Advances in Carbohydrate Chemistry and Biochemistry, Vol 56*. 56**:** 235-284. (**2001**). and the references cited therein

145. Babirad, S. A., Y. Wang, P. G. Goekjian and Y. Kishi, Preferred Conformation of C-Glycosides .3. Preferred Conformation of Carbon Analogs of 1,4-Disaccharides. *J. Org. Chem.* 52, 4825-4827 (**1987**).

146. Goekjian, P. G., T. C. Wu, H. Y. Kang and Y. Kishi, Preferred Conformation of C-Glycosides .2. Preferred Conformation of Carbon Analogs of Isomaltose and Gentiobiose. *J. Org. Chem.* 52, 4823-4825 (**1987**).

147. Goekjian, P. G., T. C. Wu, H. Y. Kang and Y. Kishi, Preferred Conformation of C-Glycosides .7. Preferred Conformation of Carbon Analogs of Isomaltose and Gentiobiose. *J. Org. Chem.* 56, 6422-6434 (**1991**).

148. Goekjian, P. G., T. C. Wu and Y. Kishi, Preferred Conformation of C-Glycosides .6. Conformational Similarity of Glycosides and Corresponding C-Glycosides. *J. Org. Chem.* 56, 6412-6422 (**1991**).

149. Haneda, T., P. G. Goekjian, S. H. Kim and Y. Kishi, Preferred Conformation of C-Glycosides .10. Synthesis and Conformational-Analysis of Carbon Trisaccharides. *J. Org. Chem.* 57, 490-498 (**1992**).

150. Miller, W. H., D. M. Ryckman, P. G. Goekjian, Y. Wang and Y. Kishi, Preferred Conformation of C-Glycosides .5. Experimental Support for the Conformational Similarity between C-Disaccharides and O-Disaccharides. *J. Org. Chem.* 53, 5580-5582 (**1988**).

151. Oleary, D. J. and Y. Kishi, Preferred Conformation of C-Glycosides .11. C-Sucrose - New Practical Synthesis, Structural Reassignment, and Solid-State and Solution Conformation of Its Octaacetate. *J. Org. Chem.* 58, 304-306 (**1993**).

152. Oleary, D. J. and Y. Kishi, Preferred Conformation of C-Glycosides .13. A Comparison of the Conformational Behavior of Several C-Furanosides, N-Furanosides, and O-Furanosides. *J. Org. Chem.* 59, 6629-6636 (**1994**).

153. Wang, Y., P. G. Goekjian, D. M. Ryckman and Y. Kishi, Preferred Conformation of C-Glycosides .4. Importance of 1,3- Diaxial-Like Interactions around the Nonglycosidic Bond - Prediction and Experimental Proof. *J. Org. Chem.* 53, 4151-4153 (**1988**).

154. Wei, A., A. Haudrechy, C. Audin, H. S. Jun, N. Haudrechybretel and Y. Kishi, Preferred Conformation of C-Glycosides .14. Synthesis and Conformational-Analysis of Carbon Analogs of the Blood-Group Determinant H-Type-Ii. *J. Org. Chem.* 60, 2160-2169 (**1995**).

155. Wei, A. and Y. Kishi, Preferred Conformation of C-Glycosides .12. Synthesis and Conformational-Analysis of Alpha,Alpha-, Alpha,Beta-, and Beta,Beta-C-Trehaloses. *J. Org. Chem.* 59, 88-96 (**1994**).

156. Wu, T. C., P. G. Goekjian and Y. Kishi, Preferred Conformation of C-Glycosides .1. Conformational Similarity of Glycosides and Corresponding C-Glycosides. *J. Org. Chem.* 52, 4819-4823 (**1987**).

157. Yuan, W., S. A. Babirad and Y. Kishi, Preferred Conformation of C-Glycosides .8. Synthesis of 1,4- Linked Carbon Disaccharides. *J. Org. Chem.* 57, 468-481 (**1992**).

158. Yuan, W., P. G. Goekjian, D. M. Ryckman, W. H. Miller, S. A. Babirad and Y. Kishi, Preferred Conformation of C-Glycosides .9. Conformational- Analysis of 1,4-Linked Carbon Disaccharides. *J. Org. Chem.* 57, 482-489 (**1992**).

159. X**=**C, Y**=**N: Andrews, J. S., T. Weimar, T. P. Frandsen, B. Svensson and B. M. Pinto, Novel Disaccharides Containing Sulfur in the Ring and Nitrogen in the Interglycosidic Linkage - Conformation of Methyl 5'- Thio-4-N-Alpha-Maltoside Bound to Glucoamylase and Its Activity as a Competitive Inhibitor. *J. Am. Chem. Soc.* 117, 10799-10804 (**1995**).

160. X**=**Y**=**C: Dondoni, A., H. M. Zuurmond and A. Boscarato, Synthesis of alpha- and beta-D-(1->-6)-C-disaccharides by Wittig olefination of formyl C-glycosides with glycopyranose 6- phosphoranes. *J. Org. Chem.* 62, 8114-8124 (**1997**).

161. X**=**Y**=**C, X**=**C, Y**=**S: Griffin, F. K., D. E. Paterson and R. J. K. Taylor, Ramberg-Backlund approaches to the synthesis of C-linked disaccharides. *Angew. Chem.-Int. Edit.* 38, 2939-2942 (**1999**).

162. X**=**N, Y**=**O: *calicheamicins* and *esperamicins*, for a review see: Smith, A. L. and K. C. Nicolaou, The enediyne antibiotics. *J. Med. Chem.* 39, 2103-2117 (**1996**).

163. X**=**C, Y**=**O: *namenamicin*: Weinstein, D. S. and K. C. Nicolaou, Synthesis of the namenamicin A-C disaccharide: towards the total synthesis of namenamicin. *J. Chem. Soc.-Perkin Trans. 1*, 545-557 (**1999**).

164. Stanek, J.; Sindlerova, M.; Cerny´, M. *Coll. Czech. Chem. Comm.*, 30, 297–303; (**1965)**

165. Bell, R. H.; Horton, D.; Miller, M. J. *Carbohydr. Res.*, 9, 201–214. (**1969**)

166. Wenzl, I., H. Kahlig, F. R. Unger and W. Schmid, A novel approach to beta-(1 -> 4)-linked thiodisaccharides starting from disulfide sugars. *Mon. Chem.* 130, 1137-1145 (**1999**).

167. Hough, L.; Sinchareonkul, L. V.; Richardson, A. C.; Akhtar, F.; Drew, M. G. B. *Carbohydr. Res.*, 9, 145–160. (**1969**)

168. Davis, B. G., R. C. Lloyd and J. B. Jones, Controlled site-selective glycosylation of proteins by a combined site-directed mutagenesis and chemical modification approach. *J. Org. Chem.* 63, 9614-9615 (**1998**).

169. Macindoe, W. M., A. H. van Oijen and G. J. Boons, A unique and highly facile method for synthesising disulfide linked neoglycoconjugates: a new approach for remodelling of peptides and proteins. *Chem. Commun.*, 847-848 (**1998**).

170. Szilagyi, L., T. Z. Illyes and P. Herczegh, Elaboration of a novel type of interglycosidic linkage: syntheses of disulfide disaccharides. *Tetrahedron Lett.* 42, 3901-3903 (**2001**).

171. Sears, P. and C. H. Wong, Carbohydrate mimetics: A new strategy for tackling the problem of carbohydrate-mediated biological recognition. *Angew. Chem.-Int. Edit.* 38, 2301-2324 (**1999**).

172. Perez, S., M. Kouwijzer, K. Mazeau and S. B. Engelsen, Modeling polysaccharides: Present status and challenges. *J. Mol. Graph.* 14, 307-& (**1996**).

173. Walker, S., D. Gange, V. Gupta and D. Kahne, Analysis of Hydroxylamine Glycosidic Linkages - Structural Consequences of the No Bond in Calicheamicin. *J. Am. Chem. Soc.* 116, 3197-3206 (**1994**).

174. Lees, W. J.; Whitesides, G. M. *J. Am. Chem. Soc.*, 115, 1860–1869 Lees, W. J. and G. M. Whitesides, Interpretation of the Reduction Potential of 6,6'-Dithiosucrose Cyclic Disulfide by Comparison of the Conformations of 6,6'- Dithiosucrose Cyclic Disulfide, 6,6'-Dithiosucrose, and Sucrose in Aqueous-Solution. *J. Am. Chem. Soc.* 115, 1860-1869 (**1993**). and references cited therein.

175. Homans, S. W., Oligosaccharide Conformations - Application of Nmr and Energy Calculations. *Prog. Nucl. Magn. Reson. Spectrosc.* 22, 55-81 (**1990**).

176. Croasmun W. R., Carlson R. M. K. *Two-Dimensioanl and related NMR methods in Structural Analyses of Oligisaccharides and Polysaccharides*, VCH Publishers, New York, Chapter 8. by Dabrovsky J: Two Dimenesional and Related NMR Methods in Structural Analysis of Oligosaccharides and Polysaccharides, p.741-783, (**1994**)

177. Sandstrom, C., H. Baumann and L. Kenne, The use of chemical shifts of hydroxy protons of oligosaccharides as conformational probes for NMR studies in aqueous solution. Evidence for persistent hydrogen bond interaction in branched trisaccharides. *J. Chem. Soc.-Perkin Trans. 2*, 2385-2393 (**1998**).

178. de la Paz, M. L., J. Jimenez-Barbero and C. Vicent, Hydrogen bonding and cooperativity effects on the assembly of carbohydrates. *Chem. Commun.*, 465-466 (**1998**).

179. Bernet, B. and A. Vasella, Intra- and intermolecular H-bonds of alcohols in DMSO - H-1-NMR analysis of inter-residue H-bonds in selected oligosaccharides: Cellobiose,

lactose, N,N '-diacetylchitobiose, maltose, sucrose, agarose, and hyaluronates. *Helv. Chim. Acta* 83, 2055-2071 (**2000**).

180. Cumming, D. A. and J. P. Carver, Virtual and Solution Conformations of Oligosaccharides. *Biochemistry* 26, 6664-6676 (**1987**).

181. Woods, R. J., Computational carbohydrate chemistry: what theoretical methods can tell us. *Glycoconjugate J.* 15, 209-216 (**1998**).

182. Martin-Pastor, M. and C. A. Bush, Conformational studies of human milk oligosaccharides using H- 1-C-13 one-bond NMR residual dipolar couplings. *Biochemistry* 39, 4674-4683 (**2000**).

183. Neubauer, H., J. Meiler, W. Peti and C. Griesinger, NMR structure determination of saccharose and raffinose by means of homo- and heteronuclear dipolar couplings. *Helv. Chim. Acta* 84, 243-258 (**2001**).

184. Tian, F., H. M. Al-Hashimi, J. L. Craighead and J. H. Prestegard, Conformational analysis of a flexible oligosaccharide using residual dipolar couplings. *J. Am. Chem. Soc.* 123, 485-492 (**2001**).

185. Tjandra, N., S. Grzesiek and A. Bax, Magnetic field dependence of nitrogen-proton J splittings in N- 15-enriched human ubiquitin resulting from relaxation interference and residual dipolar coupling. *J. Am. Chem. Soc.* 118, 6264-6272 (**1996**).

186. Martin-Pastor, M. and C. A. Bush, The use of NMR residual dipolar couplings in aqueous dilute liquid crystalline medium for conformational studies of complex oligosaccharides. *Carbohydr.Res.* 323, 147-155 (**2000**).

187. Martin-Pastor, M. and C. A. Bush, Conformational studies of human milk oligosaccharides using H- 1-C-13 one-bond NMR residual dipolar couplings. *Biochemistry* 39, 4674-4683 (**2000**).

188. Weiner, S. J.; Kollman, P. A.; Case, D. A.; Singh, U. C.; Ghio, C.; Alagona, G.; Profeta, S. Jr.; Weiner, P. A new force field for molecular mechanical simulation of nucleic acids and proteins, *J. Am. Chem. Soc.*, 106, 765–784 (**1984**).

189. Weiner, S. J.; Kollman, P. A.; Nguyen, D. T.; Case, D. A. An all atom forcefield for simulations of proteins and nucleic acid, *J. Comp. Chem.*, 7, 230–252 (**1986**).

190. Homans, S. W., A molecular mechanical force field for the conformational analysis of oligosaccharides: Comparison of theoretical and crystal structures of Man α1–3 Man β1–4 GlcNAc, *Biochemistry*, 29, 9110–9118 (**1990**).

191. Tvaroska, I. and J. P. Carver, Ab initio molecular orbital calculation of carbohydrate model compounds .5. Anomeric, exo-anomeric, and reverse anomeric effects in C-, N-, and S-glycosyl compounds. *J. Phys. Chem.* 100, 11305-11313 (**1996**).

192. J. R. Tolman, J. M. Flanagan, M. A. Kennedy, J. H.Prestegard, Nuclear Magnetic Dipole Interactions in Field-Oriented Proteins - Information for Structure Determination in Solution. *Proc. Natl. Acad. Sci. USA* 92(20), 9279-9283 (**1995**).

193. M. Zweckstetter, and A. Bax, Prediction of sterically induced alignment in a dilute liquid crystalline phase: Aid to protein structure determination by NMR. *J. Am. Chem. Soc.* 122(15), 3791-3792 (**2000**).

194. M. X. Fernandes, P. Berando, M. Pons and J. G. de la Torre, An analytical solution to the problem of the orientation of rigid particles by planar obstacles. Application to membrane systems and to the calculation of dipolar couplings in protein NMR spectroscopy. *J. Am. Chem. Soc.* 123, 12037-12047 (**2001**).

195. M. Ottiger, F. Delaglio, A. Bax, Measurement of J and dipolar couplings from simplified two- dimensional NMR spectra. *J. Magn. Reson.* 131(2), 373-378 (**1998**).

196. P. Andersson, J. Weigelt, G. Otting, Spin-state selection filters for the measurement of heteronuclear one-bond coupling constants. *J. Biomol. NMR* 12, 435-441 (**1998**).

197. P. Addersson, K. Nordstrand, M. Sunnerhagen, E. Liepinsh, I. Turovskis, G. Otting, Heteronuclear correlation experiments for the determination of one-bond coupling constants. *J. Biomol. NMR* 11, 445-450 (**1998**).

198. M. D. Sorensen, A. Meissner, O. W. Sorensen, C-13 natural abundance (SE)-E-3 and (SCT)-C-3 experiments for measurement of J coupling constants between C-13(alpha) or H- 1(alpha) and other protons in a protein. *J. Magn. Reson.* 137(1), 237-242 (**1999**).

199. P. Andersson, A. Annila, G. Otting, An alpha/beta Experiment for Spin-Selective Editing of IS Cross Peaks. *J. Magn. Reson.* 133, 364-367 (**1998**).

200. B. Brutscher, J. Boisbouvier, A. Pardi, D. Marion, J. P. Simorre, Improved sensitivity and resolution in H-1-C-13 NMR experiments of RNA. *J. Am. Chem. Soc.* 120(46), 11845-11851 (**1998**).

201. M. H. Lerche, A. Meissner, F. M. Poulsen, O. W. Sorensen, Pulse sequences for measurement of one-bond N-15-H-1 coupling constants in the protein backbone. *J. Magn. Reson.* 140(1), 259-263 (**1999**).

202. F. Cordier, A. J. Dingley, S. Grzesiek, A doublet-separated sensitivity-enhanced HSQC for the determination of scalar and dipolar one-bond J-couplings. *J. Biomol. NMR* 13(2), 175-180 (**1999**).

203. K. Pervushin, R. Riek, G. Wider, and K. Wuthrich, Attenuated T-2 Relaxation by Mutual Cancellation of Dipole-dipole Coupling and Chemical Shift Anisotropy Indicates an Avenue to NMR Structures of Very Large Biological Macromolecules in Solution. *Proc. Natl. Acad. Sci. U. S. A.* 94, 12366-12371 (**1997**).

204. J. Weigelt, Single Scan, Sensitivity- and Gradient-enhanced TROSY for Multidimensional NMR Experiments. *J. Am. Chem. Soc.* 120, 10778-10779 (1998).
M. Czisch and R. Boelens, Sensitivity Enhancement in the TROSY Experiment. *J. Magn. Reson*. 134, 158-160 (**1998**).

205. C. Griesinger, O. W. Sorensen, R. R. Ernst, Practical Aspects of the E-Cosy Technique - Measurement of Scalar Spin Spin Coupling-Constants in Peptides. *J. Magn. Reson.* 75(3), 474-492. (**1987**).

206. T. N. Pham, T. Liptaj, K. Bromek, D. Uhrin, Measurement of small one-bond proton-carbon residual dipolar coupling constants in partially oriented C-13 natural abundance oligosaccharide samples: Analysis of heteronuclear (1)J(CH)- modulated spectra with the BIRD inversion pulse. *J. Magn. Reson.* 157(2), 200-209 (**2002**).

207. Vliegenthart, J. F. G., L. Dorland and H. van Halbeek, High-Resolution, H-1-Nuclear Magnetic-Resonance Spectroscopy as a Tool in the Structural-Analysis of Carbohydrates Related to Glycoproteins. *Adv.Carbohydr.Chem.Biochem.* 41, 209-374 (**1983**).

208. Jobron, L. and O. Hindsgaul, Novel para-substituted benzyl ethers for hydroxyl group protection. *J. Am. Chem. Soc.* 121, 5835-5836 (**1999**).

209. Fukase, K., Y. Nakai, K. Egusa, J. A. Porco and S. Kusumoto, A novel oxidatively removable linker and its application to alpha-selective solid-phase oligosaccharide synthesis on a macroporous polystyrene support. *Synlett*, 1074-1078 (**1999**).

210. Rutherford, T. J., K. P. R. Kartha, S. K. Readman, P. Cura and R. A. Field, Iodine and its' interhalogen compounds: Useful reagents in carbohydrate chemistry - X. Adaptation of an NMR signal suppression pulse sequence for the selective removal of benzylic methylene signals of benzyl ether protected carbohydrates. *Tetrahedron Lett.* 40, 2025-2028 (**1999**).

211. Roumestand, C., J. Mispelter, C. Austruy and D. Canet, The Use of Band Filtering in Multidimensional Nmr - Evaluation of 2 User-Friendly Techniques. *J. Magn. Reson. Ser. B* 109, 153-163 (**1995**).

212. Emsley, L. in *Methods in Enzymology*; Oppenheimer, N.J.; James, T.L., Eds.; Academic Press: San Diego, **1994**; Vol. 239, pp. 207-246.

213. Geen, H. and R. Freeman, Band-Selective Radiofrequency Pulses. *J. Magn. Reson.* 93, 93-141 (**1991**).

214. Keglevic, D., B. Ladesic, O. Hadzija, J. Tomasic, Z. Valinger, M. Pokorny and R. Naumski, Isolation and Study of Composition of a Peptidoglycan Complex Excreted by Biotin-Requiring Mutant of Brevibacterium- Divaricatum Nrrl-2311 in Presence of Penicillin. *European Journal of Biochemistry* 42, 389-400 (**1974**).

215. Hwang, T. L. and A. J. Shaka, Reliable 2-Dimensional Rotating-Frame Cross-Relaxation Measurements in Coupled Spin Systems. *J. Magn. Reson. Ser. B* 102, 155-165 (**1993**).

216. Dauber-Ogusthorpe, P.; Roberts, V. A.; Ogusthorpe, D. J.; Wolff, D. J.; Genest, M.; Hagler, A. T. *Proteins: Structure, Function, and Genetics*, *4*, 31-47. (**1988**)

217. Pristovsek, P., J. Kidric and D. Hadzi, Bioactive Conformations of Small Peptides - a Method for Selection of Candidates Based on Conformations of Active and Inactive Analogs and Its Application to Muramyl Dipeptide. *J. Chem. Inf. Comput. Sci.* 35, 633-639 (**1995**).

218. Sanders, C. R. and J. H. Prestegard, Magnetically Orientable Phospholipid-Bilayers Containing Small Amounts of a Bile-Salt Analog, Chapso. *Biophys. J.* 58, 447-460 (**1990**).

219. Fehér K, Berger S, Kövér KE (2003). "Accurate determination of small one-bond heteronuclear residual dipolar couplings by *F1* coupled HSQC modified with a G-BIRD$^{(r)}$ module", *Journal of Magnetic Resonance* 163 (2003)

9. APPENDIX

Content

Appendix A

Table 3.1 ^{1}H and ^{13}C chemical shift data for PGM, Ad-PGM and BocTyr-PGM[a]

	PGM		Ad-PGM		BocTyr-PGM	
	δ1H	δ13C	δ1H	δ13C	δ1H	δ13C
β-GlcNAc-1	4.414	100.20	4.428	100.07	4.427	100.07
β-GlcNAc-2	3.404	55.81	3.409	56.03	3.396	56.14
β-GlcNAc-3	3.067[b]	76.53[b]	3.411	75.02	3.396	73.50
β-GlcNAc-4	3.396	73.46	3.074	76.41	3.067	70.84
β-GlcNAc-5	3.057[b]	70.70[b]	3.073	70.85	3.067	76.51
β-GlcNAc-6	3.722	60.99	3.740	61.29	3.715	61.31
β-GlcNAc-6'	3.462	60.99	3.480	61.29	3.462	61.31
β-GlcNAc(CH_3)	1.787	22.73	1.796	22.68	1.792	22.75
β-GlcNAc(NH)	7.808	-	7.768	-	7.821	-
β-GlcNAc(CO)	-	169.27	-		-	169.77
β-GlcNAc-3OH	5.063[c]	-	4.928	-	f	-
β-GlcNAc-4OH	5.003[c]	-	4.971	-	f	-
β-GlcNAc-6OH	4.343	-	4.239	-	f	-
α-MurNAc-1	5.117	89.59	5.119	89.56	5.091	89.71
α-MurNAc-2	3.477	52.38	3.488	53.99	3.502	53.99
α-MurNAc-3	3.401	74.95	3.395	75.03	3.527	71.04
α-MurNAc-4	3.672	75.67	3.683	75.66	3.425[d]	74.96[d]
α-MurNAc-5	3.506	70.93	3.533	71.04	3.670[d]	75.67[d]
α-MurNAc-6	3.602	59.32	3.603	59.38	3.583	59.53
α-MurNAc-6'	3.532	59.32	3.550	59.38	3.539	59.53
α-MurNAc-1OH	6.596	-	6.517	-		-
α-MurNAc(CH_3)	1.804	22.73	1.807	22.68	1.805	22.75
α-MurNAc(NH)	8.454	-	8.395	-	8.423	-
α-MurNAc(CO)	-	169.27	-	169.31	-	169.77
α-MurNAc-6OH	4.610	-	4.570	-		
D-Lac-α	4.462	75.42	4.470	75.38	4.454	75.40
D-Lac-β	1.270	19.17	1.262	19.09	1.253	19.05
D-Lac-CO	-	174.40	-	e	-	174.79

L-Ala^1-NH	8.026	-	7.961	-	8.088	-
L-Ala^1-α	4.351	48.14	4.349	48.10	4.329	48.26
L-Ala^1-β	1.241	18.03	1.233	18.05	1.241	18.11
L-Ala^1-CO	-	172.20	-	172.19	-	172.61
D-iGln^2-NH	8.293	-	8.240	-	8.333	-
D-iGln^2-α	4.137	51.93	4.147	51.997	4.115	52.40
D-iGln^2-αCO	-	173.15	-	173.04		
D-iGln^2-NH_2^E	7.355	-	7.289	-	7.359	-
D-iGln^2-NH_2^Z	7.008	-	6.956	-	7.016	-
D-iGln^2-β	1.711	27.35	1.935	27.55	1.996	27.21
D-iGln^2-β'	2.004	27.35	1.709	27.55	1.709	27.21
D-iGln^2-γ,γ'	2.183	31.51	2.144	31.48	2.172	31.38
D-iGln^2-δCO	-	171.67	-	171.67	-	
m-Dap^3-NH	7.969	-	7.998	-	7.857	-
m-Dap^3-α	4.174	53.09	4.161	52.50	4.115	52.40
m-Dap^3-αCO	-	171.11	-	171.14	-	
m-Dap^3-β	1.634	31.63	1.589	31.34	1.533	31.31
m-Dap^3-β'	1.577	31.63	1.471	31.34	1.586	31.31
m-Dap^3-γ	1.413	20.83	1.302	21.64	1.134	21.40
m-Dap^3-γ'	1.350	20.83	1.216	21.64	1.110	21.40
m-Dap^3-δ	1.669	32.20	1.895	27.83	1.615	31.13
m-Dap^3-δ'	1.555	32.20	1.895	27.83	1.373	31.13
m-Dap^3-ε	3.489	53.79	4.133	51.89	4.012	52.04
m-Dap^3-εCO	-	e	-	173.80	-	172.96
m-Dap^3-$\varepsilon CONH_2^E$	8.107	-	7.248	-	7.355	-
m-Dap^3-$\varepsilon CONH_2^Z$	7.287	-	6.912	-	6.938	-
m-Dap^3-εNH	7.878	-	7.647	-	8.073	-
Ad- CH_2-CO	-	-	-	169.66	-	-
Ad-CH_2(α)	-	-	1.879	49.42	-	-

Ad-βC(q)	-	-	-	e	-	-
Ad-γCH_2	-	-	1.637	36.24	-	-
Ad-γ'CH_2	-	-	1.573	36.24	-	-
Ad-δCH	-	-	1.898	27.65	-	-
Ad-εCH_2	-	-	1.556	41.79	-	-
L-Tyr-NH	-	-	-	-	7.031	-
$Bu^t(CH_3)$	-	-	-	-	1.316	28.01
L-Tyr-α	-	-	-	-	4.041	56.1
L-Tyr-CO	-	-	-	-	-	171.59
L-Tyr-β	-	-	-	-	2.659	36.28
L-Tyr-β'	-	-	-	-	2.761	36.28
L-Tyr-2,6	-	-	-	-	6.970	129.81
L-Tyr-3,5	-	-	-	-	6.567	114.77
L-Tyr-1	-	-	-	-	-	127.50
L-Tyr-4	-	-	-	-	-	155.97
L-Tyr-4OH	-	-	-	-	6.343	-
D-Ala^4-NH	8.039	-	8.103	-	8.077	-
D-Ala^4-α	4.119	48.58	4.301	47.332	4.124	48.34
D-Ala^4-β	1.212	17.61	1.187	17.91	1.190	17.56
D-Ala^4-CO	-	170.8	-	171.68	-	171.07
D-Ala^5-NH	7.547	-	8.072	-	7.513	-
D-Ala^5-α	3.803	49.15	4.161	47.30	3.731	49.46
D-Ala^5-β	1.192	18.41	1.280	16.76	1.175	18.69
D-Ala^5-CO	-	174.30	-	173.84	-	174.79

a) For solutions in DMSO-d_6 at 293K for PGM and at 300K for Ad-PGM and BocTyr-PGM. Chemical shifts are in ppm and referenced to the solvent signal (δ_{1H} = 2.500 ppm, δ_{13C} = 39.95 ppm). $CONH_2^Z$ and $CONH_2^E$ refer to one of the amide protons in Z or E position with respect to the C=O oxygen, respectively.

b) Assignment for β-GlcNAc-3 and β-GlcNAc-5 can be interchanged

c) Assignment for β-GlcNAc-3OH and β-GlcNAc-4OH can be interchanged

d) Assignment for MurNAc-H4 and MurNAc-H5 can be interchanged

e) Cannot be determined due to missing crosspeak in HMBC and overlap in the 1D ^{13}C spectra

Appendix B

Table 3.2 NOESY/ROESY cross peak intensities for PGM, Ad-PGM and BocTyr-PGM[a, b, c]

	Proton1	Proton2	PGM [d]	Ad-PGM [d]	BocTyr-PGM[e]
1	GlcNAc-1	MurNAc-4	s	s	s
2	GlcNAc-3	D-Lac-β	-	-	w [i)]
3	MurNAc-2	D-Lac-α	-	m	-
4	MurNAc-2	D-Lac-β	m	s	m
5	MurNAc-2	L-Ala^1-NH	m	m	w
6	MurNAc-2	D-iGln^2-NH	w	-	-
7	MurNAc-NH	D-Lac-α	s	s	m
8	MurNAc-NH	D-Lac-β	s	m	w
9	MurNAc(CH_3)	L-Ala^1-NH	w	w	-
10	MurNAc(CH_3)	L-Ala^1-β	-	-	w
11	MurNAc(CH_3)	D-iGln^2-NH	w	-	-
12	MurNAc(CH_3)	D-iGln^2-$CONH_2^E$	w	w	w [g)]
13	MurNAc(CH_3)	D-iGln^2-$CONH_2^Z$	w	w	-
14	MurNAc(CH_3)	D-Ala^4-β	-	-	w
15	MurNAc-3	D-Lac-β	m	m	w
16	MurNAc-3	L-Ala^1-NH	m	w	-
17	MurNAc-3	D-iGln^2-NH	w	-	-
18	MurNAc-3	D-iGln^2-$CONH_2^E$	w	-	-
19	MurNAc-4	D-Lac-β	-	-	w
20	MurNAc-4	L-Ala^1-NH	w	w	-
21	D-Lac-α	L-Ala^1-NH	s	s	s
22	D-Lac-β	L-Ala^1-NH	s	s	s [f)]
23	D-Lac-β	D-iGln^2-$CONH_2^E$	w	-	w [f)]
24	L-Ala^1-α	D-iGln^2-NH	s	s	s
25	L-Ala^1-α	D-iGln^2-$CONH_2^E$	w	w	w
26	L-Ala^1-β	D-iGln^2-NH	s	s	s
27	L-Ala^1-β	D-iGln^2-γ,γ’	-	-	w

28	L-Ala^{1}-β	D-iGln^{2}-CONH$_2^{E}$		w	w [f]
29	D-iGln^{2}-β, β'	m-Dap^{3}-αNH	m	w	w
30	D-iGln^{2}-γ,γ'	m-Dap^{3}-αNH	s	s	s
31	m-Dap^{3}-α	D-Ala^{4}-NH	s	s	s [g]
32	m-Dap^{3}-β,β'	D-Ala^{4}-NH	m	m	m
33	m-Dap^{3}-β,β'	L-Tyr-3,5	h)	h)	w
34	m-Dap^{3}-β,β'	D-Ala^{5}-NH	w	-	w
35	m-Dap^{3}-γ,γ'	D-Ala^{5}-NH	m	-	-
36	m-Dap^{3}-γγ'	L-Tyr-3,5	h)	h)	w
37	m-Dap^{3}-ε	D-Ala^{5}-NH	w	-	-
38	m-Dap^{3}-εNH	(Ad)-CH$_2$-(CO)	h)	s	h)
39	m-Dap^{3}-εNH	L-Tyr-α	h)	h)	s
40	m-Dap^{3}-εNH	L-Tyr-β,β'	h)	h)	m
41	D-Ala^{4}-α	D-Ala^{5}-NH	s	s	s
42	D-Ala^{4}-β	L-Tyr-3,5	h)	h)	w
43	Boc-Bu^{t}	L-Tyr-3,5	h)	h)	w

a) NOEs only for the dominant isomer with the reducing MurNAc moiety in α-anomeric form

b) Interresidual cross peaks are only listed. The actual number of distance restraints used for the calculations was larger, see text.

c) CONH$_2^{Z}$ and CONH$_2^{E}$ refer to one of the amide protons in Z or E position with respect to the C=O oxygen, respectively.

d) Determined from NOESY spectra recorded at 300K

e) Determined from ROESY spectra recorded at 300K

f) Ambiguous: L-Ala^{1}-β and D-Lac-β overlap

g) Ambiguous: MurNAc(CH$_3$) and GlcNAc(CH$_3$) overlap

h) Does not apply

i) Ambiguous: GlcNAc-3 and GlcNAc-5 overlap

Appendix C Insight II input file for F DISCOVER for flexible geometry systematic search

```
!
      overlap = 0.01
      begin simulation
     *    add-automatic bond torsion valence out-of-plane
      reduce
!
      scale 1-4 by 0.5
      set dielectric  = 46.000000*r
!

      Assign the torsion name ocss to
     * residue BDGL    1 atom O
     * residue BDGL    1 atom C1
     * residue BDGL    1 atom S1
     * residue BDGL    1 atom S7

      Assign the torsion name cssc to
     * residue BDGL    1 atom C1
     * residue BDGL    1 atom S1
     * residue BDGL    1 atom S7
     * residue BDGL    1 atom C7

      Assign the torsion name ssco to
     * residue BDGL    1 atom S1
     * residue BDGL    1 atom S7
     * residue BDGL    1 atom C7
     * residue BDGL    1 atom O5

      Assign the torsion name   g1 to
     * residue BDGL    1 atom O
     * residue BDGL    1 atom C5
     * residue BDGL    1 atom C4
     * residue BDGL    1 atom C3

      Assign the torsion name   g2 to
     * residue BDGL    1 atom C5
     * residue BDGL    1 atom C4
     * residue BDGL    1 atom C3
     * residue BDGL    1 atom C2

      Assign the torsion name   g3 to
     * residue BDGL    1 atom C4
     * residue BDGL    1 atom C3
     * residue BDGL    1 atom C2
     * residue BDGL    1 atom C1

      Assign the torsion name   g4 to
     * residue BDGL    1 atom C3
     * residue BDGL    1 atom C2
     * residue BDGL    1 atom C1
     * residue BDGL    1 atom O

      Assign the torsion name   g5 to
     * residue BDGL    1 atom C2
     * residue BDGL    1 atom C1
     * residue BDGL    1 atom O
     * residue BDGL    1 atom C5

      Assign the torsion name   g6 to
     * residue BDGL    1 atom C1
```

```
     * residue BDGL    1 atom O
     * residue BDGL    1 atom C5
     * residue BDGL    1 atom C4

      Assign the torsion name   n1 to
     * residue BDGL    1 atom O5
     * residue BDGL    1 atom C
     * residue BDGL    1 atom C10
     * residue BDGL    1 atom C9

      Assign the torsion name   n2 to
     * residue BDGL    1 atom C
     * residue BDGL    1 atom C10
     * residue BDGL    1 atom C9
     * residue BDGL    1 atom C8

      Assign the torsion name   n3 to
     * residue BDGL    1 atom C10
     * residue BDGL    1 atom C9
     * residue BDGL    1 atom C8
     * residue BDGL    1 atom C7

      Assign the torsion name   n4 to
     * residue BDGL    1 atom C9
     * residue BDGL    1 atom C8
     * residue BDGL    1 atom C7
     * residue BDGL    1 atom O5

      Assign the torsion name   n5 to
     * residue BDGL    1 atom C8
     * residue BDGL    1 atom C7
     * residue BDGL    1 atom O5
     * residue BDGL    1 atom C

      Assign the torsion name   n6 to
     * residue BDGL    1 atom C7
     * residue BDGL    1 atom O5
     * residue BDGL    1 atom C
     * residue BDGL    1 atom C10
!
!
      loop0 = 1
      angle0 = -180.00
      ifnum = 1
!
!
L0    force ocss in  BDGL 1  to angle0 using 100.000000
      loop1 = 1
      angle1 = -180.00
!
!
L1    force cssc in  BDGL 1  to angle1 using 100.000000
      loop2 = 1
      angle2 = -180.00
!
!
L2    force ssco in  BDGL 1  to angle2 using 100.000000
      loop3 = 1
      angle3 = -60
!
!
L3    force   g1 in  BDGL 1  to angle3 using 100.000000
      loop4 = 1
```

```
      angle4 = 60
!
!
L4    force   g2 in  BDGL 1  to angle4 using 100.000000
      loop5 = 1
      angle5 = -60
!
!
L5    force   g3 in  BDGL 1  to angle5 using 100.000000
      loop6 = 1
      angle6 = 60
!
!
L6    force   g4 in  BDGL 1  to angle6 using 100.000000
      loop7 = 1
      angle7 = -60
!
!
L7    force   g5 in  BDGL 1  to angle7 using 100.000000
      loop8 = 1
      angle8 = 60
!
!
L8    force   g6 in  BDGL 1  to angle8 using 100.000000
      loop9 = 1
      angle9 = -60
!
!
L9    force   n1 in  BDGL 1  to angle9 using 100.000000
      loop10 = 1
      angle10 = 60
!
!
L10    force   n2 in  BDGL 1  to angle10 using 100.000000
      loop11 = 1
      angle11 = -60
!
!
L11    force   n3 in  BDGL 1  to angle11 using 100.000000
      loop12 = 1
      angle12 = 60
!
!
L12    force   n4 in  BDGL 1  to angle12 using 100.000000
      loop13 = 1
      angle13 = -60
!
!
L13    force   n5 in  BDGL 1  to angle13 using 100.000000
      loop14 = 1
      angle14 = 60
!
!
L14    force   n6 in  BDGL 1  to angle14 using 100.000000
!
!
      Minimize
     *    no cross terms
     *    no morse
     *    for 500 iterations
     *    using VA09A
     *    until the maximum derivative is less than 0.0010000000 kcal/A
!
```

```
!
      archive as file number ifnum
      ifnum = ifnum + 1
!
!
R0    loop14 = loop14 + 1
      angle14 = angle14 + 0.00
      if loop14 .le.    1 then L14
      loop13 = loop13 + 1
      angle13 = angle13 + 0.00
      if loop13 .le.    1 then L13
      loop12 = loop12 + 1
      angle12 = angle12 + 0.00
      if loop12 .le.    1 then L12
      loop11 = loop11 + 1
      angle11 = angle11 + 0.00
      if loop11 .le.    1 then L11
      loop10 = loop10 + 1
      angle10 = angle10 + 0.00
      if loop10 .le.    1 then L10
      loop9 = loop9 + 1
      angle9 = angle9 + 0.00
      if loop9 .le.    1 then L9
      loop8 = loop8 + 1
      angle8 = angle8 + 0.00
      if loop8 .le.    1 then L8
      loop7 = loop7 + 1
      angle7 = angle7 + 0.00
      if loop7 .le.    1 then L7
      loop6 = loop6 + 1
      angle6 = angle6 + 0.00
      if loop6 .le.    1 then L6
      loop5 = loop5 + 1
      angle5 = angle5 + 0.00
      if loop5 .le.    1 then L5
      loop4 = loop4 + 1
      angle4 = angle4 + 0.00
      if loop4 .le.    1 then L4
      loop3 = loop3 + 1
      angle3 = angle3 + 0.00
      if loop3 .le.    1 then L3
      loop2 = loop2 + 1
      angle2 = angle2 + 10.00
      if loop2 .le.   37 then L2
      loop1 = loop1 + 1
      angle1 = angle1 + 10.00
      if loop1 .le.   37 then L1
      loop0 = loop0 + 1
      angle0 = angle0 + 10.00
      if loop0 .le.   37 then L0
!
!
      end
```

Appendix D Insight II input file for F DISCOVER for simulated annealing

```
! Simulated Annealing Protocol
!
      overlap = 0.01
! Change the next line to the cutoff value that you want to use:
      cutoff = 100.000000
! cutdis = cutoff - 1
      cutdis = 100.000000
! swtdis is always 1.5
      swtdis = 1.5
! timtmp is the exponential rate constant during
! the "Initialize dynamics" and "resume dynamics" steps.
! Default timtmp = 0.1
! For the initial heating, we usually do this fairly quickly and
! establish equilibrium, so we don't change TIMTMP when initializing
! dynamics.
! Uncomment and edit the next line if you want to change this.
!     timtmp = 0.1
!
      begin simulation
     *    add-automatic bond torsion valence out-of-plane
      reduce
!
      scale 1-4 by 0.5
! Change the dielectric constant to the value you want to use.
! distance-dependent dielectrics:  set dielectric = 1.0*r
      set dielectric  = 46.000000*r
!
!
! First minimization to reduce very high energies.
! If you want charges, delete the "and no charges" line.
      Minimize
     *    no cross terms
     *    no morse
     *    for 100 iterations
     *    using steep descents
     *    until the maximum derivative is less than 10.000000001 kcal/A
!
!
! Second minimization to drive to a low minimum.
! We don't need to minimize REALLY low, since we are about to
! heat up the molecule.
! If you want charges, delete the "and no charges" line.
! If you have > 200 nin-fixed atoms, change "VA09A" to
! "conjugate gradient".
      Minimize
     *    no cross terms
     *    no morse
     *    for 5000 iterations
     *    using VA09A
     *    until the maximum derivative is less than 1.000000001 kcal/A
!
!
! The "for ### iterations" line specifies the number of
! fsec for heating and equilibration.
! Change the temperature to suit your molecule.  If
! your molecule is restrained (e.g., rings,
! double bonds, etc), then 1000-1500K is usually good.
! If your molecule is unconstrained, 600-1000K is good.
! Steps of 1 fsec are required.
! Set timtmp to 6* the time over which the temperature will change.
```

```
! This results in a final temperature within 1.5% of your final
! temperature.  According to the manual, "the temperature difference
! between the initial and final temperature is 1/2 of the initial
! difference after TIMTMP".
! See also the TIMTMP note at the beginning of this file.
      timtmp = 1.0
! If you want charges, delete the "and no charges" line.
! The "write history" line reduces the history file output, which is
!  highly  recommended  unless  you  want  to  restart  the  calculation  if  it
fails.
      initialize dynamics
     *    write history file every 9000000 steps
     *    for 5000 iterations
     *    at 1000.000 K
     *    steps of    1.000
     *    no cross terms
     *    no morse
!
!
!    Dynamics Loop
!
      ifile = 1
!
!
! The next line specifies how many fsec to run the dynamics
! before cooling the structure.
! Also includes the heating step for each iteration
! If you want charges, delete the "and no charges" line.
! See also the TIMTMP note at the beginning of this file.
loop   timtmp = 1.0
       resume dynamics
     *    for 5000 iterations
     *    at 1000.000 K
     *    no cross terms
     *    no morse
!     *    and no charges
! The next lines specify how many fsec to cool the dynamics
! before minimizing the structure.
! The cooling occurs for ~1 psec, with an exponential decay
! to the final temperature.
! If you want charges, delete the "and no charges" line.
! See also the TIMTMP note at the beginning of this file.
      timtmp = 1.0
! You can also repeat this step, in order to cool to an intermediate
! temperature, then a final temperature.
!
      resume dynamics
     *    for 5000 iterations
     *    at 300.000 K
     *    steps of    1.000
     *    no cross terms
     *    no morse
!
!
! First minimization to reduce very high energies.
! If you want charges, delete the "and no charges" line.
      Minimize
     *    no cross terms
     *    no morse
     *    for 500 iterations
     *    using steep descents
     *    until the maximum derivative is less than 10.000000000 kcal/A
!
```

```
!
! Second minimization to drive to a low minimum.
! Adjust the "maximum derivative is less than ###"
! number to suit the level of minimization you require.
! If you have > 200 atoms, change "VA09A" to
! "conjugate gradient".
! If you want charges, delete the "and no charges" line.
      Minimize
     *    no cross terms
     *    no morse
     *    for 5000 iterations
     *    using VA09A
     *    until the maximum derivative is less than 0.001000001 kcal/A
!
!     Record Results
!
      print energy summary
      archive as file number ifile
      ifile = ifile + 1
!
!
! The next line specifies how many fsec to heat the structure
! back to the dynamics temperature.
! See also the TIMTMP note at the beginning of this file.
      timtmp = 1.0
! If you want charges, delete the "and no charges" line.
      resume dynamics
     *    for 5000 iterations
     *    at 1000.000 K
     *    no cross terms
     *    no morse
!
! Change the number below (currently 1000) to the number
! of structures you want to calculate
      if ifile .le. 1000 then loop
!
      print timings

                                                    END
```

Appendix E 2D crosssection of the 3D potential energy surface for the Glc-S-S-Man derivative. The crosssections were created by slicing the 3D surface with a plane perpendicular to the axis of the torsion angle that is held constant.

c) $\varphi_{(C1\text{-}S\text{-}S\text{-}Oring)}$ is held constant at 300^{o}

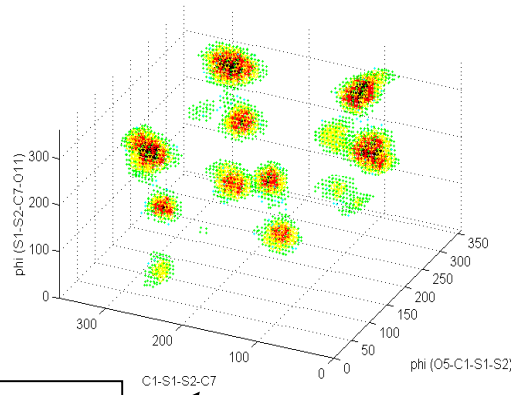

b) $\omega_{(C1\text{-}S\text{-}S\text{-}C1)}$ is held constant at 109^{o}

a) $\varphi_{(Oring\text{-}C1\text{-}S\text{-}S)}$ is held constant at 300^{o}

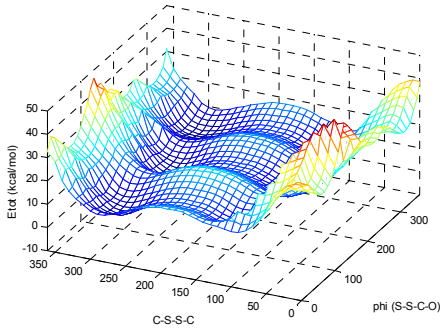

a) $\varphi_{(Oring\text{-}C1\text{-}S\text{-}S)} = 300^{o}$

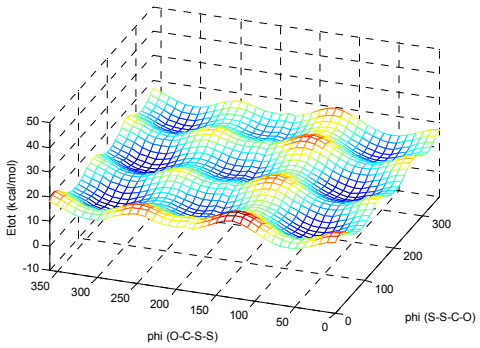

at $\omega_{(C1\text{-}S\text{-}S\text{-}C1)} = 109^{o}$

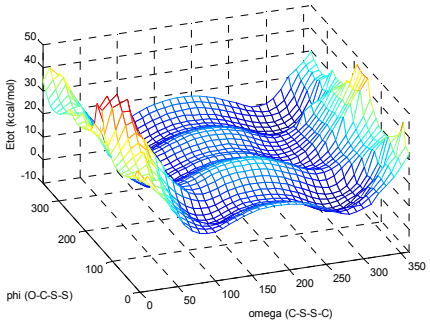

at $\varphi_{(C1\text{-}S\text{-}S\text{-}Oring)} = 300^{o}$

Appendix F 2D crosssection of the 3D potential energy surface for the Glc-S-S-Gal derivative. The crosssections were created by slicing the 3D surface with a plane perpendicular to the axis of the torsion angle that is held constant.

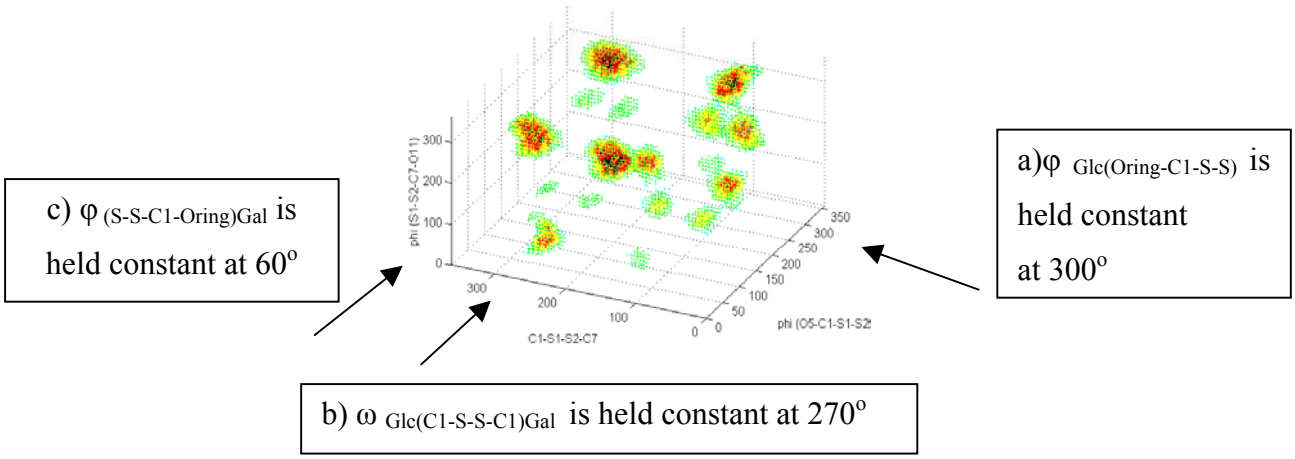

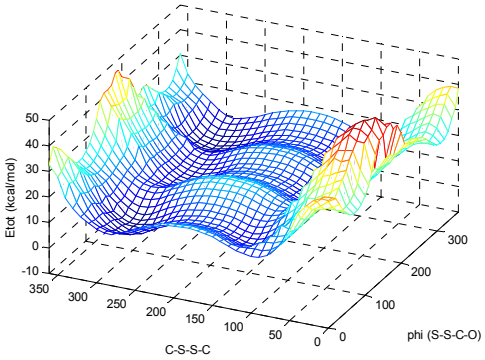

a) at φ Glc(Oring-C1-S-S) = 300°

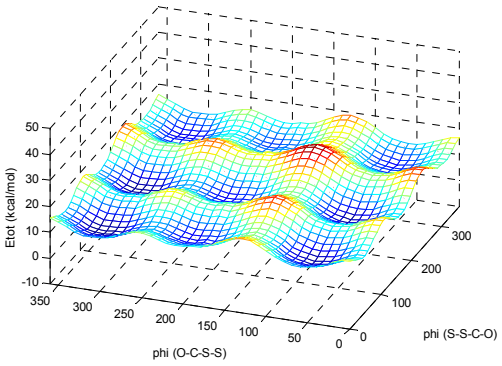

b) at ω Glc(C1-S-S-C1)Gal = 270°

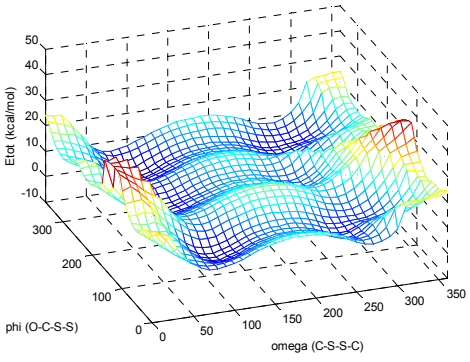

c) at φ (S-S-C1-Oring)Gal = 60°

Appendix G 2D crosssection of the 3D potential energy surface for the Glc-S-S-NAcGlc derivative. The crosssections were created by slicing the 3D surface with a plane perpendicular to the axis of the torsion angle that is held constant.

c) $\varphi_{(S\text{-}S\text{-}C1\text{-}Oring)Gal}$ is held constant at 300°

b) $\omega_{Glc(C1\text{-}S\text{-}S\text{-}C1)Gal}$ is held constant at 280°

a) $\varphi_{Glc(Oring\text{-}C1\text{-}S\text{-}S)}$ is held constant at 70°

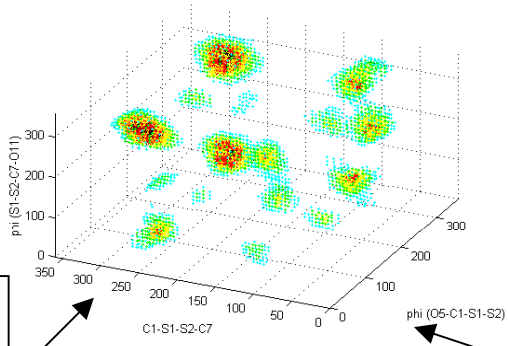

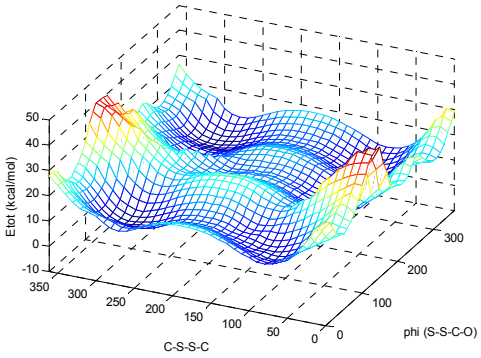

a) at $\varphi_{Glc(Oring\text{-}C1\text{-}S\text{-}S)} = 70°$

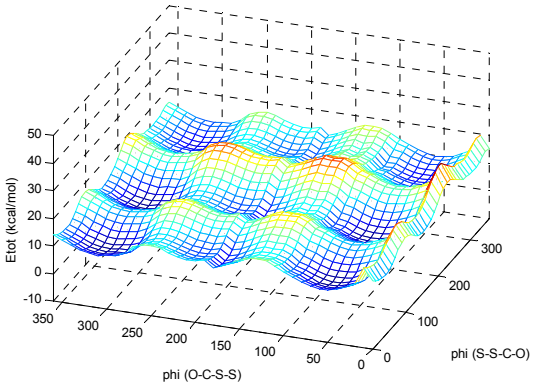

b) at $\omega_{Glc(C1\text{-}S\text{-}S\text{-}C1)Gal} = 280°$

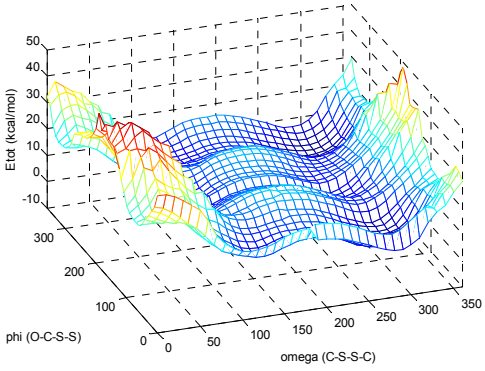

c) at $\varphi_{(S\text{-}S\text{-}C1\text{-}Oring)Gal} = 300°$

STUDIES OF CARBOHYDRATES AND PEPTIDES BY NMR SPECTROSCOPY AND MOLECULAR MODELLING

Értekezés a doktori (Ph.D.) fokozat megszerzése érdekében

kémia tudományágban

Írta: Fehér Krisztina

okleveles vegyész, angol-magyar szakforditó

Készült a Debreceni Egyetem Kémia doktori iskolája

Heterociklusos vegyületek programja keretében

Témavezető: Dr. Szilágyi László

A doktori szigorlati bizottság:

elnök:	Dr. Antus Sándor	.....
tagok:	Dr. Perczel András	.....
	Dr. Dinya Zoltán	.....

A doktori szigorlat időpontja:

Az értekezés bírálói:

....

....

A bírálóbizottság:

elnök:	.....	.....
tagok:	.....	.....
	.....	.....
	.....	.....

Az értekezés védésének időpontja: